

DIPLOMARBEIT

**Characterization of high-power near-infrared
ultrashort pulses of solid-state laser amplifiers using
spectral phase measurements**

zur Erlangung des akademischen Grades

Diplom-Ingenieur

im Rahmen des Studiums

Technische Physik

eingereicht von

Jonas Amann

Matrikelnummer 11702808

ausgeführt am Institut für Angewandte Physik
der Fakultät für Physik der Technischen Universität Wien

in Zusammenarbeit mit dem Center for Attosecond Laser Science
der School of Science, The University of Tokyo

Betreuung

Ao.Univ.Prof. Dipl.-Ing. Dr.techn. Michael Schmid

Prof. Atsushi Iwasaki

Project Assoc.Prof. Toshiaki Ando

Wien, 23.08.2023

Jonas Amann

Ao.Univ.Prof. Dipl.-Ing.
Dr.techn. Michael Schmid

Statutory Declaration

I hereby confirm that I have independently authored the present work and have not used any sources or aids other than those declared, that all sections of the work which have been taken directly or indirectly from other sources are duly marked as such, and that the work has not been submitted in identical or similar form to any other examination authority.

Eidesstattliche Erklärung

Hiermit versichere ich, dass ich die vorliegende Arbeit selbstständig verfasst und keine anderen als die angegebenen Quellen und Hilfsmittel benutzt habe, dass alle Stellen der Arbeit, die wörtlich oder sinngemäß aus anderen Quellen übernommen wurden, als solche kenntlich gemacht und dass die Arbeit in gleicher oder ähnlicher Form noch keiner Prüfungsbehörde vorgelegt wurde.

Wien, 23.08.2023

Jonas Amann

Abstract

Ultrafast laser science relies on the characterization of ultrashort pulses, which requires determining their electric field properties. This thesis focuses on the pulse characterization of two solid-state femtosecond lasers operating in the near-infrared range using self-referenced spectral interferometry (SRSI). SRSI is a technique based on linear spectral interferometry that utilizes cross-polarized wave generation to generate a reference pulse and enables the determination of both the spectral amplitude and the spectral phase of laser pulses. The experimental setup and critical parameters were carefully analyzed to ensure accurate measurements of the electric field. In the process of determining the spectral phase, a polynomial fitting was employed to obtain dispersion terms up to order four. Experimental evidence indicates that these determined dispersion terms accurately correspond to the actual dispersion terms only within a specific validity range. A method for establishing this validity range is presented. Dispersion compensation devices were implemented to minimize pulse duration by flattening the phase across the spectral bandwidth. Consequently, a pulse duration of 38 fs was achieved for a Thales ALPHA kHz laser, while a pulse duration of 271 fs was achieved for a Light Conversion PHAROS laser. Moreover, this work implemented an extended SRSI technique that takes into account the influence of an incoherent laser output component, specifically amplified spontaneous emission (ASE). The experimental findings confirmed the predictions of the extended analytical model, which also allowed the determination of the ASE spectrum of a Thales ALPHA kHz laser.

Contents

| | | |
|----------|---|-----------|
| 1 | Introduction | 5 |
| 2 | Background and Theory | 6 |
| 2.1 | Ultrashort laser pulses | 6 |
| 2.1.1 | High-order dispersion | 7 |
| 2.1.2 | Amplified Spontaneous Emission (ASE) | 9 |
| 2.2 | High-power femtosecond laser systems | 10 |
| 2.2.1 | Mode locking | 10 |
| 2.2.2 | Solid-state lasers | 11 |
| 2.2.3 | Dispersion control / pulse compression | 11 |
| 2.3 | Nonlinear optics | 13 |
| 2.3.1 | Second harmonic generation | 14 |
| 2.3.2 | Cross-polarized wave generation (XPW) | 15 |
| 2.3.3 | Optical Kerr effect | 16 |
| 2.4 | Pulse-measurement methods | 18 |
| 2.4.1 | Autocorrelation | 18 |
| 2.4.2 | Frequency-resolved optical gating (FROG) | 18 |
| 2.4.3 | GRENOUILLE | 18 |
| 2.4.4 | Spectral phase interferometry for direct electric-field reconstruction (SPIDER) | 19 |
| 2.4.5 | Spectral interferometry (SI) | 19 |
| 2.4.6 | Self-referenced spectral interferometry (SRSI) | 20 |
| 2.5 | Theory of SRSI | 20 |
| 2.5.1 | Pulse characterization procedure / SRSI algorithm | 21 |
| 2.5.2 | SRSI with consideration of an incoherent component | 25 |
| 3 | Method | 27 |
| 3.1 | Equipment | 27 |
| 3.2 | Experimental setup and optical components | 28 |
| 3.3 | Choice of calcite plate thickness | 29 |
| 3.4 | Data acquisition / procedure for measuring spectra | 31 |
| 3.5 | Software | 34 |
| 4 | Results and Discussion | 35 |
| 4.1 | SRSI pulse characterization of a Thales ALPHA kHz laser | 35 |
| 4.1.1 | Pulse characterization procedure | 35 |
| 4.1.2 | Improvement by a high-resolution spectrometer | 42 |
| 4.2 | SRSI pulse characterization of a Light Conversion PHAROS laser | 45 |
| 4.2.1 | Pulse characterization procedure | 46 |
| 4.3 | Determination of dispersion terms and validity ranges using SRSI | 49 |
| 4.3.1 | Determination of relative GDD and TOD of different pulses | 51 |
| 4.3.2 | Validity range of retrieved GDD and TOD | 52 |
| 4.4 | Consideration of ASE in SRSI pulse characterization of a Thales ALPHA kHz laser | 54 |
| 4.4.1 | Estimation of the ASE spectrum | 54 |
| 4.4.2 | Influence of ASE on the calculated fundamental and XPW spectrum | 55 |
| 5 | Conclusion | 59 |
| A | Source code | 62 |

List of Figures

| | | |
|----|---|----|
| 1 | Intensity and phase of pulses in time and frequency domain for different spectral phases . . . | 8 |
| 2 | Schematic diagram of a grating compressor | 12 |
| 3 | Simplified functionality of an AOPDF | 13 |
| 4 | Fundamental pulses with different spectral phases and the corresponding XPW pulses . . | 17 |
| 5 | Schematic representation of SRSI | 21 |
| 6 | Typical interferogram and its Fourier transform | 22 |
| 7 | Iterative SRSI algorithm | 25 |
| 8 | Experimental SRSI setup with schematic beam path | 28 |
| 9 | Interferograms for SRSI measurements measured by different spectrometers | 31 |
| 10 | Interferogram and its Fourier transform for a temporal retardation of $\tau = 560$ fs | 32 |
| 11 | Interferogram and its Fourier transform for a temporal retardation of $\tau = 1670$ fs | 32 |
| 12 | Intensity $I_{IN}(\lambda)$ of a typical interferogram of an SRSI measurement for femtosecond pulse with a center wavelength of 800 nm; interferogram measured by Ocean Optics HR4000 . . | 36 |
| 13 | Temporal signal $I_{IN}(t)$ of a femtosecond pulse with a center wavelength of 800 nm | 37 |
| 14 | Temporal interference and sum term of a femtosecond pulse | 38 |
| 15 | Spectral interference and sum term of a femtosecond pulse | 38 |
| 16 | Comparison of calculated spectra of the fundamental pulse and the reference pulse for a femtosecond pulse with a center wavelength of 800 nm | 39 |
| 17 | Calculated spectral phase of the pulse to be determined for the case with and without consideration of the non-constant phase of the reference pulse | 40 |
| 18 | Phase and spectrum of fundamental pulse and XPW spectrum determined by SRSI after coarse and fine compression | 41 |
| 19 | Intensity $I_{IN}(\lambda)$ of a typical interferogram of an SRSI measurement for a femtosecond pulse with a center wavelength of 800 nm; interferogram measured by Anritsu spectrometer . . | 42 |
| 20 | Comparison of calculated spectra of the fundamental pulse and the reference pulse for a femtosecond pulse with a center wavelength of 800 nm | 43 |
| 21 | Phase and spectrum of the fundamental pulse and XPW spectrum determined by SRSI after fine compression for a femtosecond pulse with a center wavelength of 800 nm | 44 |
| 22 | Temporal intensity of a femtosecond pulse with a center wavelength of 800 nm | 45 |
| 23 | Semi-log plot of temporal intensity of a femtosecond pulse with a center wavelength of 800 nm | 45 |
| 24 | Intensity $I_{IN}(\lambda)$ of a typical interferogram of an SRSI measurement for a femtosecond pulse with a center wavelength of 1025 nm; interferogram measured by Anritsu spectrometer . . | 47 |
| 25 | Intensity $I_{IN}(\omega)$ of a typical interferogram of an SRSI measurement for a femtosecond pulse with a center wavelength of 1025 nm; interferogram measured by Anritsu spectrometer . . | 47 |
| 26 | Temporal signal $I_{IN}(t)$ of a femtosecond pulse with a center wavelength of 1025 nm | 48 |
| 27 | Temporal interference and sum term of a fs-pulse with a center wavelength of 1025 nm . . | 48 |
| 28 | Spectral interference and sum term of a fs-pulse with a center wavelength of 1025 nm . . | 49 |
| 29 | Analytically calculated spectra of the reference pulse and the fundamental pulse for a femtosecond pulse with a center wavelength of 1025 nm | 49 |
| 30 | Spectral phase and temporal description of different femtosecond pulses with center wavelength of 1025 nm for different compressor settings | 50 |
| 31 | Spectral phase fitting of a femtosecond pulse with positive GDD | 51 |
| 32 | Spectral phase fitting of femtosecond pulse with positive GDD using a reference pulse . . | 52 |
| 33 | Validity range of GDD determined by SRSI | 53 |
| 34 | Validity range of TOD determined by SRSI | 54 |
| 35 | Separately measured and fitted fundamental and XPW spectra of a femtosecond pulse with a center wavelength of 800 nm | 55 |
| 36 | Estimation of the ASE spectrum of a femtosecond pulse with a center wavelength of 800 nm | 55 |
| 37 | Comparison of calculated fundamental and XPW spectrum with and without consideration of ASE for a femtosecond pulse with a center wavelength of 800 nm | 56 |
| 38 | Comparison of fundamental and XPW spectrum with and without consideration of ASE for a numerically simulated femtosecond pulse | 58 |

List of Abbreviations

| Abbreviation | Description |
|--------------|--|
| ASE | Amplified Spontaneous Emission |
| AOPDF | Acousto-Optic Programmable Dispersive Filter |
| CPA | Chirped-Pulse Amplification |
| FOD | Fourth-Order Dispersion |
| FROG | Frequency-Resolved Optical Gating |
| FWHM | Full Width at Half Maximum |
| GD | Group Delay |
| GDD | Group Delay Dispersion |
| GVD | Group Velocity Dispersion |
| GRENOUILLE | Grating-Eliminated No-nonsense Observation of Ultrafast Incident Laser Light E-fields |
| KLM | Kerr-Lens Mode Locking |
| SHG | Second Harmonic Generation |
| SI | Spectral Interferometry |
| SPIDER | Spectral Phase Interferometry for Direct Electric-field Reconstruction |
| SRSI | Self-Referenced Spectral Interferometry |
| Ti:Sa | Titanium-doped Sapphire |
| TOD | Third-Order Dispersion |
| VBW | Video Bandwidth |
| XPW | Cross-polarized Wave Generation |
| Yb:KGW | Ytterbium-doped Potassium Gadolinium Tungstate |

1 Introduction

Ultrafast laser science and the study of ultrashort pulses play a central role in various fields of current research, including nonlinear optics [1, 2, 3, 4], laser-plasma physics [5], micro-machining [6], and femtochemistry [7]. A major challenge in the field of ultrashort pulse physics is not only the generation but also the characterization of these pulses, where sophisticated techniques are required. For the measurement of ultrashort pulses a fundamental problem has to be solved, because for the determination of a given event in time a shorter event is needed to measure it. Since ultrashort pulses in the femtosecond range are the shortest events ever generated in the visible and near-infrared region, the only means to measure such pulses is through the pulses themselves. Modern electronic light detectors, limited by their resolution in the picosecond range, are not suitable for this purpose. The distinguishing features of ultrashort pulses extend beyond their femtosecond duration; they also possess the potential to reach extremely high peak powers. Unlike conventional continuous-wave beams, the energy of pulsed lasers is concentrated within individual pulses, resulting in these high peak powers.

In contrast to a continuous laser beam, whose electric field is sinusoidal in time, the electric field of an ultrashort pulse can be described by the product of an oscillating wave and a pulse envelope function. Another major difference is that a continuous laser beam can consist of a single frequency, whereas an important property of ultrashort pulses is their broad spectrum, which is due to the lower limit of the time-bandwidth product. Moreover, the frequency of the electric field can vary over time due to chromatic dispersion and nonlinearities. To fully characterize a pulse it is necessary to measure the time-dependent intensity and phase of the pulse's electric field (or, alternatively, its spectrum and spectral phase). Accurate pulse characterization is crucial for understanding interaction processes with matter in experiments involving ultrashort laser pulses. Key parameters important for pulse characterization, including pulse duration and spectral bandwidth, can be derived from the analysis of the electric field. Although determining the exact electric field of a pulse is challenging compared to measuring the spectrum or pulse duration, various methods exist for this purpose.

One of the first methods to characterize ultrashort pulses was autocorrelation, where two replicated pulses variably shifted in time are recombined in a nonlinear medium. Although this method allows for the measurement of intensity versus time, it does not provide information about the pulse's phase. One of the best-known methods for the complete determination of intensity and phase is frequency-resolved optical gating (FROG) [8], where FROG involves spectrally resolving the output of a standard autocorrelator. Other commonly used techniques include spectral phase interferometry for direct electric field reconstruction (SPIDER) [9] or self-referenced spectral interferometry (SRSI) [10].

This work focuses on the pulse characterization of two solid-state femtosecond lasers operating in the near-infrared range using SRSI. By determining the spectral phase of the pulses and implementing dispersion compensation devices, the pulse duration can be reduced. Within the SRSI pulse characterization, the dispersion terms up to order four will be determined, and the validity ranges (for group delay dispersion and third-order dispersion) will be estimated. Another major part of the work consists of the extension of the original SRSI method from Oksenhendler [10] by the consideration of an incoherent laser output component (in particular amplified spontaneous emission) and the experimental determination of this component. Proper selection of the parameters for the optical components of the SRSI setup and ensuring the correct minimal resolution of the spectrometer in accordance with the pulse properties are crucial for achieving high-quality pulse characterization.

The structure of the thesis is divided into a *Background and Theory* section (section 2) in which basics about the theory of ultrashort laser pulses, femtosecond laser systems, nonlinear optics, an overview of pulse measurement methods and the SRSI technique are presented. The *Methods* section (section 3) includes a description of the equipment used and the experimental setup, including all optical components. Furthermore, the data acquisition process and the software technologies employed in the research are explained in detail. This section ensures transparency and reproducibility by providing a thorough explanation of the experimental procedures. The *Results and Discussion* section (section 4) presents the analysis and interpretation of the experimental findings. A major part consists of a detailed description of the pulse characterization of the two laser systems using SRSI. Additionally, various methods for achieving a more precise determination of the spectral phase are discussed. Within a subchapter, the experimental results regarding the determination of the ASE component and its impact on the spectra of the fundamental and reference pulses calculated using SRSI are thoroughly examined.

2 Background and Theory

In this chapter, the main principles and effects relevant to ultrashort pulses and their characterization are discussed. In addition, a mathematical description of laser pulses is provided, and nonlinear effects fundamental to this study such as second-harmonic generation, the Kerr effect, and cross-polarized wave generation are described. The chapter also gives an overview of ultrashort pulse generation with high-power femtosecond laser systems and associated techniques such as mode locking, chirped-pulse amplification and dispersion control. Additionally, various methods for pulse characterization are outlined. In particular, the technique of self-referenced spectral interferometry, originally proposed by Oksenhendler et al. [10] is discussed. In this thesis, SRSI is extended by considering the influence of an incoherent laser output component due to amplified spontaneous emission (ASE).

2.1 Ultrashort laser pulses

For the description of ultrashort laser pulses, this chapter follows a similar approach as Rick Trebino and Erik Zeek in [8].

In contrast to a continuous beam, whose electric field is sinusoidal in time, an ultrashort laser pulse is a very short burst of electro-magnetic energy whose electric field comprises only a few cycles of an oscillating wave. An ultrashort pulse is therefore described as a product of an oscillating wave (e.g. sine wave) and a pulse envelope function (e.g. Gaussian profile).

Intensity and phase in the time domain

For simplicity, the electric field is assumed to be linearly polarized in this description and the possible position dependence of the electric field is not considered. The time-dependent electric field of a pulse can thus be written as:

$$\varepsilon(t) = \sqrt{I(t)} \cos(\omega_0 t - \phi(t)) = \frac{1}{2} \sqrt{I(t)} (e^{i(\omega_0 t - \phi(t))} + e^{-i(\omega_0 t - \phi(t))}) \quad (2.1)$$

with time t , carrier angular frequency ω_0 , temporal intensity $I(t)$, and temporal phase $\phi(t)$. In this description the rapidly varying carrier wave $e^{i\omega_0 t}$ is intentionally separated from the intensity $I(t)$ and phase $\phi(t)$ so that the characterization of the pulse by intensity and phase does not have to take into account all the oscillations of the pulse field. Moreover, the temporal intensity $I(t)$ and temporal phase $\phi(t)$ vary slowly in contrast to the carrier wave.

In literature, the 'analytic signal' approximation is frequently employed, which neglects the complex-conjugate term in the expression given by Equation 2.1. As a result, the expression for the electric field becomes complex. This complex pulse field multiplied by 2 and neglecting the carrier wave $e^{i\omega_0 t}$ is called complex amplitude and greatly simplifies mathematical calculations. The complex amplitude $E(t)$ is defined as:

$$E(t) = \sqrt{I(t)} e^{-i\phi(t)} \quad (2.2)$$

The temporal intensity $I(t)$ and temporal phase $\phi(t)$ can be derived from this expression Equation 2.2 as:

$$I(t) = |E(t)|^2$$

$$\phi(t) = -\arctan\left(\frac{\text{Im}[E(t)]}{\text{Re}[E(t)]}\right) \quad (2.3)$$

Intensity and phase in the frequency domain

For intensity $E(\omega)$ and phase $\phi(\omega)$ in the frequency domain, the real electric field $\varepsilon(t)$, given in Equation 2.1, is Fourier transformed:

$$E(\omega) = \int_{-\infty}^{\infty} \varepsilon(t) e^{-i\omega t} dt \quad (2.4)$$

Conversely, the following applies to the temporal electric field:

$$\varepsilon(t) = \frac{1}{2\pi} \int_{-\infty}^{\infty} E(\omega) e^{i\omega t} d\omega \quad (2.5)$$

The pulse field in the frequency domain $E(\omega)$ can be separated into intensity $I(\omega)$ (spectrum) and spectral phase $\phi(\omega)$:

$$E(\omega) = \sqrt{I(\omega)} e^{-i\phi(\omega)} \quad (2.6)$$

The spectrum and the spectral phase have components for positive and negative frequencies, where the two regions contain equivalent information because $\varepsilon(t)$ is real. The component for negative frequencies can therefore be ignored.

It is common that in the frequency domain the Fourier transform of the full real electric field $\varepsilon(t)$ is used for the description of the pulse (with negative frequency components removed) although in the time domain, the complex field $E(t)$ is used instead of the full real electric field $\varepsilon(t)$. Reasons for this convention are that the spectra are not centered around zero but around the actual center frequency (respectively wavelength) and that the temporal waveform expressed by $E(t)$ shows no rapidly oscillating behavior.

The spectral intensity (spectrum) and spectral phase can be derived from the expression Equation 2.6 as:

$$I(\omega) = |E(\omega)|^2$$

$$\phi(\omega) = -\arctan\left(\frac{\text{Im}[E(\omega)]}{\text{Re}[E(\omega)]}\right) \quad (2.7)$$

It should be noted that theoretical descriptions of pulses and calculations are performed in the frequency domain, while in experiments, with spectrometers, the measurements are usually wavelength-dependent. The relation between wavelength λ and frequency ω is given by $\omega = 2\pi c/\lambda$ thus the spectral phase and intensity can be rescaled.

The meaning of the spectral phase with respect to chromatic dispersion is discussed in detail in subsubsection 2.1.1.

2.1.1 High-order dispersion

Chromatic dispersion describes the dependence of the $k(\omega)$ vector or spectral phase $\phi(\omega)$ on frequency. High chromatic dispersion orders are of great relevance in the discussion of ultrashort pulses and are described in this chapter. The dispersion relation for the phase of a laser pulse passing through a medium can be written as [11]:

$$\phi(\omega) = k(\omega) \cdot z = (\omega/c) \cdot n(\omega) \cdot z = (\omega/c) \cdot P_{op}(\omega) \quad (2.8)$$

where $n(\omega)$ is the refractive index, z is the material thickness (distance through the medium) and $P_{op}(\omega)$ denotes the optical path length. This means that a pulse traveling through a medium accumulates spectral phase. The spectral phase can be expanded around the frequency $\omega = \omega_0$ into a Taylor series[11]:

$$\phi(\omega) = \phi|_{\omega_0} + \left.\frac{\partial\phi}{\partial\omega}\right|_{\omega_0} (\omega - \omega_0) + \frac{1}{2} \left.\frac{\partial^2\phi}{\partial\omega^2}\right|_{\omega_0} (\omega - \omega_0)^2 + \dots + \frac{1}{p!} \left.\frac{\partial^p\phi}{\partial\omega^p}\right|_{\omega_0} (\omega - \omega_0)^p. \quad (2.9)$$

The meanings of the lowest orders of the Taylor expansion corresponding to different phase distortions are described in the following. In addition, the influence of the different terms on the pulse shape is shown graphically in Figure 1. The plots were created using Python Matplotlib and the magnitude of the dispersion terms of the pulses correspond to a quantity relevant for this work (realistic values for femtosecond pulses).

Zero-order term

The first term $\phi|_{\omega_0}$ corresponds to the zero-order phase, also called absolute phase. The zero-order phase gives the relative phase of the carrier wave with respect to the envelope [8]. In many cases, the absolute phase is not of great relevance, since pulses are usually many carrier-wave cycles long and the phase shift of the carrier wave with respect to the envelope leads only to a slightly different pulse field [8]. Only for even shorter pulses, few-cycle or single-cycle pulses, the absolute phase plays a major role.

First-order term

The expression $\tau_g = \left.\frac{\partial\phi}{\partial\omega}\right|_{\omega_0}$ is defined as a group delay (GD). A group delay corresponds to a shift of the pulse on the time axis. This property is due to the Fourier Transform Shift Theorem [8]. Here the expression $E(t - \tau)$ Fourier transforms to $\varepsilon(\omega)\exp(-i\omega\tau)$ which corresponds to a shift in time. (In an analogous way, the expression $\varepsilon(\omega - \omega_0)$ Fourier transforms to $E(t)\exp(i\omega_0 t)$ which corresponds to a frequency shift.)

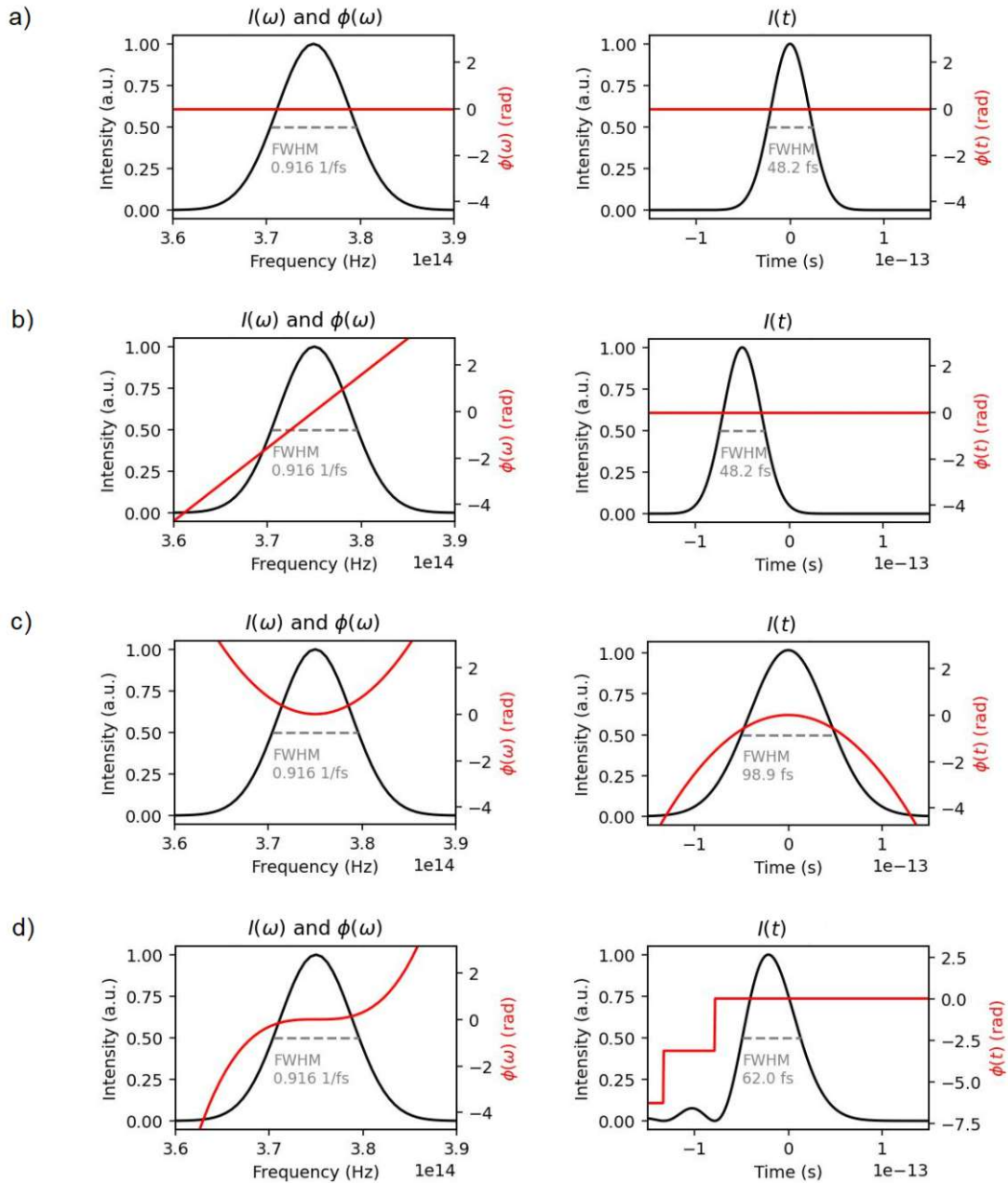


Figure 1: Intensity and phase of pulses in time and frequency domain for different spectral phases. The example pulses have a center wavelength of $3.75 \cdot 10^{14}$ Hz (800 nm) and a bandwidth (FWHM) of about $0.13 \cdot 10^{14}$ Hz (27 nm).

a) Amplitude and phase for flat spectral phase. b) A linear spectral phase ($\tau_g = 50$ fs) results in a shift in time. c) A linearly chirped pulse ($GDD = 1500$ fs²) leads to a temporal broadening of the pulse. d) Third-order dispersion ($TOD = 60000$ fs²) causes several adjacent intensity maxima in the time domain, which means oscillations of the intensity before the main pulse. Spectral phase jumps occur at times where the amplitude is zero and correspond to irrelevant discontinuities in the instantaneous frequency [8]. In the temporal description, it should be noted that the carrier wave $e^{i\omega_0 t}$ is excluded from the pulse description, leading to the removal of the linear term of the temporal phase.

Second-order term

The expression $\left. \frac{\partial^2 \phi}{\partial \omega^2} \right|_{\omega_0}$ is called group delay dispersion (GDD). Pulses with positive/negative GDD are called linearly positive/negative chirped pulses. A quadratic change in phase $\phi(t)$ results in a quadratic change in phase $\phi(\omega)$ with the opposite sign and vice versa [8]. Usually, an ultrashort pulse receives additional positive linear chirp when propagating through a dispersive material.

As shown below (Equation 2.11), the GDD term can have a non-zero value due to frequency-dependent group velocity. The frequency dependence of the group velocity means that long-wavelength components of a pulse propagate at a different velocity than short-wavelength components [4]. For a pulse with initially zero GDD, this also leads to a temporal broadening of the pulse. Due to the temporal broadening of the pulse when passing through dispersive media such as lenses, Group Velocity Dispersion (GVD) leads to distortions of the pulse to be measured.

Third-order term

The expression $\left. \frac{\partial^3 \phi}{\partial \omega^3} \right|_{\omega_0}$ corresponds to third-order dispersion (TOD) and is also called quadratic chirp [8].

Typically, a pulse with TOD is characterized by several adjacent intensity maxima in the time domain, which means oscillations of the intensity before or after the main pulse, depending on the sign of the third-order coefficient.

Higher-order terms

Complex, distorted pulses can also have high-order spectral phase components. E.g. nonlinear optical processes or propagation through long distances of fiber can lead to high-order dispersion and distort the phase [8].

Similar to the spectral phase, also the wave vector k in a medium can be expanded into a Taylor series:

$$k(\omega) = k|_{\omega_0} + \left. \frac{\partial k}{\partial \omega} \right|_{\omega_0} (\omega - \omega_0) + \frac{1}{2} \left. \frac{\partial^2 k}{\partial \omega^2} \right|_{\omega_0} (\omega - \omega_0)^2 + \dots + \frac{1}{p!} \left. \frac{\partial^p k}{\partial \omega^p} \right|_{\omega_0} (\omega - \omega_0)^p \quad (2.10)$$

The individual terms can be assigned similar meanings as the terms of the Taylor series of the spectral phase since they differ only by a factor z . Here the terms are defined as inverse group velocity $v_g^{-1} = \left. \frac{\partial k}{\partial \omega} \right|_{\omega_0}$, group velocity dispersion $GVD = \left. \frac{\partial^2 k}{\partial \omega^2} \right|_{\omega_0}$ and the p order dispersion $POD = \left. \frac{\partial^p k}{\partial \omega^p} \right|_{\omega_0}$.

Due to the relation $\phi(\omega) = k(\omega) \cdot z$ the relation $GDD = GVD \cdot z$ is valid. With the definition of group velocity $v_g = \frac{\partial \omega}{\partial k}$, the group delay dispersion can be written as:

$$GDD(\omega_0) = GVD(\omega_0) \cdot z = \left. \frac{\partial}{\partial \omega} \left(\frac{1}{v_g(\omega)} \right) \right|_{\omega_0} \cdot z \quad (2.11)$$

2.1.2 Amplified Spontaneous Emission (ASE)

Amplified Spontaneous Emission (ASE) is a phenomenon that occurs in optical laser amplifiers and laser media. It results from the fact that the gain medium is pumped with pulses that are significantly longer than the femtosecond pulses to be amplified. This means that spontaneous emission can be amplified continuously during the time the medium is population inverted. This amplified spontaneous emission reduces the population inversion and thus also reduces the energy of the amplified femtosecond pulses, which decreases the signal-to-background ratio. ASE also plays an important role in temporal intensity contrast, which is an important factor in laser-matter interaction. This means that intense pre-pulses and ASE can create a pre-plasma on the surface of a target (the material to be processed by the ultrashort pulses), thus significantly changing the properties of the target before the main pulse hits it [12].

In ASE, the emission of radiation occurs in all directions on the entire pumped spectrum of the gain medium (spectrum which is population inverted). There are strongly favored frequencies and directions, where the gain of spontaneous emission amplification is high. There is no mode structure, however (low temporal coherence) [13].

A detailed discussion on the generation of ASE in high-power CPA laser systems and calculations on the reduction of the actual gain in the presence of ASE is given in [12] and [14].

This thesis introduces an extended pulse characterization using SRSI, which incorporates an incoherent component in the analytical description, enabling the determination of the amplified spontaneous emission spectrum (refer to subsection 4.4). An alternative method for characterizing amplified spontaneous emission in femtosecond Ti:Sa lasers is described by Yong-Ho Cha et al. [15]. Their method exhibits qualitatively similar results in the retrieved ASE spectrum.

One way to get an ASE-free signal is to use cross-polarized wave (XPW) generation as this nonlinear optical effect generates a signal with the same wavelength and perpendicular polarization, see subsection 2.3.2. The measured XPW signal does not contain ASE due to the fact that XPW is a third-order nonlinear phenomenon that occurs only at high intensities, making it insignificant for small amplitudes (ASE signal is much smaller than the signal of the amplified femtosecond pulses).

2.2 High-power femtosecond laser systems

Compared to continuous-wave lasers where the output power depends on the maximum available pump power, femtosecond laser systems can achieve high peak powers by concentrating the energy in single, ultrashort optical pulses or pulse trains [16].

The generation of ultrashort pulses can be realized with a variety of lasers in the wavelength range from ultraviolet to infrared and is basically possible by two techniques: Mode locking and Q-switching. Q-switching allows sudden switching of the cavity Q-factor (quality factor) by opening and closing a shutter within the laser cavity, allowing the generation of short pulses [16]. However, most modern high-power femtosecond lasers are based on the mode locking technique, described in subsection 2.2.1. Mode locking allows large pulse repetition rates, which often means small pulse energies. To achieve higher pulse energies optical amplifier systems are used.

Dispersion control and pulse compression (see subsection 2.2.3) also play an important role in femtosecond laser systems, since only dispersion-compensated pulses achieve a minimum pulse duration.

In addition to the solid-state lasers discussed in subsection 2.2.2, there are other types of ultrafast lasers such as fiber lasers based on passively mode-locked rare-earth-doped glass fibers or mode-locked dye or diode lasers. A more detailed description of these lasers can be found in [16] or [17].

2.2.1 Mode locking

Mode locking describes the state in which many longitudinal modes of the cavity simultaneously oscillate with a fixed phase relation and the laser output is therefore a repetitive train of ultrashort optical pulses [16]. The minimum pulse duration is determined by the gain bandwidth (pulse duration is inversely proportional to gain bandwidth), so for ultrashort pulses, gain media with large bandwidth are needed. The pulse repetition rate is equal to the difference between the frequencies of two consecutive longitudinal modes and thus depends on the cavity length (longitudinal-mode separation $\Delta\nu = c/(2L)$, with the speed of light c and the resonator length L) [16].

Mode locking can be divided into active and passive mode locking. In active mode locking, the mode locker is driven by an external source and is realized by, for example, inserting an amplitude modulator or phase modulator into the laser cavity. Passive mode locking is based on a nonlinear optical effect of the mode-locker like the saturation of a saturable absorber or the Kerr effect.

An important technical implementation of passive mode locking is Kerr-lens mode locking, which is explained below following the definition by Frank Träger [16].

Kerr-lens mode locking (KLM)

KLM is based on the self-focusing property of a Kerr medium, where the optical Kerr effect (see subsection 2.3.3) is described by the intensity-dependent refractive index. The refractive index can be written as $n = n_0 + n_2 I$, where n_0 corresponds to the linear refractive index, I is the light intensity and n_2 is a positive coefficient (for a self-focusing medium). A beam with non-uniform transverse intensity distribution (like a Gaussian distribution) crossing a Kerr medium will experience a different refractive index and phase shift at the beam center than at the edge of the beam. This transversely varying phase shift corresponds to the behavior of a lens, where the focal length decreases for larger beam intensities. If the nonlinear Kerr medium is now placed in front of an aperture, then a beam with a high intensity will be more tightly focused and a larger proportion of the beam will be transmitted through the aperture. This means that the losses decrease as the pulse intensity increases, leading to mode locking.

2.2.2 Solid-state lasers

This chapter will describe the structure and operation of typical solid-state lasers, such as the Thales ALPHA kHz (Ti:Sa) and PHAROS PH2-20W (Yb:KGW) lasers used in this work. These solid-state lasers rely on Kerr-lens mode locking (KLM) and chirped-pulse amplification (CPA). Basically, the pulses generated by the Kerr lens mode-locked oscillator are stretched, amplified, and then compressed again. The combination of stretching, amplifying and compressing corresponds to the concept of the CPA technique (first applied to an optical amplifier by Donna Strickland and Gerard Mourou [18]) and reduces the damage risk related to nonlinear effects [19]. Stretching before amplification can be achieved by dispersive elements (e.g. optical glass as in the case of the Thales ALPHA kHz laser or a diffraction grating as in the case of PHAROS PH2-20W laser). Compression of the pulse after amplification is possible by inducing opposite dispersion (prism compressor or diffraction grating). The two essential components, oscillator and amplifier, are explained in the following.

Oscillator:

In principle an oscillator consists of a cavity (technical implementation e.g. with chirped mirrors) which also contains the population-inverted gain medium. The gain medium is usually pumped with continuous-wave laser modules. In the cavity, a large number of longitudinal standing waves (modes) oscillate within the bandwidth of the gain medium. To generate ultrashort pulses, a fixed phase relationship between the modes must be established (mode-locking). As mentioned above, one possibility is the Kerr lens mode-locking technique where a nonlinear Kerr medium is placed in front of an aperture in the oscillator [16].

Amplifier:

Usually, as in the case of Thales ALPHA kHz (Ti:Sa) and PHAROS PH2-20W (Yb:KGW) solid-state lasers, the amplifiers contain the same gain media as the oscillators (Ti:Sa and Yb:KGW crystal, respectively) which are pumped by continuous-wave pump modules. Usually a Pockels cell is used to inject the seed pulse from the oscillator into the amplifier and to extract the amplified pulse. Inside the resonator, it is necessary that the pulse to be amplified experiences a gain over many round-trips. This is possible either by a regenerative amplifier, where a Pockels cell is used inside the amplifier cavity and thus is traversed by the pulse in each round-trip (considerable dispersion of higher-order is accumulated in each round-trip) or by a multipass amplifier where the pulse to be amplified is guided along slightly different paths through the gain medium and thus traverses the Pockels cell only at entry [20].

Two commercially available high-power femtosecond solid-state lasers used in this work are described in subsection 3.1.

2.2.3 Dispersion control / pulse compression

In femtosecond laser systems it is important to be able to compensate for dispersion since the shortest possible pulses require pulses with a constant spectral phase. For example, pulses accumulate spectral phase during propagation in a medium, which must be compensated. In the case of CPA, the pulses are intentionally stretched (inducing dispersion) to amplify the signal, and then compressed again. In the following, two possibilities for dispersion control and pulse compression are presented: prism or grating pairs and pulse-shaping by an AOPDF. Further possibilities would be e.g. chirped mirrors, Gires-Tounois interferometers, liquid-crystal spatial light modulators or deformable-mirror pulse shapers, see [16] and [21] for detailed descriptions.

Prism / grating compressor

Since transparent media lead to positive group delay dispersion, but in experiments often pulses with minimum time duration (without chirp) are needed, it is necessary to compress the pulses with optical systems. Systems that induce negative group delay dispersion can be based on angular dispersion of prisms and gratings. The principle of building an optical system with prisms or gratings is based on the first element providing angular dispersion and the second element recollimating the spectral components. In the first element, different wavelengths will be deflected unequally, resulting in varying travel times for the different wavelength components of the pulse before being recollimated in the second element. Using two pairs of these elements, the original beam profile can be preserved, since the lateral displacement of the spectral components (spatial chirp) of the two pairs can cancel out. This is demonstrated in the case of a symmetric grating pair, as shown in Figure 2. Prism and grating pairs are used for introducing pos-

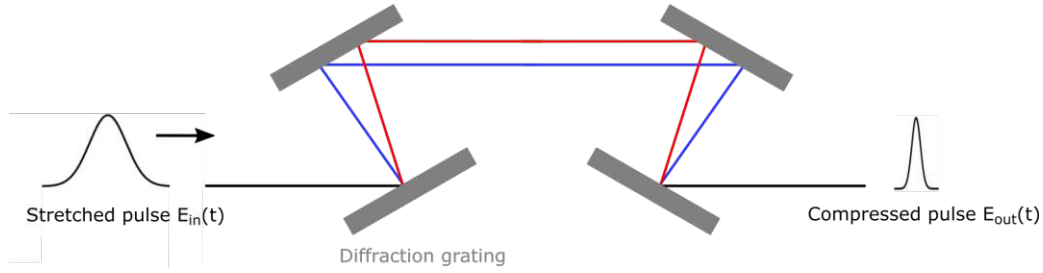


Figure 2: Schematic diagram of a grating compressor. It can be seen that different wavelengths are unequally deflected, resulting in different travel times for the different wavelength components.

itive group delay dispersion (and third-order dispersion), called a stretcher, and for introducing negative group delay dispersion (and third-order dispersion), called a compressor. For prism pairs, it should be noted that when determining the total induced GDD and TOD, not only the angular dispersion but also the contributions of the GDD and TOD induced by the glass itself should be taken into account.

The GDD and TOD introduced by the prism pairs depend on the wavelength-dependent refractive index, the mean wavelength and the distance between the prisms. For grating pairs the introduced GDD and TOD depend on the angle of reflection of the grating, the mean wavelength and the grating constant (grating spacing). A method for calculating the GDD and TOD values based on these parameters is provided in [16] and [21].

Pulse shaper / AOPDF

Pulse shaping using an acousto-optic programmable dispersive filter (AOPDF) was developed for adaptive compensation of group delay time dispersion in laser systems by Pierre Tournois [22]. The design includes a programmable acousto-optical cell where the principle is based on the acousto-optic interaction in an anisotropic birefringent medium (e.g. TeO₂ crystal). Naftaly Menn [23] defines the acousto-optic interaction as the phenomenon that acoustic waves, which correspond to periodic variations of the density of the medium, induce periodic variations of the refractive index affecting the propagation of electromagnetic waves. An acousto-optical cell (or Bragg cell) is an optically transparent material that is acoustically coupled to a transducer.

In an AOPDF, the acousto-optical longitudinal Bragg cell transfers the amplitude and phase modulation of the acoustic wave directly to an optical diffracted beam by acousto-optical diffraction. For this purpose an acoustic wave is generated by a transducer. The wave propagates with velocity v through the crystal (in the direction of the light beam z) and spatially reproduces the temporal shape of the transducer signal. It should be noted that the acoustic wave can be considered as fixed modulated grating when the laser beam impinges on the crystal since the speed of light is orders of magnitude larger than the speed of the acoustic wave v . In the case of phase-matching (momentum and energy conservation), two optical modes (two polarizations) can be efficiently coupled by acousto-optic interaction. The phase-matching conditions can be expressed as [24]:

$$\begin{aligned} \mathbf{k}_{\text{diff}}(\omega_{\text{opt,diff}}) &= \mathbf{k}_{\text{in}}(\omega_{\text{opt,in}}) + \mathbf{k}_{\text{ac}}(\omega_{\text{ac}}) \\ \omega_{\text{opt,diff}} &= \omega_{\text{opt,in}} + \omega_{\text{ac}} \end{aligned} \quad (2.12)$$

where $(\mathbf{k}_{\text{diff}}, \omega_{\text{opt,diff}})$, $(\mathbf{k}_{\text{in}}, \omega_{\text{opt,in}})$ and $(\mathbf{k}_{\text{ac}}, \omega_{\text{ac}})$ represent the wave vectors and angular frequencies of the optical diffracted beam, optical input beam and acoustic beam, respectively. The optical input beam is usually polarized parallel to the fast axis polarization of the birefringent crystal (mode 1). Locally (at a certain position on the z -axis) there is only one spatial frequency in the acoustic grating, at which only one optical frequency can be diffracted. At this position $z(\omega)$ a part of the energy is diffracted onto the slow axis polarization (mode 2). This means that each optical frequency ω propagates a certain distance in the crystal before the phase-matched spatial frequency is encountered in the acoustic grating. The pulse leaving the device in mode 2 consists of all the spectral components diffracted at the different positions z . This mode 2 pulse differs from the input pulse because the velocities of the two modes are different (slow axis, fast axis) and thus each diffracted frequency experiences a different time delay. The amplitude of each frequency component of the optical diffracted beam (mode 2) can be manipulated by the acoustic power at the position z where the frequency is diffracted. The functionality of an AOPDF is also illustrated in Figure 3.

As discussed, the optical diffracted beam is a function of the electric transducer signal, so with the right

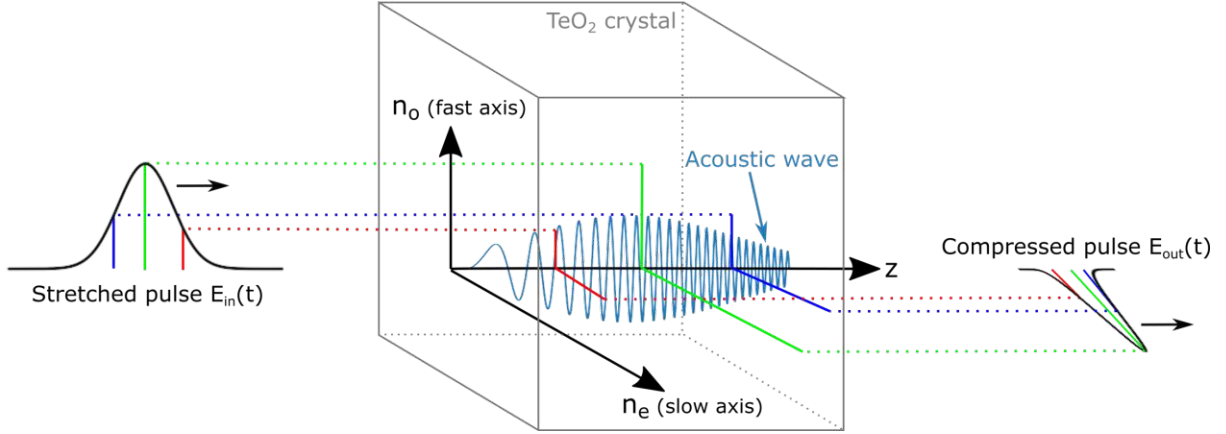


Figure 3: Simplified functionality of an AOPDF. An acoustic wave propagating in an anisotropic birefringent medium induces periodic variations of the refractive index affecting the propagation of the input pulse. The optical input beam is polarized onto the fast axis polarization of the birefringent crystal (mode 1). Locally (at a certain position on the z -axis) there is only one spatial frequency in the acoustic grating, at which only one optical frequency can be diffracted. At this position $z(\omega)$ a part of the energy is diffracted onto the slow axis polarization (mode 2). This means that each optical frequency ω propagates a certain distance in the crystal before the phase-matched spatial frequency is encountered in the acoustic grating. The output pulse consists of all the spectral components diffracted at the different positions z . The output pulse (mode 2) differs from the input pulse because the velocities of the two modes are different (slow axis, fast axis) and thus each diffracted frequency experiences a different time delay. The figure shown is an adaptation based on the illustrations found in [24] and [25].

choice of the temporal shape of this signal (and the spatial shape of the acoustic wave generated by it) an almost arbitrary group-delay distribution as a function of frequency can be generated [21]. In this study, a WB-800 Dazzler AOPDF pulse shaper was utilized within a Thales ALPHA kHz laser system, which is described in more detail in subsection 3.1.

For a more detailed description of the operation, please refer to the literature [16], [21], [22] and [24].

2.3 Nonlinear optics

Nonlinear optics describes phenomena in which a material system's response (polarization density) to an applied optical electric field has a nonlinear dependence on the strength of the optical field. For the occurrence of nonlinear optical effects, high light intensities are needed to modify the optical properties of a material system by the presence of light. In contrast to linear optics where the induced polarization depends linearly on the electric field strength, in nonlinear optics the polarization $\mathcal{P}(t)$ is expressed as a power series in the real field strength $\varepsilon(t)$ [4]:

$$\mathcal{P}(t) = \epsilon_0[\chi^{(1)}\varepsilon(t) + \chi^{(2)}\varepsilon^2(t) + \chi^{(3)}\varepsilon^3(t) + \dots] \equiv \mathcal{P}^{(1)}(t) + \mathcal{P}^{(2)}(t) + \mathcal{P}^{(3)}(t) + \dots \quad (2.13)$$

where $\chi^{(1)}$ is the linear susceptibility, $\chi^{(2)}$ is the second-order nonlinear susceptibility, and $\chi^{(3)}$ is the third-order nonlinear susceptibility. The expressions $\mathcal{P}^{(1)}(t)$, $\mathcal{P}^{(2)}(t)$, and $\mathcal{P}^{(3)}(t)$ correspond to first-, second-, and third-order nonlinear polarization, respectively. In Equation 2.13, the expressions $\mathcal{P}(t)$ and $\varepsilon(t)$ are scalar quantities.

In a more general case of nonlinear susceptibility, it is described as a tensorial complex quantity linking the complex amplitudes of the electric field and polarization. The following conventions are adapted from Boyd et al. [4] and Trebino et al. [8]. The vectorial electric field of an optical wave $\varepsilon_i(t)$ (with Cartesian components $i = 1, 2, 3$) is described as the sum of different monochromatic plane waves with the spatially slowly varying complex field amplitudes $E_i(\omega_n)$ and the carrier frequencies ω_n :

$$\varepsilon_i(t) = \frac{1}{2} \sum_n E_i(\omega_n) e^{i\omega_n t} + c.c. \quad (2.14)$$

The number n of different monochromatic plane waves with discrete frequencies ω_n depends on the optical field considered. In order to describe all second-order nonlinear optical mixing processes, the optical

field incident on the nonlinear medium can be described by two distinct frequency components [4]. For third-order nonlinear optical mixing processes, three distinct frequency components of the optical field must be taken into account. The electric field is written as the product of a carrier sine wave and the relatively slowly varying complex envelope function as in Equation 2.1 and Equation 2.2. Note that in this description the spatial dependence ($e^{-i\mathbf{k}\cdot\mathbf{r}}$) is suppressed for reasons of simplicity and must be considered for a complete description. The expression 'c.c.' denotes complex conjugate.

For the case of second-order nonlinear polarization $\mathcal{P}_i^{(2)}(t)$, the second-order susceptibility tensor $\chi_{ijk}^{(2)}(\omega_n + \omega_m, \omega_n, \omega_m)$ which relates the amplitude of the nonlinear polarization to the product of the field amplitudes gives the following relation [4]:

$$\mathcal{P}_i(\omega_n + \omega_m) = \frac{1}{4}\epsilon_0 \sum_{jk} \sum_{(nm)} \chi_{ijk}^{(2)} E_j(\omega_n) E_k(\omega_m) e^{i(\omega_n + \omega_m)t} + c.c. \quad (2.15)$$

Here the indices ijk are the Cartesian components and the notation (nm) indicates that a summation is performed over n and m where the sum $\omega_n + \omega_m$ is fixed and ω_n and ω_m can each vary. Note that in the notation used, as also employed by Boyd et al. [4], the values of ω_n and ω_m can be positive and negative, whereby the value of ω_n can have a different sign than the value of ω_m . Additionally, the notation states that the electric field envelope for a negative frequency is equivalent to its conjugate complex field envelope ($E(-\omega_n) \equiv E^*(\omega_n)$) with both the frequency and \mathbf{k} -vector being negative. As shown in Equation 2.15, the product of the two input waves with frequencies ω_n and ω_m results in a contribution to the nonlinear polarization oscillating with frequency $\omega_n + \omega_m$ (both ω_n and ω_m can assume positive or negative values independently).

For the case of third-order susceptibility, the expression for the nonlinear polarization from Equation 2.15 can be extended to [4]:

$$\begin{aligned} \mathcal{P}_i(\omega_o + \omega_n + \omega_m) \\ = \frac{1}{8}\epsilon_0 \sum_{jkl} \sum_{(mno)} \chi_{ijkl}^{(3)} E_j(\omega_o) E_k(\omega_n) E_l(\omega_m) e^{i(\omega_o + \omega_n + \omega_m)t} + c.c. \end{aligned} \quad (2.16)$$

This effect describes four-wave mixing, as three waves enter a nonlinear medium and a fourth wave is generated. Note that all the frequencies ω_o , ω_n and ω_m can assume positive or negative values independently.

It should also be noted that second-order nonlinear processes can only occur in non-centrosymmetric crystals (crystals with no inversion symmetry) [4]. Third-order nonlinear processes can occur in centrosymmetric and non-centrosymmetric media. An exact description of the nonlinear susceptibility is possible using quantum mechanics, but some qualitative properties can also be obtained using a classical model. In the classical picture, the electric field shifts the electrons in the medium, and the nonlinear polarization due to the field-dependent susceptibility can be calculated on the basis of the anharmonic oscillator model [26]. In this model, the electrons of the dielectric medium are assumed to be held in equilibrium by a potential well, where the potential well is quadratic in lowest order. Only at large field strengths, where the electron is far from equilibrium, the deviation of the potential from a quadratic form becomes noticeable.

There exist numerous nonlinear phenomena whereby for this work, the optical Kerr effect (see subsection 2.2.1) and cross-polarized wave generation (see subsection 2.3.2) are of great relevance.

2.3.1 Second harmonic generation

One of the historically most important nonlinear effects is the second-harmonic generation (SHG) which was discovered in 1961 by Franken et al. [1]. This discovery is often associated with the beginning of the field of nonlinear optics. Franken et al. guided ruby laser light into a quartz crystal and observed the generation of radiation with doubled frequency. Powers [26] describes the process as follows: The induced polarization in a material by an optical field is important to understanding SHG. If nonlinearities are included in the polarization expression, this allows that energy exchange from optical inputs at different frequencies is possible. Thus, it is possible that optical fields with one frequency ω can induce a nonlinear polarization with a component with twice the frequency. The induced polarization oscillating with twice the fundamental frequency drives a field that radiates energy of that doubled frequency (=second-harmonic generation). Since SHG is a second-order nonlinear process, a non-centrosymmetric crystal structure is required.

Second harmonic generation is a special case of sum frequency generation, where two input photons with

the same frequencies ω_1 generate a third photon with frequency $\omega_3 = 2\omega_1$. Starting from Equation 2.15, the amplitude of the nonlinear polarization can be expressed as [4]:

$$\mathcal{P}_i(\omega_1 + \omega_1) = \frac{1}{2}\epsilon_0 \sum_{jk} \chi_{ijk}^{(2)} E_j(\omega_1) E_k(\omega_1) e^{i(2\omega_1)t} + c.c. \quad (2.17)$$

In the case that the input field polarization is along the x-axis, the result simplifies to:

$$\mathcal{P}_i(\omega_1 + \omega_1) = \frac{1}{2}\epsilon_0 \chi_{ixx}^{(2)} E_x^2(\omega_1) e^{i(2\omega_1)t} + c.c. \quad (2.18)$$

For the sum frequency generation to occur efficiently, the phase-matching condition discussed in the following must be satisfied.

Phase-matching

In sum frequency generation the intensity of the generated field at frequency $\omega_3 = \omega_1 + \omega_2$ (conservation of energy) depends on the wavevector mismatch $\Delta k = k_1 + k_2 - k_3$ (conservation of momentum). The efficiency of the sum frequency generation decreases if the condition of perfect phase-matching $\Delta k = 0$ is not satisfied (for a detailed derivation see [4]). Only a wavevector mismatch of zero ($\Delta k = 0$) corresponds to the maintenance of a constant phase relationship between the interacting waves along the propagation direction and consequently to a coherent superposition. The perfect phase-matching ($\Delta k = 0$) with collinear beams can be written using the relation ($k = \frac{\omega}{c_0/n(\omega)}$) between wave vector k , refractive index n , angular frequency ω , and speed of light in vacuum c_0 as:

$$n(\omega_1)\omega_1 + n(\omega_2)\omega_2 = n(\omega_3)\omega_3 \quad (2.19)$$

For the case of second-harmonic generation ($\omega_1 = \omega_2$ and $\omega_3 = 2\omega_1$) the equation reduces to:

$$n(\omega_1) = n(2\omega_1) \quad (2.20)$$

Assuming that the incoming and outgoing beams are parallel and have the same polarization, and that the refractive index $n(\omega)$ increases with increasing frequency (normal dispersion), this equation cannot be satisfied [4]. One way to fulfill the phase-matching condition is phase-matching by angle tuning. This is based on the optical property of birefringence, the dependence of the refractive index on the polarization direction of the light. Another possibility is noncollinear phase-matching where two partial beams within the nonlinear crystal must cross at a certain angle. Further explanation and calculations of the phase-matching condition can be found in [4] and [26].

2.3.2 Cross-polarized wave generation (XPW)

Cross-polarized wave generation is a third-order nonlinear optical process by four-wave mixing. It involves the interaction between three incident waves, leading to the generation of a new wave at the same frequency but with an orthogonal polarization component [27]. When a linearly polarized input beam enters the nonlinear crystal, the output signal consists of the (depleted) initial wave and a component orthogonally polarized to it. This requires a medium with anisotropy of the third-order nonlinear susceptibility such as BaF₂ or YVO₄ [27]. In cubic crystals, a [001] orientation (z-cut crystal) or a [011] orientation (holographic cut) is commonly used, with the holographic cut showing a higher conversion efficiency in cross-polarized wave generation [28].

Minkovski et al. [27] provide a theoretical description of the efficiency of XPW generation. It is observed that in addition to the input pulse energy, the efficiency of XPW generation also depends on the thickness of the crystal, the orientation (periodic dependence of the efficiency on the crystal rotation), and the anisotropy of the $\chi^{(3)}$ tensor of the crystal. Note that these theoretical estimates predict an XPW efficiency of at most 10%.

Starting from Equation 2.16, the amplitude of the nonlinear polarization for the degenerate four-wave-mixing process can be expressed as:

$$\begin{aligned} \mathcal{P}_i(\omega_1 + \omega_1 - \omega_1) = & \frac{1}{8}\epsilon_0 \sum_{jkl} \left[\chi_{ijkl}^{(3)} E_j(\omega_1) E_k(\omega_1) E_l(-\omega_1) e^{i\omega_1 t} \right. \\ & + \chi_{ijkl}^{(3)} E_j(\omega_1) E_k(-\omega_1) E_l(\omega_1) e^{i\omega_1 t} \\ & \left. + \chi_{ijkl}^{(3)} E_j(-\omega_1) E_k(\omega_1) E_l(\omega_1) e^{i\omega_1 t} \right] + c.c. \end{aligned} \quad (2.21)$$

where the three involved field frequencies entering the nonlinear medium are ω_1 , ω_1 and $-\omega_1$ (respectively the k-vectors are k_1 , k_1 and $-k_1$). The generated wave has therefore the same frequency as the input signal. The k-vector of the generated wave corresponds to k_1 which is why this is a self-phase-matched process.

The electric field envelope of a negative frequency as in the notation of Equation 2.21 corresponds to a conjugate complex field envelope where its corresponding frequency and k-vector are both negative. Such a third-order effect, where a k-vector is subtracted, is called a *induced grating* effect because the intensity due to two beams exhibits a sinusoidal spatial dependence which then induces a sinusoidal modulation of the properties of the medium, similar to a diffraction grating [8]. Such a process can then be described as the diffraction of the third beam (with negative frequency and k-vector) off the induced grating (Bragg-grating).

In the case where two input beams are polarized in the y-direction, the *diffracted* third input beam is polarized in the x-direction and considering only the $\chi_{xxyy}^{(3)}$ component of the susceptibility tensor, the result can be simplified to:

$$\mathcal{P}_x(\omega_1 + \omega_1 - \omega_1) = \frac{1}{8} \epsilon_0 \chi_{xxyy}^{(3)} E_x(-\omega_1) E_y^2(\omega_1) e^{i\omega_1 t} + c.c. \quad (2.22)$$

Simplified, omitting the polarization direction and frequency, the nonlinear polarization of the third-order frequency-degenerate nonlinear XPW effect can thus be expressed as in [29]:

$$\mathcal{P}^{(3)}(t) \propto \chi^{(3)} |E(t)|^2 E(t) + c.c. \quad (2.23)$$

The generated field is proportional to $\mathcal{P}^{(3)}$, so the generated XPW field $E_{\text{XPW}}(t)$, depending on the fundamental input field $E_F(t)$, can be written as [29]:

$$E_{\text{XPW}}(t) \propto |E_F(t)|^2 E_F(t) \quad (2.24)$$

As previously stated, the generated XPW field $E_{\text{XPW}}(t)$ is polarized perpendicular to the fundamental input field $E_F(t)$, allowing for easy separation from the incident beam.

Temporal filtering characteristic

Cross-polarized wave generation is a third-order nonlinear optical effect that occurs only at very high intensities. This results in a temporal filtering property (for pulses with only one prominent temporal intensity peak) that shortens the generated XPW signal in time, which can also be seen in Equation 2.24. The pulse duration of a fundamental pulse E_F to generate the XPW signal has therefore a longer duration than the generated XPW pulse E_{XPW} . This also means that the spectral phase of the XPW pulse is flattened and the spectrum is broadened which is due to the time-bandwidth product. Jullien et al. [29] showed a possible pulse duration shortening up to a factor of $\sqrt{3}$.

It is observed that for large values of GDD or higher-order dispersion of the fundamental pulse, the temporal filtering property mainly flattens the phase of the XPW pulse and broadens the spectrum only slightly (example shown in Figure 4 b). For small values of GDD or higher-order dispersion where the phase is already relatively flat, the temporal filtering property mainly means a broadening of the XPW spectrum (example shown in Figure 4 a) and c).

2.3.3 Optical Kerr effect

The optical Kerr effect is described by the intensity-dependent refractive index [26]:

$$n = n_0 + n_2 I = n_0 + \frac{n_2}{2} |E|^2 \quad (2.25)$$

where n_0 corresponds to the linear (weak-field) refractive index, I is the light intensity, E is the electric field and n_2 is a positive coefficient (for a self-focusing medium). The nonlinear index n_2 depends on the linear refractive index and the third-order nonlinear susceptibility $\chi^{(3)}$ (derivation in Powers [26]). The Kerr effect is also known as the quadratic electro-optic effect since the refractive index is proportional to the square of the electric field of the incident light itself. This means that in this electro-optic effect, the field of the incident light itself is responsible for the change in the refractive index and no external field is required for this effect to occur. The Kerr effect is the basis for the Kerr-lens mode locking method, which is an important method for generating ultrashort pulses, see subsection 2.2.1. In addition, the nonlinear optical effects of self-focusing and self-phase modulation are due to the Kerr effect.

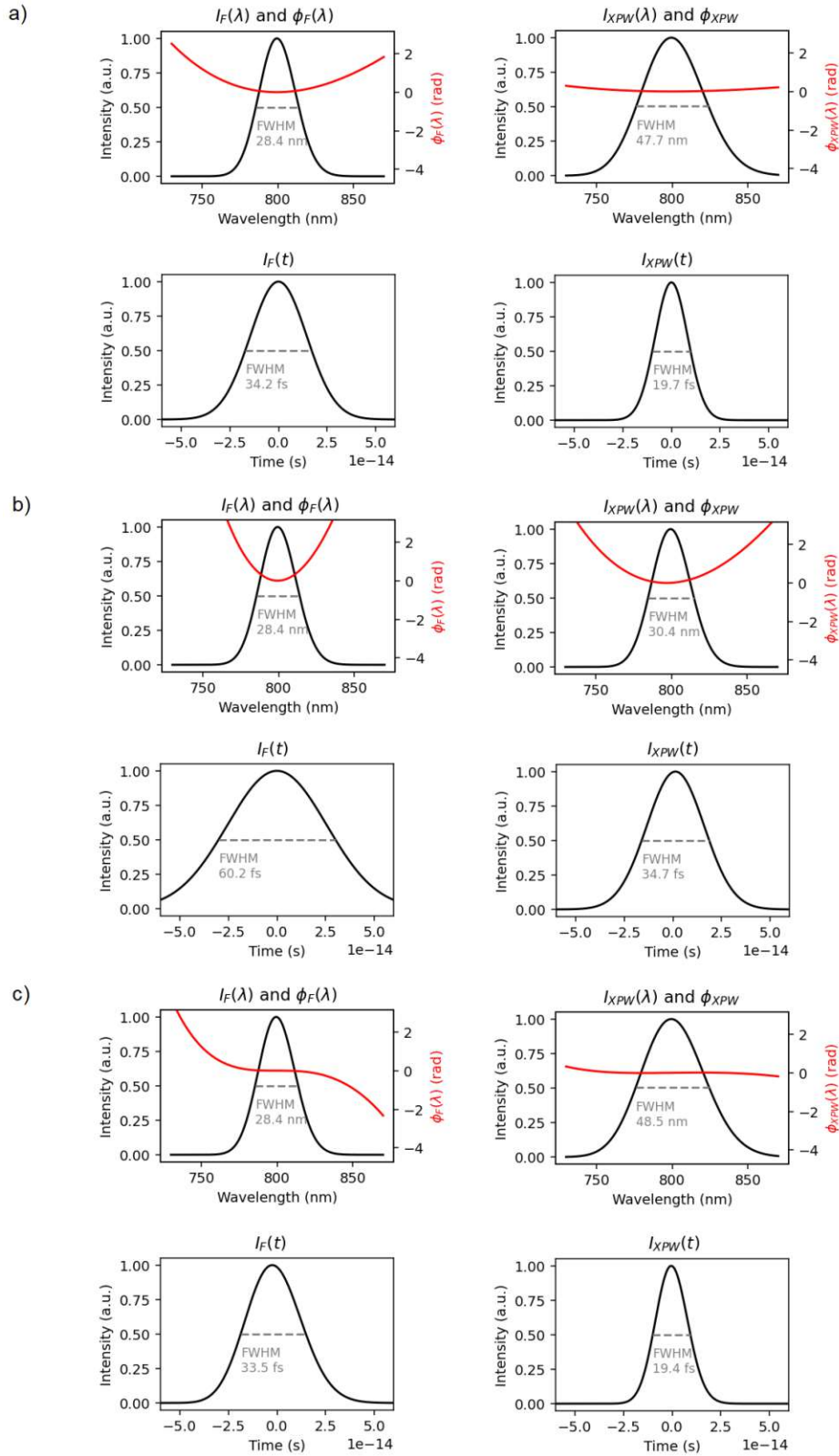


Figure 4: The spectra (FWHM = 28.8 nm, center wavelength = 800 nm) and spectral phases for fundamental pulses with different spectral phases and the corresponding generated XPW pulses are shown. The generated XPW pulses can be calculated by utilizing the relation specified in Equation 2.24. A spectral broadening and flattening of the phase of the generated XPW pulse can be seen due to the temporal filtering property of XPW. a) Slightly chirped fundamental pulse (GDD = 100 fs²). Mainly a broadening of the XPW spectrum can be observed. b) Chirped fundamental pulse (GDD = 600 fs²). Mainly a flattening of the spectral phase of the XPW pulse can be observed. c) Fundamental pulse with third-order dispersion (TOD = 3000 fs³) and the corresponding XPW pulse.

2.4 Pulse-measurement methods

As mentioned in the introduction, the full characterization of a pulse requires measuring the time-dependent intensity and phase of its electric field (or its spectrum and spectral phase). This cannot be achieved using electronic light detectors alone, as they have limited time resolution. Instead, pulse characterization techniques rely on nonlinear optical effects. There are various methods available for pulse characterization, and this section highlights some of the most commonly used ones such as autocorrelation, frequency-resolved optical gating and spectral interferometry. In this work, the characterization of two femtosecond lasers is achieved through the use of self-referenced spectral interferometry (SRSI). Consequently, a comprehensive discussion of this method is provided, including the treatment of an additional incoherent component in the laser output signal.

2.4.1 Autocorrelation

One of the earliest ultrashort-pulse measurement techniques is autocorrelation, where the intensity of the pulse versus time can be measured. The input pulse is divided into two pulses, which are recombined in a non-linear medium (e.g. SHG crystal). One of the partial pulses is delayed variably in time (delay τ) before the recombination. When using an SHG crystal, the intensity of the generated field is proportional to the product of the intensities of the two partial pulses $I_{\text{SHG}}(t, \tau) \propto I(t)I(t - \tau)$ [8]. Detectors are too slow to resolve the time dependence of the signal $I_{\text{SHG}}(t, \tau)$, which is why the measurement records the time integral (autocorrelation) [8]:

$$A(\tau) = \int_{-\infty}^{\infty} I(t)I(t - \tau)dt \quad (2.26)$$

The autocorrelation contains information about the pulse length since no second harmonic generation will occur if the pulses don't overlap in time. With this method, the phase cannot be determined, and the phase-matching-bandwidth condition requires a thin SHG crystal, resulting in a weak SHG signal and poor measurement sensitivity [30].

2.4.2 Frequency-resolved optical gating (FROG)

FROG is an advanced technique that measures the intensity and phase of a pulse invented by R. Trebino et al. [8, 31, 32]. In a FROG system, the femtosecond pulses are divided into two replicas each. One of the replicas is time-delayed compared to the other and then spatially overlapped in a nonlinear medium to produce higher harmonics. The spectrum of these higher harmonics is measured, together with the locally resolved time delay between the superimposed beams [33].

The special feature of the FROG method is that the ultrashort pulse measurements are not performed purely in the time domain (autocorrelation) or the frequency domain (spectrum) but in a hybrid domain, the time-frequency domain [8]. So the measurements are simultaneously resolved in the time and frequency domain. This means that FROG analyzes the spectrum of a standard autocorrelation output. So instead of measuring the signal energy versus the delay as in an autocorrelator, FROG measures the signal spectrum versus the delay [8]. A phase-retrieval algorithm allows for determining the temporal pulse intensity and phase from this signal.

In a FROG setup, depending on the design, up to five or more degrees of freedom are involved, which makes the alignment of the setup difficult [30].

There are several variants of FROG based on different nonlinear optical processes. The most common geometry is the second-harmonic generation FROG. There also exist third-harmonic generation FROG geometries. Third-order FROG geometries include the Polarization Gating, Self-Diffraction, and Transient Grating FROG techniques. For a detailed description of all subgroups see Trebino et al. [8].

2.4.3 GRENOUILLE

GRENOUILLE (grating-eliminated no-nonsense observation of ultrafast incident laser light e-fields) is one of several techniques for measuring femtosecond pulses and determining the full electric field described by pulse intensity and phase. Pulse measurements with high accuracy and real-time capability (single-shot measurements) are possible with this technique [33]. GRENOUILLE is a specialized, simple setup of the frequency-resolved optical gating (FROG) method. As with FROG, a phase-retrieval algorithm allows for determining the pulse intensity and phase versus time from the measured signal.

A conventional FROG setup corresponds to a frequency-resolved autocorrelator, where the autocorrelator

is a complex, expensive and alignment-sensitive setup. GRENOUILLE simplifies the setup by replacing the beam splitter, the delay line and the beam combining optics with a Fresnel biprism. In addition, a thick nonlinear crystal is used to obtain a stronger signal and to spectrally resolve the autocorrelation signal due to the small phase-matching bandwidth [34].

2.4.4 Spectral phase interferometry for direct electric-field reconstruction (SPIDER)

SPIDER is a self-referencing interferometric method to perform full intensity and phase measurements of ultrashort pulses first proposed by C. Iaconis and I. Walmsley [9]. In their original proposal [9], the principle is as follows. Two replicas of the pulse to be characterized are separated by a certain time delay. This pulse pair is superimposed with a stretched pulse in a nonlinear medium, which generates the sum frequency. The stretched pulse is derived from the input pulse and undergoes significant temporal broadening when passed through a highly dispersive optical element, such as a block of glass or a pair of diffraction gratings. Due to this high chirp, each frequency component of the pulse appears at a different time. The two temporally separated pulse replicas of the pulse to be characterized are thus mixed with a different temporal (and also spectral) component of the stretched pulse. Because the stretched pulse is highly chirped, this corresponds to a mixing of a replica pulse with a quasi-monochromatic frequency. This sum-frequency mixing in the nonlinear medium results in two pulse replicas which are frequency shifted and spectrally sheared. The sum-frequency signal is analyzed by a spectrometer. The generated spectral interferogram of the frequency-converted and spectrally sheared pulse pair is recorded, whereby the intensity $I_{IN}(\omega)$ can be written as [9]:

$$\begin{aligned} I_{IN}(\omega) &= |E(\omega) + E(\omega - \Omega)e^{-i\omega\tau}|^2 \\ &= \left| |E(\omega)|e^{-i\phi(\omega)} + |E(\omega - \Omega)|e^{-i\phi(\omega - \Omega)}e^{-i\omega\tau} \right|^2 \\ &= |E(\omega)|^2 + |E(\omega - \Omega)|^2 + 2|E(\omega)E(\omega - \Omega)| \cos(\phi(\omega) - \phi(\omega - \Omega) - \omega\tau) \end{aligned} \quad (2.27)$$

$E(\omega)$ is the first unknown upconverted field, $E(\omega - \Omega)$ is the second unknown upconverted field (shifted by spectral shear Ω), τ is the time delay, and $\phi(\omega)$ is the spectral phase. In contrast to FROG, the phase-retrieval algorithm to determine the phase from the interferogram is noniterative and requires only two one-dimensional Fourier transforms [9]. The third term provides the spectral phase as the phase difference between spectral components separated by the shear Ω , modified by the term $\omega\tau$, which arises due to the delay τ between the two upconverted fields $E(\omega)$ and $E(\omega - \Omega)$ [9].

2.4.5 Spectral interferometry (SI)

Spectral interferometry (SI) or interferometry in the frequency domain was first introduced in the 1970s by C. Froehly et al. [35]. The operation is based on the interference between an unknown signal $E(t)$ and a reference signal with known electric field $E_{ref}(t)$. The two time-delayed signals with delay τ are collinearly fed into a spectrometer, where the measured spectrum can be described as follows [8]:

$$\begin{aligned} I_{IN}(\omega) &= |E_{ref}(\omega) + E(\omega)e^{-i\omega\tau}|^2 \\ &= \left| |E_{ref}(\omega)|e^{-i\phi_{ref}(\omega)} + |E(\omega)|e^{-i\phi(\omega)}e^{-i\omega\tau} \right|^2 \\ &= |E_{ref}(\omega)|^2 + |E(\omega)|^2 + 2|E_{ref}(\omega)E(\omega)| \cos(\phi_{ref}(\omega) - \phi(\omega) - \omega\tau) \end{aligned} \quad (2.28)$$

$E_{ref}(\omega)$ and $E(\omega)$ are the electric fields of the reference and unknown signals, $\phi_{ref}(\omega)$ is the spectral phase of the reference signal, $\phi(\omega)$ is the spectral phase of the unknown signal, τ is the time delay, and ω is the angular frequency. The measured SI interferogram thus consists of the two individual spectra of the reference and the unknown signal and an interference term which depends on the phase difference $\phi_{ref}(\omega) - \phi(\omega)$ and the delay τ . The crucial point in SI is that the electric field or intensity and phase of the reference pulse must be known and must not correspond to the unknown pulse itself, otherwise the spectral phase cancels out in the interference term. Also, the spectrum of the reference pulse must be broader than that of the unknown pulse to allow a correct characterization.

The assumption of an ideal reference pulse, represented by a Dirac- δ -pulse $\delta(t)$, implies a pulse with an infinitely broad spectrum of constant intensity and a constant phase. Consequently, the bandwidth of the amplitude of the cos-modulated interference term ($2|E_{ref}(\omega)E(\omega)| \cos(\phi_{ref}(\omega) - \phi(\omega) - \omega\tau)$) would correspond to the spectral bandwidth of the pulse to be determined, while the argument of the interference term (taking into account the modulation $\omega\tau$) would correspond to the spectral phase.

One way to generate a reference pulse with a known spectral phase and a broader spectrum than the unknown pulse for pulse characterization using SI is the self-referenced spectral interferometry technique described below.

2.4.6 Self-referenced spectral interferometry (SRSI)

SRSI is a femtosecond pulse characterization technique to determine the spectral amplitude and phase originally developed by Oksenhendler et al. [10]. SRSI is based on spectral interferometry, where the reference pulse is self-created from the pulse to be characterized. The self-created reference pulse results from pulse shaping optimization and non-linear temporal filtering. The pulse shaping optimization is achieved by an acousto-optic programmable dispersive filter. The non-linear temporal filtering is achieved by a frequency-conserving non-linear optical effect (e.g. cross-polarized wave generation).

By generating a reference pulse with a known spectral phase and wider bandwidth than the pulse to be measured, it is possible to perform the measurements by spectral interferometry. This method is linear, analytical, accurate and therefore simplifies the measurement setup and algorithm in contrast to other techniques like FROG or SPIDER [10].

In this work, this technique is used to characterize the pulses of two femtosecond laser systems, which is why a detailed discussion of the SRSI design and algorithm is given below in subsection 2.5.

2.5 Theory of SRSI

This chapter describes the method proposed by Oksenhendler et al. for pulse characterization using self-referenced spectral interferometry (SRSI) [10], which provides a description of the full electric field of an ultrashort pulse. In addition to explaining the setup, functionality, and characterization procedure, the chapter also covers an extension of the SRSI technique that incorporates an incoherent laser output component.

SRSI represents an extended version of spectral interferometry (SI), where SI operates on the principle of using two collinear pulses, a known reference pulse and an unknown, fundamental pulse to be characterized. These pulses are temporally delayed and interfere with each other. In the case of SRSI, this reference pulse is self-created. To determine the phase and amplitude of the fundamental pulse, it is essential to have knowledge of the amplitude and phase of the reference pulse. In order to measure the phase and amplitude of the fundamental pulse accurately, it is necessary for the reference pulse to possess a broader spectrum compared to the input fundamental pulse. Without this condition, the phase of certain frequencies cannot be measured [10]. Furthermore, to ensure accurate pulse characterization using SRSI, it is crucial for the reference pulse to have a flat spectral phase. The generation of the self-created reference pulse in SRSI involves two main steps: pulse shaping for reference pulse optimization (using an acousto-optic programmable dispersive filter, prism or grating compressor) and the utilization of the frequency-conserving non-linear optical effect known as cross-polarized wave generation. The pulse shaping (phase flattening) is performed within the laser system itself, prior to the SRSI setup, thus affecting both the fundamental pulse being determined and the reference pulse. As the spectral phase of the fundamental pulse is altered in this process, it becomes necessary to deduce the phase of the original fundamental pulse before the pulse shaping process. The spectral phase introduced to achieve an output with a flat phase yields the initial spectral phase to be measured [10]. In many cases, including this thesis, a flat phase of the fundamental pulse is desired to obtain the shortest possible pulse duration, eliminating the need for determining the initial spectral phase of the pulse.

In the experimental setup, the beam follows a specific sequence of optical elements. These elements include: first polarizer, calcite plate (retardation plate), first focusing lens, XPW crystal, recollimating lens, second polarizer, second focusing lens and spectrometer. A schematic representation of the experimental setup with its optical elements as well as the changing amplitudes and polarizations of the pulses after passing through the respective elements is shown in Figure 5. The input pulse is approximately vertically polarized using the first polarizer, whereas the laser output beam itself is already approximately vertically polarized. Using the calcite plate and its birefringent property, a replica pulse is generated. The optical axis of the retardation plate is parallel to the crystal's front surface and therefore perpendicular to the direction of incidence of the input beam but slightly rotated with respect to the polarization direction of the input beam. The dependence of the refractive index on the polarization leads to a time delay and the splitting of the input pulse into two partial pulses with polarization perpendicular to each other. The delay between these pulses corresponds to the time τ . By rotating the calcite plate and thus

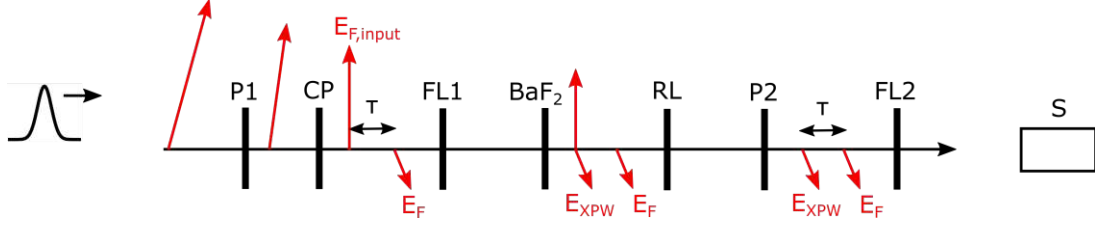


Figure 5: Schematic representation of the optical elements in SRSI setup and the changing amplitudes and polarizations of the pulses after passing through the respective elements. The interference between the fundamental pulse E_F and the XPW pulse E_{XPW} with time delay τ is then measured by a spectrometer. P1: first polarizer; CP: calcite plate; FL1: first focusing lens; BaF₂: XPW crystal; RL: recollimating lens; P2: second polarizer; FL2: second focusing lens; S: spectrometer;

changing the orientation of the optical axis, the ratio of the intensities between the beams polarized parallel and perpendicular with respect to the optical axis can be changed. The optical axis is rotated only a few degrees with respect to the polarization direction of the input beam. Thus, the vertically polarized partial pulse has a higher intensity than the horizontally polarized pulse. The stronger, vertically polarized pulse exiting the calcite plate $E_{F,input}$ serves as input pulse for the XPW generation. The weaker, horizontally polarized wave exiting the calcite plate corresponds to the unknown fundamental pulse E_F to be characterized, which is shifted by the time τ compared to the pulse $E_{F,input}$. Since the optical axis corresponds to the slow axis, the pulse E_F precedes the pulse $E_{F,input}$. The first focusing lens is used to focus the beam into the BaF₂ crystal, ensuring a sufficient intensity for XPW generation. Since the input pulse $E_{F,input}$ is stronger than the pulse E_F , it is possible to obtain a horizontally polarized XPW signal E_{XPW} generated in the XPW crystal which has an intensity similar to the fundamental pulse E_F . Due to the similar intensity of the reference pulse and the fundamental pulse, it is possible to generate a well measurable interference signal. This implies that after the XPW crystal, there are two horizontally polarized components: a pulse E_F to be determined, and a time-delayed reference pulse E_{XPW} . The reference pulse has a broader spectrum and a flatter phase due to the temporal filtering property of XPW generation. After the BaF₂ crystal, the diverging beam is collimated with a recollimating lens and all vertically polarized pulses are blocked by a second polarizer. The beam is then focused into a spectrometer using a second focusing lens, where the interferogram $I_{IN}(\omega)$ of the two pulses E_F and E_{XPW} is recorded.

As in spectral interferometry, the measured signal $I_{IN}(\omega)$ can be expressed as [10]:

$$\begin{aligned}
 I_{IN}(\omega) &= |E_{XPW}(\omega) + E_F(\omega)e^{-i\omega\tau}|^2 \\
 &= \left| |E_{XPW}(\omega)|e^{-i\phi_{XPW}(\omega)} + |E_F(\omega)|e^{-i\phi_F(\omega)}e^{-i\omega\tau} \right|^2 \\
 &= S_0(\omega) + 2|f(\omega)|\cos(\phi_{XPW}(\omega) - \phi_F(\omega) - \omega\tau) \\
 &= S_0(\omega) + f(\omega)e^{i\omega\tau} + f^*(\omega)e^{-i\omega\tau}
 \end{aligned} \tag{2.29}$$

with the interference term between the unknown and the reference pulses:

$$f(\omega) = E_{XPW}(\omega)E_F^*(\omega) = |E_{XPW}(\omega)|e^{-i\phi_{XPW}(\omega)} \cdot |E_F(\omega)|e^{i\phi_F(\omega)} \tag{2.30}$$

and the sum of the spectral intensities of the pulses:

$$S_0(\omega) = |E_{XPW}(\omega)|^2 + |E_F(\omega)|^2 \tag{2.31}$$

Note that the term $e^{i\omega\tau}$ corresponds to the interference of the signal seen in the interferogram $I_{IN}(\omega)$, where successive peaks are separated by the distance $\Delta\omega = 2\pi/\tau$.

In the following the algorithm is presented how the amplitude and phase of the fundamental pulse can be determined from the measured interferogram.

2.5.1 Pulse characterization procedure / SRSI algorithm

For the estimation of the spectral phase and amplitude of the unknown, fundamental pulse based on the measured interference signal $I_{IN}(\omega)$, a similar procedure is followed as in [10] and [36]. The steps necessary to achieve this are discussed in this chapter.

Processing of the measured signal

Usually the measured interferogram $I_{IN}(\lambda)$ is recorded by the spectrometer in the wavelength domain (data points with intensity and wavelength information). By the relation $f = c/\lambda$, with the frequency f , speed of light c and wavelength λ , the interferogram can be represented also in the frequency domain $I_{IN}(\omega)$. A typical interferogram of a femtosecond pulse is illustrated in Figure 6. To perform a Fourier

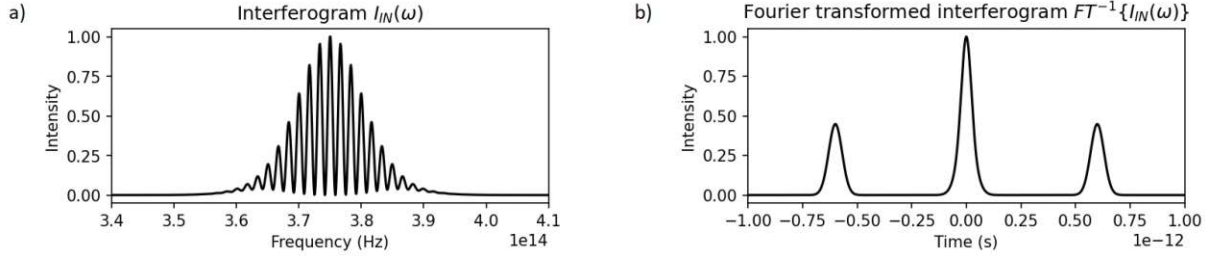


Figure 6: Typical interferogram and its Fourier transform for a femtosecond pulse, whereby the fundamental pulse has a center wavelength of 800 nm. The intensities of the fundamental and the XPW pulse were assumed to be equal. a) Intensity $I_{IN}(\omega)$ of the interferogram. b) The temporal signal $I_{IN}(t)$ corresponds to the Fourier transformed signal of $I_{IN}(\omega)$ consisting of the sum term $S_0(t)$ (peak centered around $t = 0$) and the interference terms $f(t \pm \tau)$ (peaks centered around $t = \pm \tau$).

transform of this spectrum using the fast Fourier transform algorithm, the intensities must be equidistantly distributed. Since this is not the case, the data points are linearly interpolated. Thus, it is possible to display the intensities of the interferogram in the frequency domain with an equidistant step size. The step size must be smaller than the smallest distance between two data points of the raw data.

The step size (pixel spacing) can be described in terms of a frequency interval Δf , or a wavelength interval $\Delta \lambda$. In this context, Δf can be expressed as a function of $\Delta \lambda$:

$$\Delta f = \left. \frac{df}{d\lambda} \right|_{\lambda_i} \cdot \Delta \lambda = -\frac{c}{\lambda_i^2} \cdot \Delta \lambda \quad (2.32)$$

where c is the speed of light and λ_i is the wavelength under consideration.

Analogously, the following relation is valid for the wavelength interval $\Delta \lambda$:

$$\Delta \lambda = \left. \frac{d\lambda}{df} \right|_{f_i} \cdot \Delta f = -\frac{c}{f_i^2} \cdot \Delta f \quad (2.33)$$

where f_i is the frequency under consideration. Note the relation $\omega = 2\pi f$ when performing calculations involving angular frequency.

Extracting the sum term and the interference term

The signal $I_{IN}(\omega)$ is composed of a sum term $S_0(\omega)$ and an interference term $f(\omega)$ (see Equation 2.29). In the following, it is discussed how the terms $S_0(\omega)$ and $f(\omega)$ can be extracted from the measured signal. The measured signal $I_{IN}(\omega)$ is transformed from the frequency domain to the time domain by an inverse Fourier transform, as illustrated in Figure 6, and can be expressed as:

$$\mathcal{FT}^{-1}\{I_{IN}(\omega)\}(t) = S_0(t) + f(t - \tau) + f^*(t + \tau) \quad (2.34)$$

The first term $S_0(t)$ corresponds to the sum of the field autocorrelation functions of each pulse and is therefore centered around $t = 0$ [10]. The terms $f(t - \tau)$ and $f^*(t + \tau)$ are the cross-correlation functions shifted by τ [10]. They are centered at $t = \tau$ and $t = -\tau$. The functions $f(t - \tau)$ and $f^*(t + \tau)$ are symmetrically mirrored about $t = 0$ and contain the same information, so in the following only $f(t - \tau)$ is considered. The peaks $S_0(t)$ and $f(t - \tau)$ are separated by the time delay τ , which corresponds to the delay of the replicate pulse through the calcite plate. The delay τ is proportional to the thickness of the calcite plate. It is important that the delay τ is large enough to separate the peaks properly. If the peaks do not overlap, it is possible to extract $S_0(t)$ and $f(t - \tau)$ (or $f^*(t + \tau)$) from the temporal signal using a window function. For the choice of the window function, for example, a fourth-order super-Gaussian function with a width of half the gap between $S_0(t)$ and $f(t - \tau)$ (corresponding to half the time delay between reference pulse and fundamental pulse $\tau/2$) is suitable, see [36]. The super-Gaussian window of order four is defined as $\exp[-((t - \tau)/(2\sigma^2))^4]$ with the window width σ , time t and time shift τ .

By Fourier transform of the separated signals $S_0(t)$ and $f(t - \tau)$ the signals $S_0(\omega)$ and $f(\omega)e^{i\omega\tau}$ can be obtained. When performing the transformation of $f(t - \tau)$ in practice, the signal is centered around $t = 0$.

Calculating amplitudes of fundamental and reference pulse

With the equations Equation 2.30 and Equation 2.31 it is possible to find expressions for the absolute values of the amplitude for the reference pulse $|E_{\text{XPW}}(\omega)|$ and the fundamental pulse $|E_{\text{F}}(\omega)|$ [10]. Assuming that the XPW spectral components are more intense than input pulse ones at each frequency the analytical expressions are given by:

$$|E_{\text{XPW}}(\omega)| = \frac{1}{2} \left(\sqrt{S_0(\omega) + 2|f(\omega)|} + \sqrt{S_0(\omega) - 2|f(\omega)|} \right) \quad (2.35)$$

$$|E_{\text{F}}(\omega)| = \frac{1}{2} \left(\sqrt{S_0(\omega) + 2|f(\omega)|} - \sqrt{S_0(\omega) - 2|f(\omega)|} \right) \quad (2.36)$$

If the input pulse spectral components at each frequency are more intense than those of the XPW signal, the analytical expressions for the amplitudes of the reference pulse $|E_{\text{XPW}}(\omega)|$ and the fundamental pulse $|E_{\text{F}}(\omega)|$ are:

$$|E_{\text{XPW}}(\omega)| = \frac{1}{2} \left(\sqrt{S_0(\omega) + 2|f(\omega)|} - \sqrt{S_0(\omega) - 2|f(\omega)|} \right) \quad (2.37)$$

$$|E_{\text{F}}(\omega)| = \frac{1}{2} \left(\sqrt{S_0(\omega) + 2|f(\omega)|} + \sqrt{S_0(\omega) - 2|f(\omega)|} \right) \quad (2.38)$$

The obtained amplitudes are only accurate if the measured interferogram is well-resolved and the interference term $f(\omega)$ can be precisely determined. Therefore, the spectrometer must have a sufficient resolution.

Alternativeley, the XPW spectrum and the fundamental spectrum can be measured separately (each signal is measured independently without interference from the other signal, achieved by modifying the experimental setup accordingly, see subsection 3.4). Because the magnitudes of the separately measured intensities of the XPW spectrum $I_{\text{XPW}}^M(\omega)$ and the fundamental spectrum $I_{\text{F}}^M(\omega)$ do not match the magnitude of the intensities of the two signals during the SRSI measurement, they must be scaled. This is possible by fitting the sum of the two intensities multiplied by a scaling factor to the sum term $S_0(\omega)$ (Equation 2.31) obtained from the interferogram:

$$S_0(\omega) = I_{\text{XPW}}(\omega) + I_{\text{F}}(\omega) = c_{\text{XPW}} \cdot I_{\text{XPW}}^M(\omega) + c_{\text{F}} \cdot I_{\text{F}}^M(\omega) \quad (2.39)$$

The superscript M , refers to the fact that it is a directly measured spectrum. The coefficients c_{XPW} and c_{F} are determined using a least-squares routine (by a *Python SciPy* routine). For this the following integral is minimized:

$$\int |S_0(\omega) - c_{\text{XPW}} \cdot I_{\text{XPW}}^M(\omega) - c_{\text{F}} \cdot I_{\text{F}}^M(\omega)| d\omega \quad (2.40)$$

Or in the discrete case the following sum is minimized:

$$\sum_{i=0}^N |(S_0)_i - c_{\text{XPW}} \cdot (I_{\text{XPW}}^M)_i - c_{\text{F}} \cdot (I_{\text{F}}^M)_i| \quad (2.41)$$

The absolute values of the amplitude for the reference pulse $|E_{\text{XPW}}(\omega)|$ and the fundamental pulse $|E_{\text{F}}(\omega)|$ can thus be written as:

$$|E_{\text{XPW}}(\omega)| = \sqrt{c_{\text{XPW}} \cdot I_{\text{XPW}}^M(\omega)} \quad (2.42)$$

$$|E_{\text{F}}(\omega)| = \sqrt{c_{\text{F}} \cdot I_{\text{F}}^M(\omega)} \quad (2.43)$$

Calculating the spectral phase

With the interference term $f(\omega) = E_{\text{XPW}}(\omega)E_{\text{F}}^*(\omega)$ (see Equation 2.30) the following relation can be established:

$$\arg[f(\omega)] = \phi_{\text{F}}(\omega) - \phi_{\text{XPW}}(\omega) \quad (2.44)$$

with the spectral phases of the reference pulse $\phi_{\text{XPW}}(\omega)$ and the fundamental pulse $\phi_{\text{F}}(\omega)$. If the spectral phase of the generated reference pulse is assumed to be nearly flat this corresponds to a constant phase $\phi_{\text{XPW}}(\omega) = \text{constant}$. This means that in this approximation the argument of the spectral interference term $\arg[f(\omega)]$ is set equal to the spectral phase of the fundamental pulse $\phi_{\text{F}}(\omega)$ (neglecting the constant phase term), which simplifies the equation Equation 2.44 to:

$$\phi_{\text{F}}(\omega) \approx \arg[f(\omega)] \quad (2.45)$$

Thus, using Equation 2.36 and Equation 2.45, the fundamental pulse can be fully characterized to a first approximation, since both amplitude $|E_{\text{F}}(\omega)|$ and phase $\phi_{\text{F}}(\omega)$ have been determined. This approximation is accurate in case of a completely flat phase of the reference pulse. Since the phase of the reference pulse is flatter than that of the fundamental pulse due to XPW generation, but not completely flat, the phase determined by $\arg[f(\omega)]$ is only an initial estimate.

Consideration of a non-constant spectral phase of the reference pulse:

Until now, a flat phase of the reference pulse has been assumed for determining the phase of the unknown, fundamental pulse. This is only a good approximation for the characterization of pulses with small dispersion. In general, the reference pulse has a non-constant phase, which can be taken into account as in the following iterative algorithm for determining the phase of the fundamental pulse (also illustrated in Figure 7).

The fundamental pulse $E_{\text{F}}(\omega)$ is described by the amplitude $|E_{\text{F}}(\omega)|$ (see Equation 2.36) and the spectral phase $\phi_{\text{F}}(\omega)$ which is estimated in the first iteration step with $\phi_{\text{F}}(\omega) = \arg[f(\omega)]$ (as in equation Equation 2.45). Using an iterative algorithm considering the phase of the reference pulse, the phase $\phi_{\text{F}}(\omega)$ will be determined more accurately.

For this purpose, the reference pulse is approximated by the expression $E_{\text{XPW}}(t) \propto |E_{\text{F}}(t)|^2 E_{\text{F}}(t)$ (Equation 2.24), whereby the expression $E_{\text{F}}(t)$ is calculated by Fourier transform of $E_{\text{F}}(\omega)$. By inverse Fourier transform of $E_{\text{XPW}}(t)$, the spectral phase of the reference pulse can be obtained $\phi_{\text{XPW}}(\omega) = \arg[(\mathcal{FT}^{-1}\{E_{\text{XPW}}(t)\})]$. The obtained phase $\phi_{\text{XPW}}(\omega)$ can thus be used to calculate a new estimate for $\phi_{\text{F}}(\omega)$ using equation Equation 2.44. The phase $\phi_{\text{F}}(\omega)$ is used in the next iteration step to compute a new estimate of $E_{\text{F}}(\omega)$. This new estimate of $E_{\text{F}}(\omega)$ in turn provides a more accurate estimate of the phase of the reference pulse. This iterative process is continued until convergence. The iteration steps until convergence depend, among other things, on the strength of the dispersion of the input pulse and are approximately in the range of 10^0 to 10^2 .

In the iterative calculation of $E_{\text{XPW}}(t)$, linear spectral phase may accumulate [37]. A linear spectral phase corresponds to a shift of the pulse in the time domain. Therefore, this problem is easily fixed by centering the pulse $E_{\text{XPW}}(t)$ around $t = 0$ after each calculation.

It is important to note that the spectral phase is meaningless for an intensity of the pulse equal to zero. This means that the calculation of the spectral phase is meaningful only in a wavelength range where the intensity has a value larger than zero. The calculation of the phase in the following is always performed only for a range in which the intensity is larger than 5% of the peak intensity.

Phase flattening

To achieve the highest accuracy when determining the amplitude and phase of the fundamental pulse it is essential to have a reference pulse with an almost flat spectral phase across the entire spectrum. The criterion for a good approximation of the spectral phase for the fundamental pulse by $\phi_{\text{F}} \approx \arg[f(\omega)]$ is that the spectral phase of the reference pulse is completely flat. This can be achieved by e.g. an AOPDF pulse shaper, prism or grating compressor.

Due to the temporal sharpening of the XPW effect, the chirp can be minimized by maximizing the bandwidth of the generated XPW signal while manipulating the second-order dispersion of the fundamental input pulse by a dispersion compensation device (e.g. grating compressor or AOPDF). Thus, an initial compression of the reference pulse can be achieved because the reference pulse (and also the fundamental pulse) is now approximately chirp-free. Another possibility is to determine the spectral phase and dispersion terms of the fundamental pulse using the SRSI algorithm and compensate for the dispersion based on these findings.

If a flat phase of the fundamental pulse is determined by the SRSI algorithm, this corresponds with high accuracy to the actual phase, since the reference pulse has an even flatter phase due to the property of temporal filtering of the XPW effect.

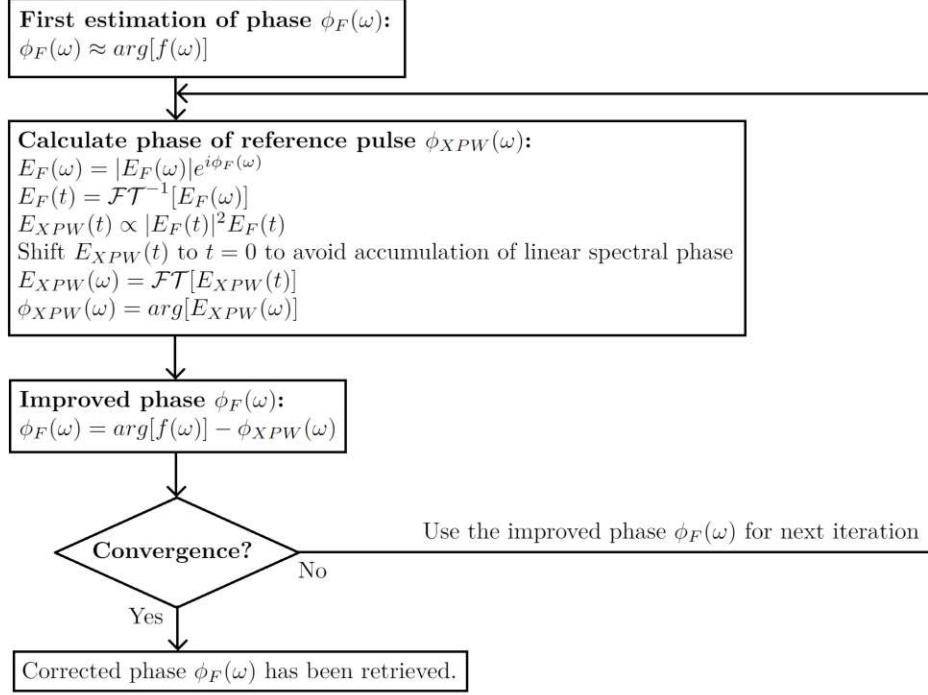


Figure 7: Iterative algorithm for determining the phase of the fundamental pulse $\phi_F(\omega)$. In general, the reference pulse has a non-constant phase $\phi_{XPW}(\omega)$, which can be taken into account as described in this flowchart to obtain a better estimate for the phase of the fundamental pulse.

Since dispersion compensation is performed by the AOPDF or grating compressor within the laser system, it is crucial to consider the phase changes introduced by these dispersion compensation devices to accurately determine the original pulse's phase (phase before dispersion compensation).

Temporal amplitude and phase

By inverse Fourier transform, the electric field of the pulse in the time domain can be calculated from the amplitude and phase in the frequency domain. From the obtained temporal amplitude an estimation of the pulse duration can be made (FWHM of the intensity). Due to the carrier frequency (average frequency of the pulse ω_0) the temporal phase has a large linear part, which is why in the literature the carrier wave $e^{i\omega_0 t}$ is often excluded from the description of the pulse.

2.5.2 SRSI with consideration of an incoherent component

So far, the analytical description of SRSI, as originally proposed by Oksenhendler et al. [10], has been presented without considering an incoherent part of the laser output signal. The influence of an incoherent component, specifically the ASE signal, which is particularly important for ultrashort pulse lasers, is discussed in this section. It is important when considering ASE that Equation 2.29 has to be extended. Considering the incoherent component $I_{ASE}(\omega)$, the following relation [38] now holds:

$$I_{IN}(\omega) = |E_{ASE}(\omega)|^2 + |E_{XPW}(\omega) + E_F(\omega)e^{-i\omega\tau}|^2 = S_0(\omega) + f(\omega)e^{i\omega\tau} + f^*(\omega)e^{-i\omega\tau} \quad (2.46)$$

with the unchanged interference term between the unknown and the reference pulses:

$$f(\omega) = E_{XPW}(\omega)E_F^*(\omega) \quad (2.47)$$

and the sum of the spectral intensities of the pulses including the intensity of the ASE signal:

$$S_0(\omega) = |E_{ASE}(\omega)|^2 + |E_{XPW}(\omega)|^2 + |E_F(\omega)|^2 \quad (2.48)$$

When considering an incoherent component, Equation 2.35 to Equation 2.38 are no longer valid, so $I_F(\omega)$ and $I_{XPW}(\omega)$ cannot be calculated exactly with these formulas. Therefore, the XPW spectrum and the output spectrum corresponding to the fundamental spectrum, including an incoherent component, are

measured separately (each signal is measured independently without interference from the other signal, achieved by modifying the experimental setup accordingly, see subsection 3.4). Because the magnitudes of the separately measured intensities of the XPW spectrum ($I_{XPW}^M(\omega)$) and the laser output spectrum ($I_{FA}^M(\omega) = I_F(\omega) + I_{ASE}(\omega)$) do not match the magnitude of the intensities of the two signals during the SRSI measurement, they must be scaled. This is possible by fitting the sum of the two intensities multiplied by a scaling factor to the sum term $S_0(\omega)$ (Equation 2.48) obtained from the interferogram [38]:

$$S_0(\omega) = I_{ASE}(\omega) + I_{XPW}(\omega) + I_F(\omega) = c_{XPW} \cdot I_{XPW}^M(\omega) + c_{FA} \cdot I_{FA}^M(\omega) \quad (2.49)$$

The superscript M , refers to the fact that it is a directly measured spectrum. The coefficients c_{XPW} and c_{FA} are determined using a least-squares routine (by a *Python SciPy* routine). For this the following integral is minimized:

$$\int |S_0(\omega) - c_{XPW} \cdot I_{XPW}^M(\omega) - c_{FA} \cdot I_{FA}^M(\omega)| d\omega \quad (2.50)$$

Or in the discrete case the following sum is minimized:

$$\sum_{i=0}^N |(S_0)_i - c_{XPW} \cdot (I_{XPW}^M)_i - c_{FA} \cdot (I_{FA}^M)_i| \quad (2.51)$$

Using Equation 2.47, the intensity $I_F(\omega)$ can be expressed as:

$$I_F(\omega) = \frac{|f(\omega)|^2}{I_{XPW}(\omega)} = \frac{|f(\omega)|^2}{c_{XPW} \cdot I_{XPW}^M(\omega)} \quad (2.52)$$

Since the intensity of the laser output $I_{FA}(\omega)$ is composed of the coherent part $I_F(\omega)$ and the incoherent part $I_{ASE}(\omega)$, the intensity $I_{ASE}(\omega)$ can be expressed as follows:

$$I_{ASE}(\omega) = I_{FA}(\omega) - I_F(\omega) = c_{FA} \cdot I_{FA}^M(\omega) - \frac{|f(\omega)|^2}{c_{XPW} \cdot I_{XPW}^M(\omega)} \quad (2.53)$$

Thereby the intensity $I_F(\omega)$ is calculated as in Equation 2.52.

An alternative calculation of the intensity $I_{ASE}(\omega)$ can be derived from Equation 2.48. After transforming the equation and using Equation 2.52, $I_{ASE}(\omega)$ can be expressed as:

$$I_{ASE}(\omega) = S_0(\omega) - I_F(\omega) - I_{XPW}(\omega) = S_0(\omega) - \frac{|f(\omega)|^2}{c_{XPW} \cdot I_{XPW}^M(\omega)} - c_{XPW} \cdot I_{XPW}^M(\omega) \quad (2.54)$$

The expressions for calculating the ASE intensity have also been obtained in this form by Iliev et al. [38].

If the incoherent ASE component is taken into account, the analytical formulas for calculating the coherent component of the laser output signal (Equation 2.35) and the XPW signal (Equation 2.36) as in [10] are no longer valid. This is due to the fact that the sum term $S_0(\omega)$ has to be extended by the incoherent part $I_{ASE}(\omega)$. If the calculation is carried out, solutions for the coherent part of the laser output signal and the XPW signal can be found using Equation 2.47 and Equation 2.48. These contain the term for the ASE signal which must be known or determined as described before.

Assuming that the XPW spectral components are more intense than input pulse ones at each frequency and considering ASE, the analytical expressions for the amplitudes $|E_{XPW}(\omega)|$ and $|E_F(\omega)|$ are given by:

$$|E_{XPW}(\omega)| = \frac{1}{2} \left(\sqrt{S_0(\omega) - I_{ASE}(\omega) + 2|f(\omega)|} + \sqrt{S_0(\omega) - I_{ASE}(\omega) - 2|f(\omega)|} \right) \quad (2.55)$$

$$|E_F(\omega)| = \frac{1}{2} \left(\sqrt{S_0(\omega) - I_{ASE}(\omega) + 2|f(\omega)|} - \sqrt{S_0(\omega) - I_{ASE}(\omega) - 2|f(\omega)|} \right) \quad (2.56)$$

If the input pulse spectral components at each frequency are more intense than those of the XPW signal, the analytical expressions for the amplitudes $|E_{XPW}(\omega)|$ and $|E_F(\omega)|$ are:

$$|E_{XPW}(\omega)| = \frac{1}{2} \left(\sqrt{S_0(\omega) - I_{ASE}(\omega) + 2|f(\omega)|} - \sqrt{S_0(\omega) - I_{ASE}(\omega) - 2|f(\omega)|} \right) \quad (2.57)$$

$$|E_F(\omega)| = \frac{1}{2} \left(\sqrt{S_0(\omega) - I_{ASE}(\omega) + 2|f(\omega)|} + \sqrt{S_0(\omega) - I_{ASE}(\omega) - 2|f(\omega)|} \right) \quad (2.58)$$

This allows a comparison of the results for the calculated intensities of the laser output signal and the XPW signal with and without consideration of an incoherent component.

3 Method

The following sections outline the experimental and theoretical approaches and methods employed in this work. A detailed description of the equipment specifications, including laser systems, spectrometers, and optical components utilized in the experimental setup will be provided. Furthermore, an estimation for the required calcite plate thickness is performed. The procedure for data acquisition and the description of the spectra measurement will be outlined, along with an explanation of the software used for data processing and evaluation.

3.1 Equipment

The equipment used in the experiments includes, in addition to the actual SRSI setup, two femtosecond solid-state laser sources and two types of spectrometers. An overview of these lasers and spectrometers, along with their respective specifications, is provided below.

Ti:Sa laser - Thales ALPHA kHz

The Thales ALPHA kHz laser is a custom-build high-repetition-rate (5 kHz) Ti:Sa laser system for generating ultrashort pulses. The basics of such a solid-state laser based on Kerr-lens mode locking and chirped pulse amplification is described in subsection 2.2.2. The average power measured in the laboratory for the amplified signal is 2.3 W, which corresponds to 0.46 mJ energy per pulse at a repetition rate of 5 kHz. The bandwidth (FWHM) of the generated amplified pulse is in the range of more than 30 nm with an average wavelength of about 800 nm. This allows pulse durations of down to 30 fs, enabling applications in high-order harmonic generation, time-resolved spectroscopy, laser engraving and many others. Other features of the ALPHA kHz laser series are the fully diode-pumped design and a beam diameter of 15 mm. The dimension of the system is $1.5 \times 6 \text{ m}^2$. A grating compressor is used for dispersion control and pulse compression which allows to manipulate and compensate second- and third-order dispersion. The diffraction grating is mounted on a motorized translation stage where the compressor length (and thus GDD / TOD) can be adjusted by software. An additional pulse shaper (AOPDF Fastlite Dazzler), positioned after the oscillator between the stretcher and the amplifier module, allows the manipulation of dispersion. By measuring the spectral phase and feedback into the pulse shaper, the dispersion can be almost completely compensated and pulses with a duration in the range of 30 fs can be achieved. An overview of the properties of the ALPHA kHz laser series can be found in the manual [39].

Yb:KGW laser - Light Conversion PHAROS PH2-20W

The PHAROS PH2-20W laser is a high-repetition-rate (up to 1 MHz) Yb:KGW laser system for generating ultrashort pulses. Yb:KGW (potassium gadolinium tungstate) is a rare-earth-doped (ytterbium-doped) laser gain medium commonly used for solid-state femtosecond lasers. Also this solid-state laser uses Kerr-lens mode locking and chirped pulse amplification as described in subsection 2.2.2. The average output power is up to 20 W and the average wavelength is 1025 nm. According to the manufacturer, a pulse bandwidth (FWHM) of 8.2 nm and a pulse duration of down to 223 fs is possible. Some features of the PHAROS laser are the compact ($0.73 \times 0.42 \text{ m}^2$), thermally-stabilized and sealed design, the built-in pulse picker to adjust the repetition rate by software and the robust optomechanical design, which ensures a stable operation in varying environments. An adjustable grating compressor is used for dispersion control and pulse compression which allows to manipulate and compensate second- and third-order dispersion. The diffraction grating is mounted on a motorized translation stage where the compressor length (and thus GDD / TOD) can be adjusted by software. An overview of the PHAROS laser series and its operation can be found in the manual [40].

Ocean Optics HR4000CG-UV-NIR spectrometer

The HR4000CG-UV-NIR is a miniature dispersive spectrometer for high-resolution measurements of spectra. A diffraction grating is used to separate the light into its component wavelengths and using a mirror and lens system, the dispersed light is directed to a CCD detector which records the spectrum. A wavelength range from 200 to 1100 nm at an optical resolution (FWHM) of 0.75 nm is supported (the wavelength difference between adjacent CCD pixels is about 0.25 nm). The integration time for the recording of the spectrum can be continuously selected between 4 ms and 20 s. The python-seabreeze library provides an interface to the Ocean Optics HR4000 spectrometer. This allows real-time recording of the spectrum for direct pulse characterization. The HR4000CG-UV-NIR manual [41] provides detailed information about the device's functionality and its potential applications.

Anritsu MS9740B spectrometer

The Anritsu optical spectrum analyzer is a dispersive spectrometer that allows high-resolution, wide dynamic range spectra to be recorded. A diffraction grating is used to disperse the signal into different wavelengths, which are then measured by the photodetector. This means that the intensities of the different wavelengths are recorded in sequence. A wavelength range from 600 to 1750 nm at a minimum resolution of 0.03 nm is supported. The video bandwidth (VBW) is the bandwidth of the photodetector used to measure the individual wavelengths and can be set between 1 MHz and 200 Hz. The VBW affects the speed and accuracy of the spectrum analysis, with a higher VBW resulting in a faster display of the spectrum because the detection filter is faster. A narrower VBW, on the other hand, helps to suppress noise as the signal is averaged over a longer time. The sweep time (time needed to measure and display the spectrum) depends not only on the VBW but also on the point averaging and the measured wavelength range. The Anritsu manual [42] provides detailed information about the device's functionality and its potential applications.

Since the intensities of the wavelength intervals are recorded sequentially, a fluctuation of the intensity of the entire input signal means fluctuations in the measured spectrum. These fluctuations can be reduced by point averaging (per measured wavelength) or sweep averaging (multiple sweeps).

WB-800 Dazzler pulse shaper

The Fastlite WB-800 Wide Band Dazzler is an ultrafast pulse shaper based on the principle of an acousto-optic programmable dispersive filter (AOPDF). The operation of an AOPDF is described in subsection 2.2.3. The pulse shaping system enables a precise programming of spectral phase and amplitude for ultrafast laser pulses. The wavelength tuning range is from 680 to 920 nm with a spectral resolution of 0.6 nm (at 800 nm). Dazzler systems can be installed inside a CPA system and allow to compensate high-order phase distortions, thereby enabling the generation of ultrashort pulses. In this study, a Dazzler is integrated into a Thales ALPHA kHz laser system, positioned after the laser oscillator between the stretcher and the amplifier module. Dispersion compensation up to the fourth-order through an input mask in the software is possible. By employing an input file for the Dazzler that includes the spectral phase relative to wavelength, an 'arbitrary' spectral phase of the output pulse can be predefined (the phase must fall within specific value ranges and avoid jumps, refer to [24]). Consequently, compensation for even higher-order dispersion terms becomes attainable. Detailed information regarding the operational principles and applications for the Dazzler pulse shaper can be found in the manual [24].

3.2 Experimental setup and optical components

The experimental SRSI setup with all optical components is shown in Figure 8. The individual components and their functionality are described in the following.

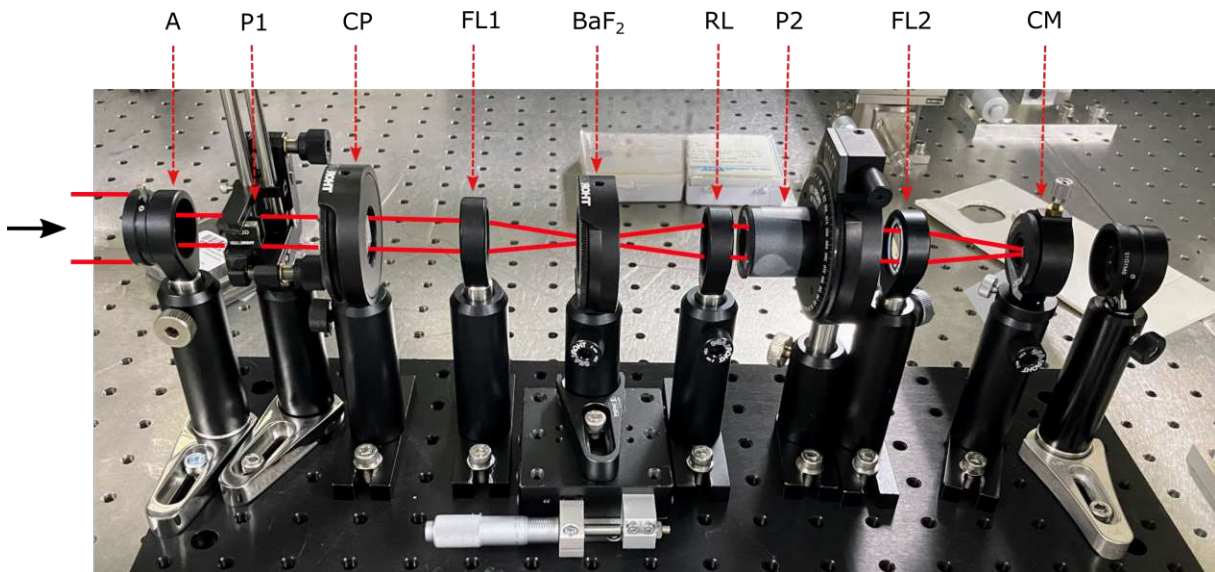


Figure 8: Experimental SRSI setup with schematic beam path.

A: aperture; P1: first polarizer; CP: calcite plate; FL1: first focusing lens; BaF₂: XPW crystal; RL: recollimating lens; P2: second polarizer; FL2: second focusing lens; CM: cable mount;

Aperture: The round adjustable aperture selects the inner part of the beam profile. This is necessary because the input beam (15 mm diameter) is wider than the first polarizer ($5 \times 5 \text{ mm}^2$).

First polarizer: The first polarizer with fixed polarization direction and a size of $5 \times 5 \times 5 \text{ mm}^3$ polarizes the input beam vertically. This polarizer is a broadband polarizing beamsplitter cube, which is composed of two prisms positioned at right angles. One of these prisms includes a dielectric coating that enables the cube to split light into s-polarized and p-polarized components. The s-polarized component is reflected by 90° , while the p-polarized component is transmitted. It is important to note that the glass prisms used in the polarizing beamsplitter cube are made of high-dispersion flint, which also induces dispersion.

Calcite plate: Using the calcite plate and its birefringent property, a replica pulse is generated as described in subsection 2.5. The stronger, vertically polarized pulse exiting the calcite plate will serve as input pulse for the XPW generation. The weaker, horizontally polarized pulse corresponds to the unknown, fundamental pulse to be characterized. The orientation of the calcite plate is chosen so that the vertically polarized partial pulse has a higher intensity than the horizontally polarized pulse. A 3 mm thick calcite plate is used for the characterization of the ALPHA kHz laser pulses with an average wavelength of 800 nm. For the characterization of the PHAROS laser pulses with wavelength 1025 nm, a 10 mm thick plate is used. For the estimation of the thicknesses see subsection 3.3.

Focusing lens: The first focusing lens with a focal length 50 mm focuses the two partial pulses with perpendicular polarization into the XPW crystal. It should also be noted that the crystal should not be placed directly in the focal point of the first focusing lens, since the high intensity may exceed the destruction threshold of the crystal. On the other hand, placing the crystal too far away from the focal point will result in a weak XPW generation.

The coated lens is made of N-BK7 and has a center thickness of 5.3 mm. It should be noted that the lens also introduces dispersion.

XPW crystal / BaF₂ crystal: The vertically polarized partial pulse has a higher intensity than the horizontally polarized pulse. Thus, it is possible to obtain a horizontally polarized XPW signal generated in the XPW crystal which has an intensity similar to the unknown, fundamental pulse. The thickness of the BaF₂ crystal is 1 mm. The XPW crystal is rotatably mounted to allow the crystal orientation to be adjusted to maximize XPW efficiency. In addition, the entire mount of the XPW crystal is mounted on a linear translation stage to allow the crystal to be variably moved around the focal point of the first focusing lens. A holographic ([011]) crystallographic orientation is used.

Recollimating lens: The recollimating lens with a focal length of 50 mm collimates the diverging partial beams and guides them into the second polarizer.

Second polarizer: The second polarizer of size $5 \times 5 \times 5 \text{ mm}^3$ is rotatably mounted to align the polarization direction so that the vertically polarized pulses are blocked and only the XPW signal and the replica of the fundamental signal generated in the calcite crystal are transmitted. The polarizer is a polarizing beamsplitter cube, like the first polarizer.

Second focusing lens: The second focusing lens with focal length 50 mm focuses the interfering partial beams into a fiber optic cable which can be connected to the spectrometer.

Cable mount: The cable mount is used to fix the fiber optic cable that is connected to the spectrometer. Two adjusting screws allow the cable to be moved in the plane perpendicular to the direction of incidence of the pulses in order to optimally guide the focused beam into the cable.

3.3 Choice of calcite plate thickness

In this section, a suitable thickness of the calcite plate and the required resolution of the spectrometers for pulse characterization of the different laser systems are determined. It should be noted that the pulses of the ALPHA kHz laser and the PHAROS laser differ in their average wavelength, bandwidth and pulse duration.

One of the crucial steps in pulse characterization using SRSI is the separation of the sum term $S_0(t)$ and the interference term $f(t + \tau)$ in the time domain by a super-Gaussian window function after the inverse Fourier transform of the measured interferogram $I_{IN}(\omega)$. For this procedure, the temporal retardation τ must be much larger than the pulse duration of the pulse to be determined. The temporal retardation is determined by the thickness of the calcite plate. At the same time, the distance between two peaks in the interferogram $I_{IN}(\omega)$ is inversely proportional to the temporal retardation, so that if the retardation is too large, the interferogram can no longer be resolved by the spectrometer.

In general, two peaks in the interferogram have a spacing of $\Delta\omega = 2\pi/\tau$. This can be seen in Equation 2.29 by the term $e^{i\omega\tau}$.

The distance $\Delta\omega$ between two peaks in the frequency domain can be rewritten for the wavelength domain as described in Equation 2.33. The distance in the frequency domain between two peaks $\Delta\omega$ is constant for different frequencies ω_i considered. In contrast, $\Delta\lambda$ depends on the frequency/wavelength. Thus, the signal can be better resolved by the spectrometer (assuming that the spectrometer has about the same resolution on the whole wavelength range) when the pulse has a larger average wavelength. Example: If we assume a fixed time delay of $\tau = 2$ ps we obtain the same values for the distance $\Delta\omega$ between two peaks in the interferogram independent of the frequency ω_i . In contrast, the distance $\Delta\lambda$ between two peaks in the interferogram is about 1.06 nm at a wavelength of 800 nm ($\omega_i = 2.36 \cdot 10^{15}$ rad/s) and about 1.75 nm at a wavelength of 1025 nm ($\omega_i = 1.84 \cdot 10^{15}$ rad/s).

Thickness of the calcite plate for ALPHA kHz laser

The retardation with a calcite plate of thickness $\Delta s = 3$ mm corresponds approximately to a temporal retardation of $\tau = 1.67$ ps at a mean wavelength of 800 nm ($\tau = \frac{\Delta s}{c/n_o} - \frac{\Delta s}{c/n_e}$, with speed of light c , ordinary refractive index $n_o(800 \text{ nm}) = 1.6488$ [43], and extraordinary refractive index $n_e(800 \text{ nm}) = 1.4819$ [43]). In this estimate of retardation, higher dispersion terms such as GDD induced by the calcite were neglected, and the pulse shape and pulse duration before and after the calcite plate were assumed to be the same.

The calculated temporal retardation of 1.67 ps is much larger than the expected pulse duration in the order of 30 fs. This also means that the sum term $S_0(t)$ and the interference term $f(t)$ can be well separated. When performing the SRSI pulse characterization in subsection 4.1, this separation of the two terms can be seen in Figure 13.

The distance $\Delta\lambda$ between two peaks in the spectrum around 800 nm ($\omega_i = 2.36 \cdot 10^{15}$ rad/s) is 1.3 nm (calculated by Equation 2.33 using $\Delta\omega = 2\pi/\tau$).

The used pixel spacing of the Anritsu spectrometer is 0.05 nm, resulting in an actual resolution of 0.059 nm (internally calculated by the spectrometer and displayed on its monitor; for more information, refer to the handbook [42]). As a consequence, the interferogram can be well resolved with this setup as shown in Figure 9 a). On the other hand, the Ocean Optics HR4000 spectrometer has a resolution of 0.75 nm, which indicates that the fine structures of the interferogram are not adequately resolved with this spectrometer as shown in Figure 9 b).

It is important to highlight that the resolution of the recorded interferograms significantly influences the pulse characterization process using SRSI. Very low resolution can hinder the clear separation and distinction of two adjacent peaks within the interferogram. Even if the maxima and minima can be clearly separated, insufficient resolution also leads to a weakened contrast of the interference pattern, i.e. a smaller amplitude of the interference signal, which subsequently affects the evaluation of the interferogram. Therefore, a high resolution is crucial for accurate and effective pulse characterization using SRSI. The measured interferograms of the same signal for the two spectrometers can be seen for comparison in Figure 9. The resulting effect on the determined spectral phases will be discussed in subsection 4.1.

The experiment was also carried out with a 1 mm thick calcite plate. This gives a temporal retardation of about $\tau = 560$ fs (one third of the temporal retardation of the 3 mm calcite plate). Compared to a pulse with a duration of around 30 fs, this time delay is still large. However, it is possible that the clear separation of the sum term $S_0(t)$ and the interference term $f(t \pm \tau)$ cannot be achieved (see Figure 10), as there may be some overlap between the two signals which may result in reduced accuracy of pulse characterization using SRSI.

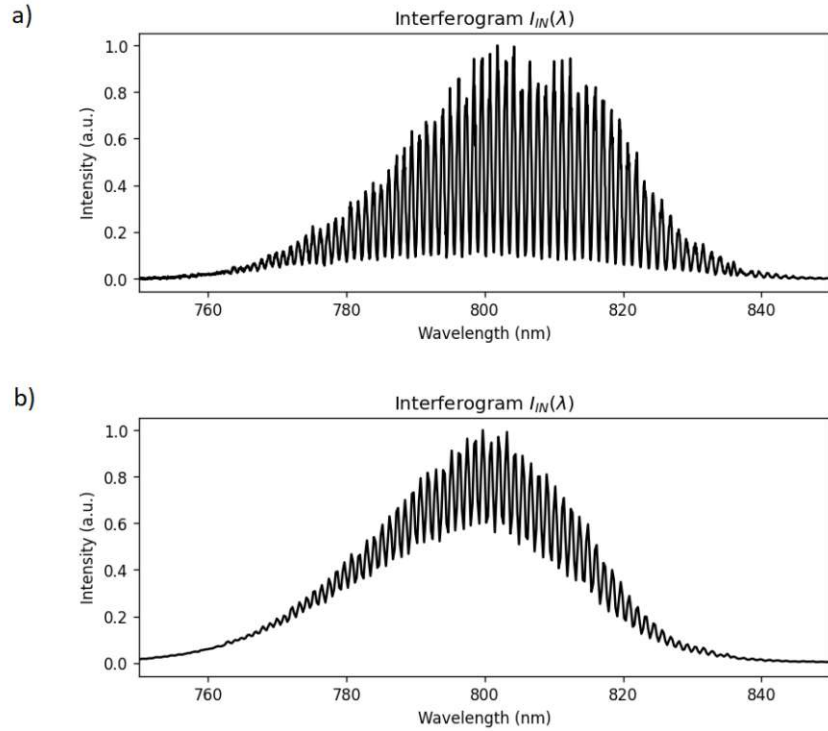


Figure 9: Intensity $I_{IN}(\lambda)$ of a typical interferogram of an SRSI measurement for a calcite plate with a thickness of 3 mm and a dispersion-compensated femtosecond pulse with a center wavelength of 800 nm measured by different spectrometers. a) Interferogram recorded by Anritsu MS9740B spectrometer with an optical resolution about 0.059 nm. b) Interferogram recorded by Ocean Optics HR4000 spectrometer with an optical resolution about 0.75 nm. Insufficient resolution leads to a weakened contrast of the interference pattern.

Thickness of the calcite plate for PHAROS laser

The retardation with a calcite plate of thickness $\Delta s = 10$ mm corresponds approximately to a temporal retardation of $\tau = 5.44$ ps at a mean wavelength of 1025 nm ($\tau = \frac{\Delta s}{c/n_o} - \frac{\Delta s}{c/n_e}$, with speed of light c , ordinary refractive index $n_o(1025 \text{ nm}) = 1.6432$ [43], and extraordinary refractive index $n_e(1025 \text{ nm}) = 1.4799$ [43]). The temporal retardation is thus much larger than the approximate pulse duration of about 300 fs. This implies that the sum term $S_0(t)$ and the interference term $f(t)$ can be effectively separated, as demonstrated in subsection 4.2, Figure 26.

As described earlier, the spectrum can be better resolved for a higher average wavelength. However, the thick calcite plate results in closely spaced peaks in the interferogram, requiring a spectrometer with high resolution. The distance $\Delta\lambda$ between two peaks in the spectrum around 1025 nm is 0.64 nm (calculated by Equation 2.33 using $\Delta\omega = 2\pi/\tau$). The used pixel spacing of the Anritsu spectrometer is 0.05 nm, resulting in an actual resolution of 0.059 nm. As a consequence, the interferogram can be well resolved with this setup. The Ocean Optics HR4000 spectrometer has a resolution of 0.75 nm, which means that the interferogram cannot be resolved adequately with this spectrometer.

The experiment was also carried out with a 3 mm thick calcite plate. This gives a temporal retardation of about $\tau = 1670$ fs. For a pulse with an approximate duration of 300 fs, this temporal retardation is too small to clearly separate the sum term $S_0(t)$ and the interference term $f(t \pm \tau)$ with a super-Gaussian window function, since the two signals overlap, see Figure 11.

3.4 Data acquisition / procedure for measuring spectra

As previously mentioned, it is important for the fundamental signal to have a similar intensity to the XPW signal generated in the non-linear crystal. This yields the highest contrast of the fringes resulting from the interference of both pulses, thereby achieving a high signal-to-noise ratio in the spectrum obtained. For the pulse characterization, three spectra are measured: the XPW spectrum $I_{XPW}(\omega)$, the

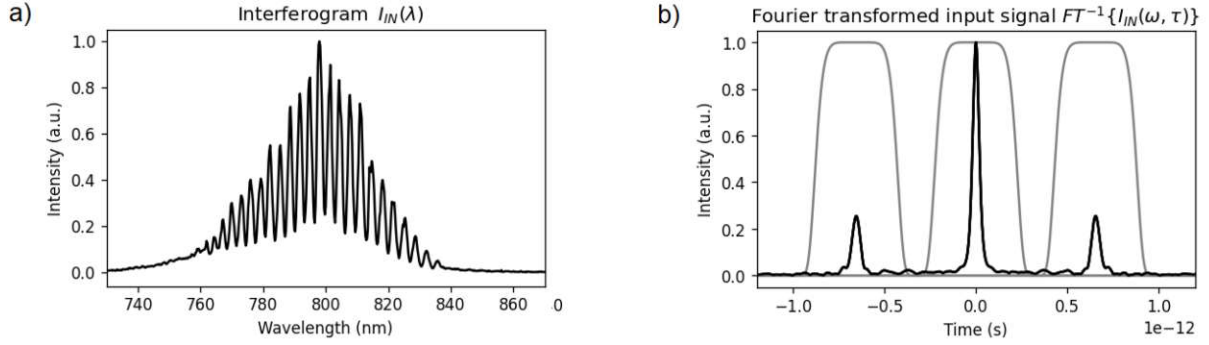


Figure 10: Measured interferogram and its Fourier transform for a calcite plate with a thickness of 1 mm (temporal retardation of $\tau = 560$ fs between the fundamental and the XPW pulse), whereby the fundamental pulse has a center wavelength of 800 nm and an approximate pulse duration of 30 fs. a) Intensity $I_{IN}(\lambda)$ of the interferogram. b) The temporal signal $I_{IN}(t)$ corresponds to the Fourier transformed signal of $I_{IN}(\omega)$ consisting of the sum term $S_0(t)$ (peak centered around $t = 0$) and the interference terms $f(t \pm \tau)$ (peaks centered around $t = \pm\tau$). (Spectrometer: Ocean Optics HR4000)

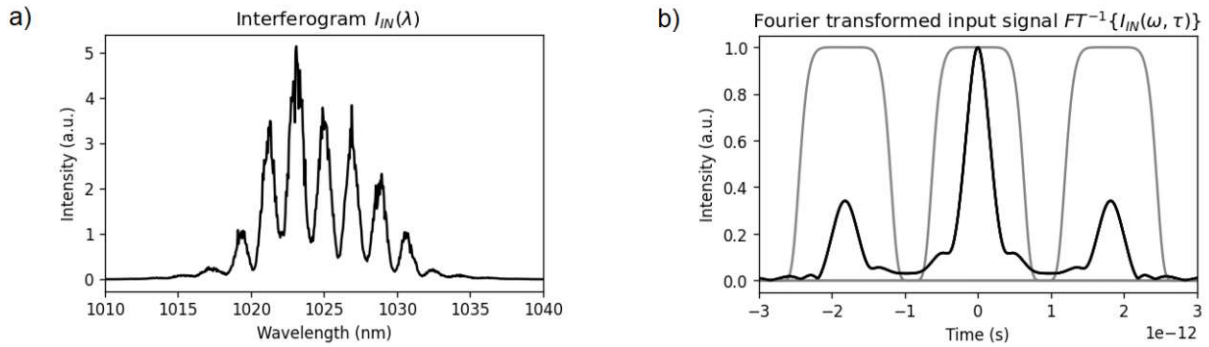


Figure 11: Measured interferogram and its Fourier transform for a calcite plate with a thickness of 3 mm (temporal retardation of $\tau = 1670$ fs between the fundamental and the XPW pulse), whereby the fundamental pulse has a center wavelength of 1025 nm and an approximate pulse duration of 300 fs. a) Intensity $I_{IN}(\lambda)$ of the interferogram. b) The temporal signal $I_{IN}(t)$ corresponds to the Fourier transformed signal of $I_{IN}(\omega)$. The sum term $S_0(t)$ (peak centered around $t = 0$) and the interference terms $f(t \pm \tau)$ (peaks centered around $t = \pm\tau$) cannot be separated properly. (Spectrometer: Anritsu MS9740B)

fundamental spectrum (laser output spectrum) $I_F(\omega)$, and the interferogram $I_{IN}(\omega)$. In the measured spectrum of the laser output signal, an incoherent component (ASE) is neglected and the pure coherent fundamental signal $I_F(\omega)$ is assumed. A treatment that considers the incoherent part is discussed in subsection 4.4. Please note that the term 'fundamental spectrum' or 'laser output spectrum' refers to the output signal of the laser after passing through the optical elements of the SRSI setup. Otherwise, the spectrum could be measured directly at the laser output, but this would neglect the induced dispersion caused by the optical elements of the SRSI setup.

SRSI allows the analytical computation of both the fundamental and XPW spectra from the measured interferogram. However, the separate measurement of these spectra allows a comparison to evaluate the accuracy of the pulse characterization by SRSI. To measure the spectra, the procedure is as follows.

In the first step, the calcite plate and the BaF₂ crystal are removed from the SRSI setup. Then the polarization directions of the two polarizers are aligned perpendicular to each other to obtain best extinction.

In the second step, to measure the pure XPW spectrum, the following procedure is carried out: The calcite plate is reinserted into the SRSI setup and aligned to maintain extinction (optical axis parallel to the polarization of the beam). Now the BaF₂ crystal can be inserted and rotated to obtain maximum XPW generation. The generated XPW signal is polarized at 90° with respect to the input signal, which

is why it is transmitted by the second polarizer. At this point also the setting of the grating compressor of the laser is optimized. The compressor allows a change of the GDD, whereby the measured XPW spectrum reaches a maximum bandwidth with the best compensation of the GDD by the compressor.

In the third step, to measure the fundamental spectrum $I_F(\omega)$ (output signal of the laser), the procedure begins by removing the BaF₂ crystal from the setup. Subsequently, the calcite plate is rotated by a few degrees from its previous position. By rotating the calcite plate and thus changing the orientation of the optical axis, the ratio of the intensities between the beams polarized parallel and perpendicular with respect to the optical axis can be changed. A time-delayed replica pulse $E_F(t - \tau)$ is generated due to the birefringent property of calcite. The replica pulse should have a lower intensity than the pulse with perpendicular polarization $E_{F,\text{input}}(t)$ that is needed to generate the XPW signal. Note that the magnitude of the intensity of the spectrum of the replica pulse should be similar to the previously measured magnitude of the intensity of the XPW spectrum in order to observe the largest possible interference contrast when measuring the interferogram $I_{\text{IN}}(\omega)$. Due to the slight rotation of the calcite plate, the two partial pulses are not polarized exactly parallel or perpendicular to the polarization direction of the second polarizer. This results in leakage of the input pulse into the spectrometer. Since we want to measure an interference-free spectrum of the output signal, the polarization direction of the second polarizer is adjusted to extract only the time-delayed replica pulse $E_F(t - \tau)$ and block $E_{F,\text{input}}(t)$ with perpendicular polarization. For this purpose, the polarizer is rotated until no interference is present in the measured spectrum. Another way to adjust the second polarizer and to block the fundamental signal $E_{F,\text{input}}(t)$ is to rotate the polarization direction of the second polarizer until the measured spectrum has a minimum intensity. This second approach is necessary, for example, if the spectrometer cannot resolve the interference pattern.

If the second polarizer is not optimally adjusted, the interference between the time-delayed replica pulse of the fundamental pulse generated by the calcite plate $E_F(t - \tau)$ and the fundamental pulse $E_{F,\text{input}}(t)$ polarized perpendicular to $E_F(t - \tau)$ can be described mathematically as in the following. For this, it is assumed that the amplitude $|E_{F,\text{input}}(\omega)|$ does not differ from the amplitude $|E_F(\omega)|$ except for a constant factor. The interferogram $I_{\text{IN}}(\omega)$ has to be extended in that case by a term $\text{const} \cdot E_{F,\text{input}}(\omega)$ (multiplication by constant factor since only a part is transmitted by the second polarizer) and is given by:

$$\begin{aligned} I_{\text{IN}}(\omega) &= |E_{\text{XPW}}(\omega) + E_F(\omega)e^{-i\omega\tau} + \text{const} \cdot E_{F,\text{input}}(\omega)|^2 \\ &= S_0(\omega) + f(\omega)e^{i\omega\tau} + f^*(\omega)e^{-i\omega\tau} \end{aligned} \quad (3.1)$$

with the new 'interference term' $f(\omega)$:

$$\begin{aligned} f(\omega) &= (E_{\text{XPW}}(\omega) + \text{const} \cdot E_{F,\text{input}}(\omega)) \cdot E_F^*(\omega) \\ &= E_{\text{XPW}}(\omega) \cdot E_F^*(\omega) + \text{const}' \cdot |E_F(\omega)|^2 \end{aligned} \quad (3.2)$$

and the new 'sum term' $S_0(\omega)$:

$$S_0(\omega) = |E_{\text{XPW}}(\omega) + \text{const} \cdot E_{F,\text{input}}(\omega)|^2 + |E_F(\omega)|^2 \quad (3.3)$$

The expression $\arg[f(\omega)] = \phi_F(\omega) - \phi_{\text{XPW}}(\omega)$ (Equation 2.44) is no longer valid for $E_{F,\text{input}}(\omega)$ not equal to zero, so the estimate for the phase $\phi_F(\omega) \approx \arg[f(\omega)]$ no longer holds.

As described in this step, by rotating the calcite plate and thus changing the orientation of the optical axis, the ratio of the intensities between the partial beams polarized parallel and perpendicular with respect to the optical axis can be changed. Due to the slight rotation of the calcite plate, the two partial pulses are not polarized exactly parallel or perpendicular to the polarization direction of the second polarizer and the second polarizer has to be readjusted. An alternative approach could involve rotating the first polarizer rather than adjusting the calcite plate. This change would result in an equivalent effect on the intensity ratio between the partial beams. This way the second polarizer would have to be adjusted only once. However, changing the polarization direction of the first polarizer will result in a change of the total intensity, since the beam of the laser output is linearly polarized.

In a fourth step, after the correct adjustment of the second polarizer, whereby the fundamental pulse $E_{F,\text{input}}(t)$ is blocked in order not to interfere with the replica pulse $E_F(t - \tau)$, the BaF₂ crystal can be inserted. This crystal must also be rotated until XPW generation and the resulting reference phenomena are suppressed. The spectrum measured in this way corresponds to the output signal (fundamental signal) of the laser whereby the generation of an XPW signal was completely suppressed.

In a final step, the interferogram $I_{IN}(\omega)$ can now be measured by rotating the BaF₂ crystal. Depending on the rotation angle, the intensity of the generated XPW signal can be varied. Amplitudes of the replica pulse $|E_F(\omega)|$ and the XPW pulse $|E_{XPW}(\omega)|$ of the same order are needed for an interferogram with good contrast. Note that the achievable intensity of the XPW pulse is limited by the value determined in step two, and even this limitation cannot be completely attained. This occurs because, as a result of the rotation of the calcite plate in step three, the input pulse is split into two perpendicularly polarized partial pulses. Consequently, the intensity of the pulse used to generate the XPW pulse $E_{F,input}(t)$ experiences a certain attenuation compared to the input pulse before the calcite plate. Therefore the magnitude of the XPW spectrum measured separately in step two does not match the magnitude of the XPW signal that contributes to the generation of the interferogram.

An example of the spectra obtained using this procedure for the femtosecond pulses of the ALPHA kHz laser is shown in Figure 19 a).

3.5 Software

This chapter explains the software implementation, technologies and the software libraries used to implement the SRSI algorithm (for the pulse characterization procedure and ASE determination, see subsection 2.5.1 and subsection 2.5.2). All evaluations were realized using Python, importing various libraries for subtasks. In Appendix A, the Python implementation of the SRSI algorithm is described, demonstrated by the characterization of pulses from a Thales ALPHA kHz laser. An overview of the software packages used and their application is given in the following.

Python: The entire SRSI algorithm for pulse characterization including graphical presentation was implemented using Python. Python is an interpreted, interactive, object-oriented programming language. It contains modules, exceptions, dynamic typing, dynamic data types and classes. There are interfaces to many system calls and libraries. Another advantage is portability: Python is executable on many Unix variants and on Windows. Documentation can be found at <https://docs.python.org>.

Pandas: Pandas is an open-source software library for Python used for data analysis, data mining and data modeling. Advantages of this library include existing tools for reading and writing data between in-memory data structures and various formats such as CSV and text files. The integrated handling of missing data is an additional beneficial feature. In this work, the library is mainly used in the evaluation to read the spectra stored by the spectrometers in CSV files and to structure the data into datasets for further evaluation. Documentation can be found at <https://pandas.pydata.org>.

SciPy: The open-source Python library SciPy is widely used for scientific computing applications. It provides various functionalities such as optimization, integration, interpolation, algebraic and differential equation routines. Detailed documentation can be found at <https://docs.scipy.org>. Of particular importance in this work are the algorithms for Fourier transform, optimization/minimization of scalar functions of two variables and for finding global maxima of functions.

NumPy: NumPy is an open-source Python library optimized for array computing and includes many numerical computing tools and mathematical functions and algebra routines, documentation at <https://numpy.org>. NumPy was used in this work for interpolation tasks, mathematical functions and phase unwrapping.

python-seabreeze: The python-seabreeze library provides an interface to the Ocean Optics HR4000 spectrometer. This allows real-time recording of the spectrum for direct pulse characterization. Therefore a continuous pulse characterization is possible, with one cycle being performed in a few seconds. The evaluation includes the determination of the phase and amplitude of the pulse as well as further evaluations. Documentation can be found at <https://python-seabreeze.readthedocs.io>.

Matplotlib: The library Matplotlib is used for visualization of static, animated and interactive graphs in Python, see documentation at <https://matplotlib.org>. All data visualization plots in this work were generated using this library. The interactive mode allows continuous updating of the plots, so that with the additional use of the python-seabreeze library continuous pulse characterization is possible.

4 Results and Discussion

In this chapter the results of experiments conducted to characterize two high-power solid-state femtosecond lasers using SRSI are presented and discussed. The retrieval of the full electric field enabled the determination of various parameters, including pulse durations and the dispersion terms (group delay dispersion, third-order dispersion and fourth-order dispersion) of the pulses. It is explained how a flattened spectral phase across the entire bandwidth is achieved by incorporating dispersion compensation devices. Furthermore, the chapter presents the results of pulse characterization using an extended SRSI model that considers an incoherent component of the laser output and allows the ASE spectrum to be obtained.

4.1 SRSI pulse characterization of a Thales ALPHA kHz laser

For pulse characterization, it is crucial to adjust the optical elements of the SRSI setup according to the instructions provided in subsection 3.4. Selecting an appropriate thickness for the calcite plate, as detailed in subsection 3.3, ensures the acquisition of an interferogram with distinct fringes, enabling the evaluation and retrieval of the pulse characteristics.

The evaluation for the pulse characterization is done as in subsection 2.5.1 where the algorithm to retrieve the pulse characteristics is described. In the following, the individual steps of the evaluation are described on the basis of an example pulse (dispersion-compensated pulse with pulse duration of about 38 fs, center wavelength of 800 nm and bandwidth of about 30 nm from a Thales ALPHA kHz laser source). The calcite plate used for this experiment has a thickness of 3 mm.

Using the Ocean Optics HR4000 spectrometer, the spectrum is recorded with an integration time of 100 ms over the entire wavelength range with an optical resolution (FWHM) of 0.75 nm. The python-seabreeze library allows a real-time recording of the spectrum. Therefore a continuous pulse characterization is possible, with one cycle being performed in a few seconds. The evaluation includes the determination of the phase and amplitude of the pulse, calculation of the dispersion parameters and pulse duration as well as the graphical display of the amplitude and phase in the time and the frequency domain. In the process of pulse characterization by SRSI, the spectral phase is flattened iteratively by dispersion compensation in the grating compressor as well as the Dazzler pulse shaper to obtain a reference pulse optimization. The pulse shaping (dispersion compensation) is performed within the laser system itself, prior to the SRSI setup, thus affecting both the fundamental pulse being determined and the reference pulse. The spectral phase introduced to achieve an output with a flat phase yields the initial spectral phase to be measured [10]. When aiming for the shortest pulse duration of the fundamental signal, optimizing the reference pulse simultaneously optimizes the fundamental pulse. In many cases, as in this thesis, the generation of the shortest possible pulses is desired. This is why the process of pulse characterization through SRSI not only involves characterizing the pulse but also results in an optimization of the fundamental pulse. It should be noted here that the low resolution of this spectrometer causes the interference term to be too small. This is evident from the visibly reduced size of the interference pattern. The small interference term directly affects the calculated amplitudes for the XPW and fundamental pulse spectra (amplitude calculations by Equation 2.35 – Equation 2.38). Hence, in the subsequent step, a second spectrometer (Anritsu MS9740B) with higher resolution (0.059 nm) will be employed.

Therefore, after initial pulse characterization using the Ocean Optics HR4000 spectrometer and optimizing the spectral phase through the dispersion control devices of the laser, the pulse characterization is performed again using the Anritsu spectrometer, which requires several minutes to record the spectrum. Due to the higher resolution (0.059 nm) of the Anritsu spectrometer, a more precise determination of the amplitude and phase is possible. For recording the spectrum with the Anritsu spectrometer the VBW was set to 200 Hz and the point average to 1000.

It should be noted that in the following evaluation, a possible incoherent part of the laser output is ignored. A calculation that takes into account an incoherent part is performed in subsection 4.4.

4.1.1 Pulse characterization procedure

In the following paragraphs, the experimental procedure of pulse characterization for the Thales ALPHA kHz laser is performed according to the theoretical description in subsection 2.5.1.

Processing of the measured signal

The spectrometer (Ocean Optics HR4000) records the intensities for the wavelength range 194–1120 nm with an approximate pixel spacing of 0.25 nm. The individual wavelengths are not equidistantly spaced. The spectra (XPW spectrum, fundamental spectrum, and interferogram) are recorded as described in subsection 3.4 and are shown in Figure 12 a) for the example of a dispersion-compensated femtosecond pulse with a center wavelength of 800 nm. The interferogram $I_{IN}(\lambda)$ shown in this figure serves as input for the evaluations presented in Figure 12 b) to Figure 16 a).

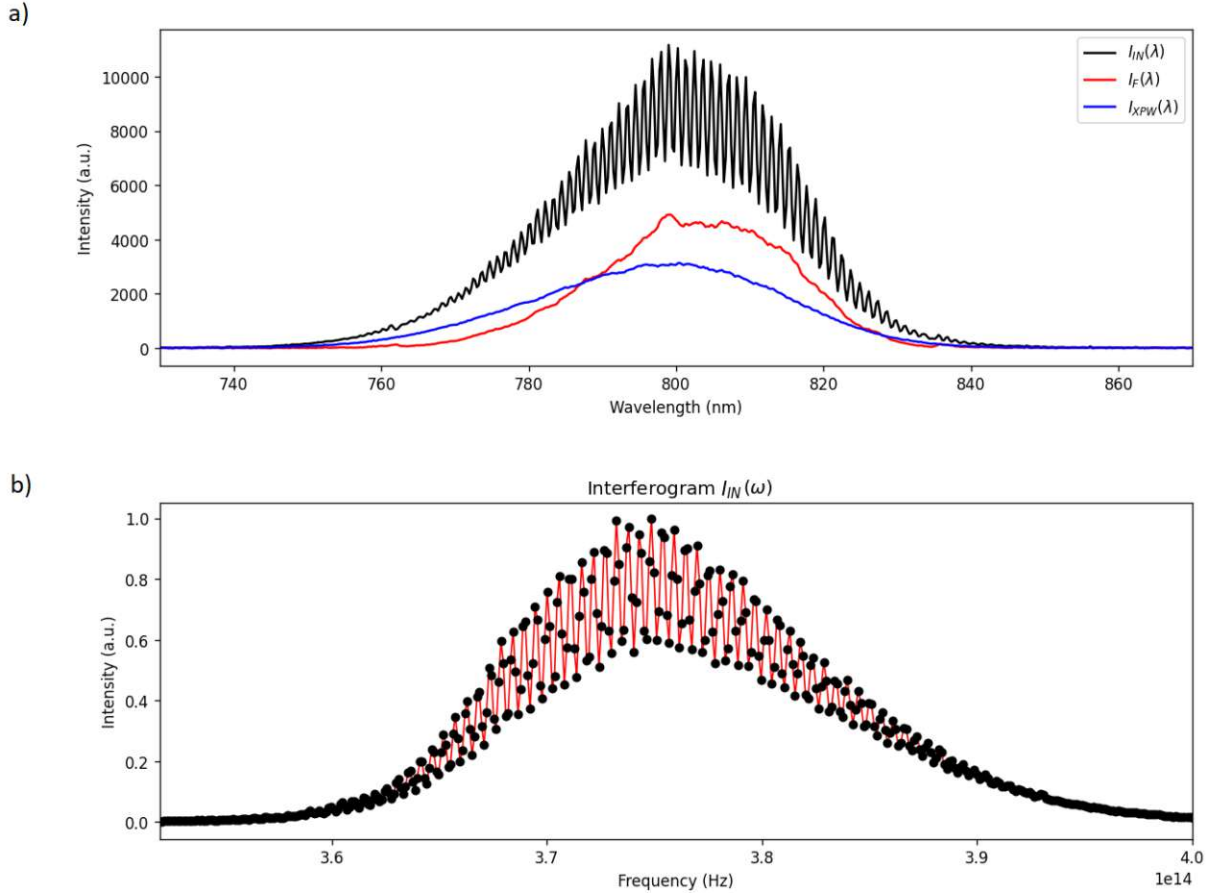


Figure 12: Typical interferogram of an SRSI measurement for a calcite plate with a thickness of 3 mm and a dispersion-compensated femtosecond pulse with a center wavelength of 800 nm, displayed in the wavelength and frequency domain. a) Intensity $I_{IN}(\lambda)$ of the interferogram in the wavelength domain. The interferogram $I_{IN}(\lambda)$ serves as input for the evaluations presented in Figure 13 to Figure 16 a). Also shown are the intensities of the separately measured XPW spectrum $I_{XPW}(\lambda)$ and fundamental spectrum $I_F(\lambda)$. b) Intensity $I_{IN}(\omega)$ of the interferogram in the frequency domain. Black dots correspond to the measuring points of the spectrometer. The red line corresponds to the linear interpolation. The interferogram was recorded with an Ocean Optics HR4000 spectrometer (resolution about 0.75 nm).

As described in subsection 2.5.1, the spectrum data is mapped to a frequency range between 0 and $4.2 \cdot 10^{14}$ Hz and linearly interpolated to obtain equidistant data points which are needed for the later fast Fourier transform. The pixel spacing of the Ocean Optics HR4000 spectrometer corresponds to a frequency interval $|\Delta f| = 1.2 \cdot 10^{11}$ Hz (at wavelength 800 nm and a pixel spacing in the wavelength domain of 0.25 nm, for the calculation see Equation 2.32). Since the evaluation is later performed using the Anritsu spectrometer, with a pixel spacing of 0.05 nm (equivalent to a frequency interval $|\Delta f| = 2.3 \cdot 10^{10}$ Hz at 800 nm), an interpolation step size of 10^{10} Hz is chosen. The obtained spectrum in the frequency domain $I_{IN}(\omega)$ can be seen in Figure 12 b).

It should be noted that spline interpolation or interpolation using the zero-filling method as described in Dorrer et al. [44] does not significantly affect the retrieved amplitude or phase of the pulse to be determined.

Extracting the sum term and the interference term

The measured signal in the frequency domain $I_{IN}(\omega)$ is composed of a sum term $S_0(\omega)$ and an interference term $f(\omega)$ (see Equation 2.29). The following shows how the terms $S_0(\omega)$ and $f(\omega)$ can be extracted from the measured signal. For this purpose, the inverse Fourier transform of $I_{IN}(\omega)$ is calculated (using fast Fourier transform). This yields a temporal signal $I_{IN}(t)$ (see Equation 2.34) containing the sum of the field autocorrelation functions $S_0(t)$ and the correlation functions $f(t - \tau)$ and $f^*(t + \tau)$. The temporal signal is depicted in Figure 13. The signal exhibits fluctuations across the entire range, which may be attributed to fluctuations in laser output power and noise within the measured interferogram. A signal near the main pulses, however, can be important for pulse characterization to identify pre-pulses.

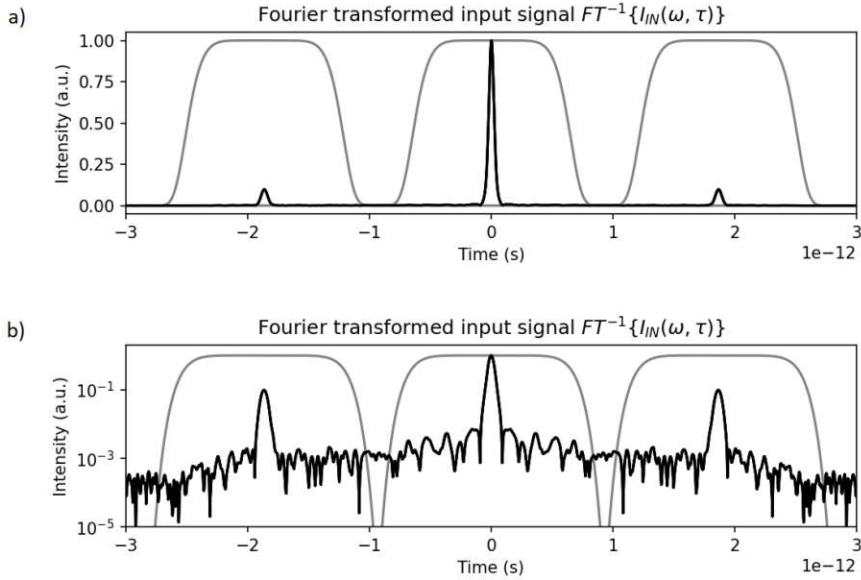


Figure 13: The real part of the temporal signal $I_{IN}(t)$ is shown in a). The real part of the temporal signal in a semi-logarithmic plot is shown in b). This temporal signal is the inverse-Fourier-transformed signal $I_{IN}(\omega)$ measured by the SRSI setup. The signal $I_{IN}(t)$ contains the sum term $S_0(t)$ centered around $t = 0$ and the two interference terms $f(t - \tau)$ and $f^*(t + \tau)$, which are centered around $t = \tau$ and $t = -\tau$. By multiplying a super-Gaussian window function of order four (shown in gray) with the temporal signal $I_{IN}(t)$, the sum term $S_0(t)$ and the interference term $f(t - \tau)$ (or $f^*(t + \tau)$) can be separated. The pulse characterized here is a dispersion-compensated femtosecond pulse with a center wavelength of 800 nm.

The peaks $S_0(t)$ and $f(t - \tau)$ are separated by the time delay τ , which corresponds to the delay of the pulse replica created by the calcite plate. The retardation with a calcite plate of thickness $\Delta s = 3$ mm corresponds approximately to a temporal retardation of $\tau = 1.68$ ps at a mean wavelength of 800 nm (for the calculation see subsection 3.3). For a calcite plate with a thickness of 3 mm, the peaks $S_0(t)$ and $f(t - \tau)$ are well separated so that the temporal signals do not overlap.

Thus, by multiplying the super-Gaussian window function with the temporal signal $I_{IN}(t)$, the sum term $S_0(t)$ and the interference term $f(t - \tau)$ can be extracted (depicted in Figure 14). In this figure the temporal signal from Figure 13, separated into interference term and sum term, is shown in more detail and beyond the primary peaks, a subtle signal adjacent to the peaks becomes evident. This signal contributes to the finer features in its Fourier-transformed counterpart. For instance, narrowing the width of the super-Gaussian window function in the temporal domain to cut off this side signal leads to a smoother Fourier-transformed signal (resulting in a correspondingly smoothed spectrum and spectral phase of the fundamental and XPW signals, determined by SRSI). In addition to the envelope, the figure also illustrates the carrier wave.

After centering the interference term $f(t - \tau)$ around $t = 0$, $S_0(t)$ and $f(t)$ can be Fourier transformed to obtain the now separated components $f(\omega)$ and $S_0(\omega)$ (depicted in Figure 15).

Calculating amplitudes of fundamental and reference pulse

Using the sum term $S_0(\omega)$ and interference term $f(\omega)$, the amplitudes of the reference pulse $|E_{XPW}(\omega)|$ (XPW signal) and the fundamental pulse $|E_F(\omega)|$ (pulse to be determined) can be determined. In case all XPW spectral components are more intense than the ones of the input pulse at each frequency the

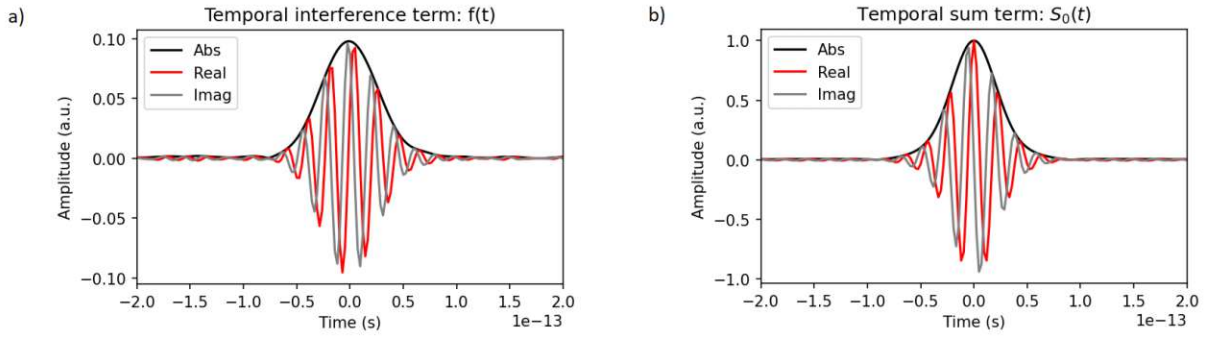


Figure 14: The plot shows the interference term (a) and the sum term (b), which were extracted from the signal $I_{IN}(t)$ by multiplication with a super-Gaussian window. Thereby the sum term corresponds to the sum of the field autocorrelation functions of the fundamental and the reference pulse. The interference term corresponds to the cross-correlation of the two pulses. The pulse characterized here is a dispersion-compensated femtosecond pulse with a center wavelength of 800 nm.

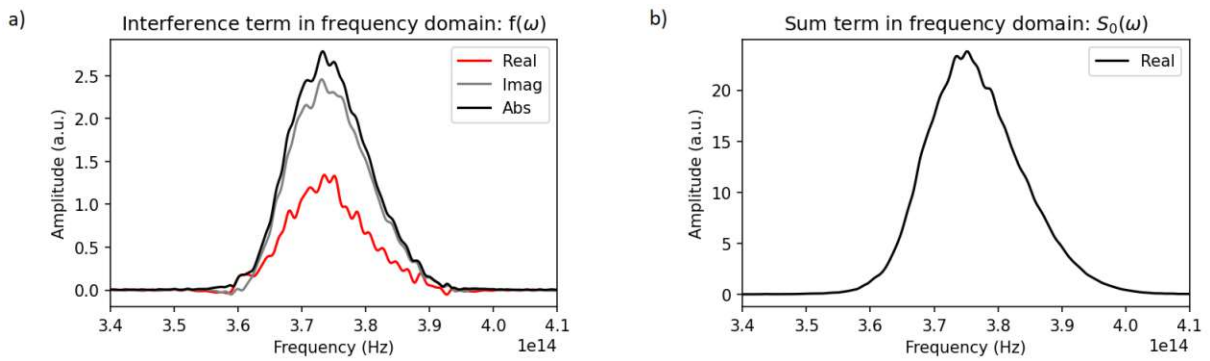


Figure 15: The plot shows the interference term (a) and the sum term (b) extracted from the measured SRSI signal $I_{IN}(\omega)$. Note that the sum term in the frequency domain is the Fourier transformed sum of the field autocorrelation functions of the fundamental and the reference pulse $S_0(t)$ and therefore the sum of the spectral intensities of the reference and the fundamental pulse, see Equation 2.31. This leads to a purely real signal $S_0(\omega)$. The pulse characterized here is a dispersion-compensated femtosecond pulse with a center wavelength of 800 nm.

expressions Equation 2.35 and Equation 2.36 are used. The intensity ratio between the XPW and fundamental signal was adjusted by rotating the calcite plate. The intensities of the XPW and the fundamental spectrum are shown in Figure 16. It should be noted that the spectrum of the XPW signal should be wider than the spectrum of the fundamental pulse. This condition is fulfilled.

If the resolution of the spectrometer used is too small, the magnitude of the observed interference pattern in the measured interferogram $I_{IN}(\omega)$ is too small. This results in a too small magnitude of the interference term $f(\omega)$. The magnitudes of the XPW and fundamental spectra calculated using the sum term $S_0(\omega)$ and interference term $f(\omega)$ therefore differ from the actual values. An estimation of the actual magnitudes of the intensities of the XPW and fundamental spectra is possible by measuring the XPW spectrum $I_{XPW}^M(\omega)$ and the fundamental spectrum $I_F^M(\omega)$ separately and fitting the magnitudes of these independent spectra to the sum term S_0 obtained from the interferogram as described in Equation 2.39. In Figure 16, a comparison between the intensities of the XPW and fundamental spectra calculated from the measured interferogram using the SRSI algorithm (see Equation 2.35 – Equation 2.38) and the separately measured and scaled spectra (see Equation 2.42 – Equation 2.43) is shown. The two XPW spectra and the fundamental spectra show a similar shape. Note that the ratio of the maximum intensity of the fundamental spectrum to the maximum intensity of the XPW spectrum depends on the calculation method. The comparison of the XPW and the fundamental spectrum shows that the XPW signal has about twice the intensity of the fundamental signal in case the spectra are measured and scaled separately. In the spectra derived from the measured interferogram using the SRSI algorithm, the XPW signal appears to be approximately eight times larger than the fundamental signal. This discrepancy can be overcome by using a spectrometer with higher resolution, as demonstrated in subsection 4.1.2.

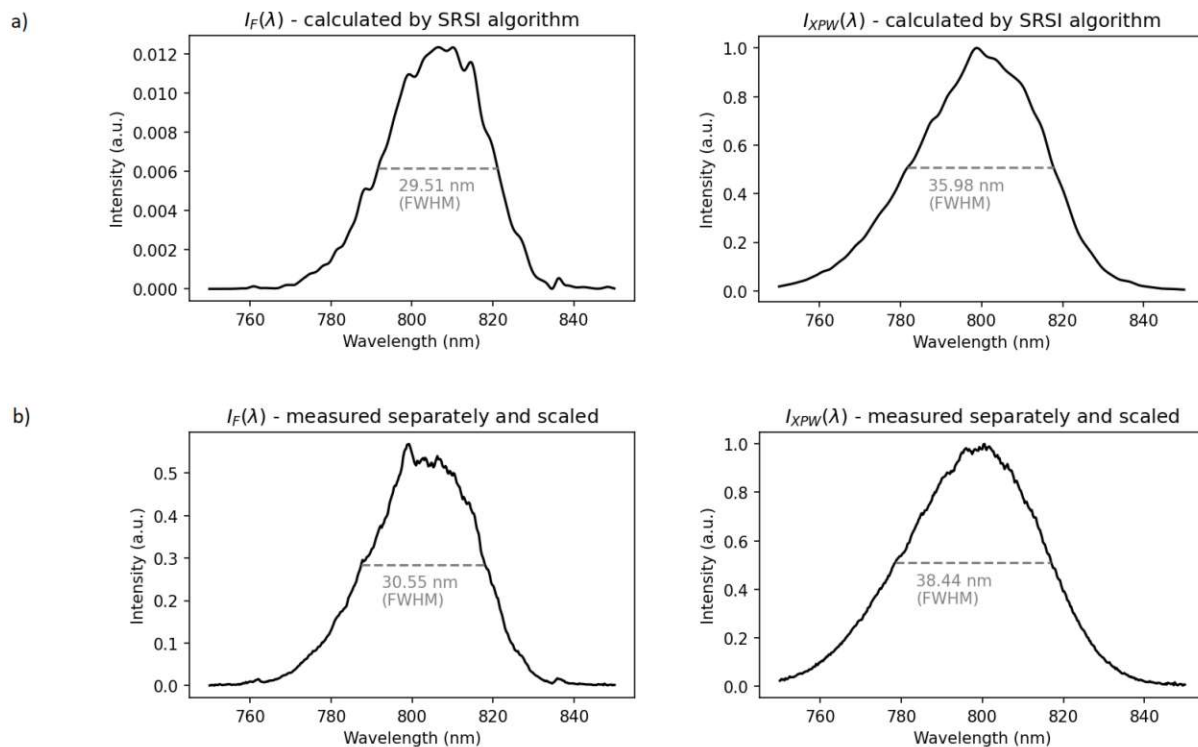


Figure 16: a) The intensities of the XPW and fundamental spectra calculated from the measured interferogram using the SRSI algorithm (see Equation 2.35 – Equation 2.38) are shown. b) The separately measured and scaled spectra (see Equation 2.42 – Equation 2.43) are shown.

It can be seen that the ratio of the maximum intensity of the fundamental spectrum to the maximum intensity of the XPW spectrum depends on the calculation method. This variance can be attributed to the limited resolution of the Ocean Optics HR4000 spectrometer.

In each case, the intensities are scaled with respect to the maximum intensity of the reference signal $I_{XPW}(\lambda)$. The pulse characterized here is a dispersion-compensated femtosecond pulse with a center wavelength of 800 nm.

Calculating the spectral phase

The spectral phase of the fundamental pulse $\phi_F(\omega)$ is estimated by $\arg[f(\omega)]$ (see Equation 2.45). A flat phase of the reference pulse (XPW signal) is assumed in this approximation.

In contrast to the previous evaluations, a sample pulse without a flat phase is now considered. In this context, the spectral phase of an initially dispersion-compensated pulse was modified using the Dazzler pulse shaper, inducing a second-order dispersion ($GDD = 400 \text{ fs}^2$). The resultant spectral phase of this altered pulse is depicted in Figure 17. It indicates a complex structure with a positive second-order dispersion as well as higher-order dispersion.

One possibility to improve the accuracy of the determined spectral phase is to consider the non-constant phase of the reference pulse as described in subsection 2.5.1. By using an iterative algorithm (see Figure 7) a better estimation of the phase of the pulse to be determined can be performed. The determined spectral phase for a positively chirped pulse with and without consideration of the non-constant phase of the reference pulse is shown in Figure 17. The change of the spectral phase also changes the temporal amplitude of the pulse to be determined, thereby influencing the pulse duration ($FWHM = 35.4 \text{ fs}$ for pulse without phase correction and $FWHM = 38.2 \text{ fs}$ for pulse with correction). As described in Equation 2.44, the spectral phase of the pulse to be determined is equal to the sum of the argument $\arg[f(\omega)]$ and the phase of the reference pulse. In the case of a pulse with a significant GDD, the reference pulse will also exhibit a slight positive chirp. Considering this factor in the spectral phase calculation of the fundamental pulse leads to a larger second-order dispersion compared to assuming a constant phase for the reference pulse.

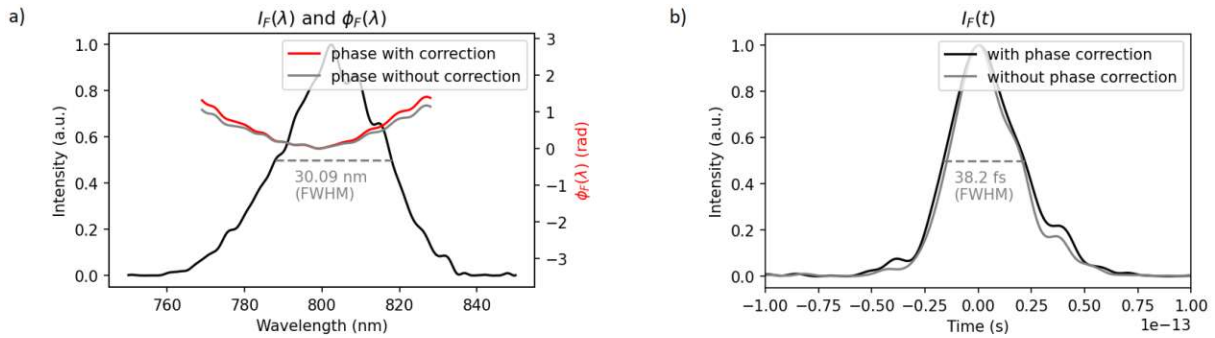


Figure 17: a) The calculated spectral phase of the fundamental pulse $\phi_F(\lambda)$ is shown in gray for the case without iterative correction to account for the non-constant phase of the reference pulse. For the case when the non-constant phase of the reference pulse is taken into account, the spectral phase is shown in red. The phase indicates a positive group delay dispersion (400 fs^2) and also higher-order dispersion terms. By changing the spectral phase, the temporal amplitude of the pulse to be determined $I_F(t)$ also changes. b) The temporal intensity of the fundamental pulse is illustrated in gray for the scenario where the non-constant phase of the reference pulse is not taken into account (FWHM = 35.4 fs). The temporal intensity is depicted in black for the scenario involving the iterative phase correction (FWHM = 38.2 fs). The pulse described is a femtosecond pulse with a center wavelength of 800 nm.

Phase flattening

Another way to improve the accuracy of the determination of the spectral phase is to use a pulse shaper (AOPDF, grating or prism compressor) which is introduced before the SRSI setup. By adjusting e.g. the second, third and fourth-order dispersion it is tried to achieve a spectral phase as flat as possible since the determination of a flat phase by SRSI is a very good estimate of the actual phase (detailed explanation in subsection 2.5.1). However, the original input pulse to be measured has now been changed by the pulse shaper. The change of the spectral phase in the pulse shaper to reach the flat phase corresponds to the spectral phase of the originally measured input pulse [10].

The procedure of phase flattening is basically done in two steps.

Coarse compression: manual phase adjustment

With the software for the Dazzler pulse shaper used, the dispersion terms up to order four can be varied manually by means of an input mask. To do this, the phase is determined as discussed in the previous steps and fitted to a fourth-degree polynomial to estimate the dispersion terms up to order four (for details of the determination of dispersion terms see subsection 4.3). The dispersion terms are only an estimate, since the determination of the phase by SRSI is only meaningful for a certain deviation from a flat phase (estimate of the validity range in subsection 4.3.2). In the Dazzler pulse shaper, the dispersion can be compensated using the estimated dispersion terms. After correcting the phase in the pulse shaper, the determined phase is flatter. This procedure can be iterated. An alternative approach to achieving coarse compression, without the need to determine the spectral phase, involves maximizing the bandwidth of the generated XPW signal while manipulating the second-order dispersion of the fundamental input pulse using the laser's grating compressor or Dazzler pulse shaper. The spectral broadening of the XPW signal is a result of the temporal filtering property of the XPW effect, with the most significant broadening occurring when the input pulse is dispersion-compensated.

Fine compression: phase adjustment by feedback of the determined phase

In order to compensate for the dispersion of the fundamental input pulse in the Dazzler pulse shaper even more (also higher dispersion order terms), an additional iterative feedback approach can be chosen. The phase of the fundamental pulse is determined as described above and can be used by the pulse shaper to further correct the input pulse [10]. An input file for the Dazzler containing the spectral phase versus wavelength allows to compensate the dispersion by subtracting the values of the determined spectral phase for the different wavelengths from the corresponding values in the file. The input file used for the Dazzler has a value range of 750 - 850 nm, which is why the phase within this range is determined using SRSI. As mentioned before, the determined values of the spectral phase outside the spectral bandwidth of the pulse, at intensities close to zero, are not reliable. Nonetheless, these values are applied to the

input file because the phase modulation induced by the Dazzler beyond the pulse spectrum's bandwidth has a negligible impact on pulse manipulation.

By employing this phase feedback loop with the Dazzler, it becomes possible to achieve even further phase flattening. For a comparison of the determined spectral phase of the pulse to be determined before and after the iterative feedback loop for dispersion compensation see Figure 18 a) and b).

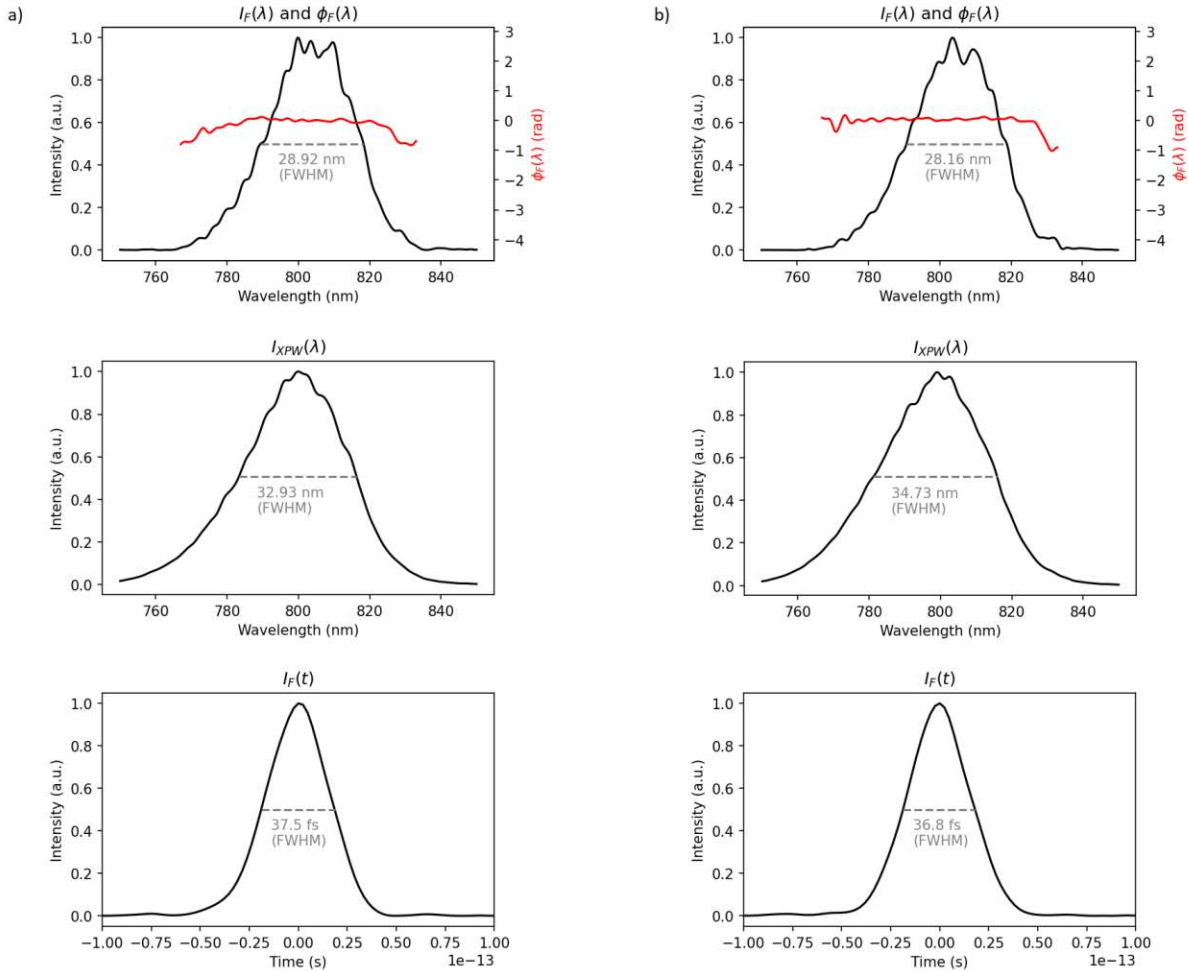


Figure 18: a) Phase and spectrum of fundamental pulse and XPW spectrum determined by SRSI after coarse compression with a Dazzler pulse shaper by a fourth-order polynomial (without fine compression by feedback of the measured phase into the pulse shaper). Additionally, the temporal intensity of the fundamental pulse is shown. b) Phase and spectrum of fundamental pulse and XPW spectrum determined by SRSI after fine compression (two iterations of the feedback loop). Additionally, the temporal intensity of the fundamental pulse is shown. Note that the XPW spectrum is wider and the temporal pulse width is shorter after fine compression. The interferogram $I_{IN}(\omega)$ was measured by the Ocean Optics HR4000 spectrometer.

To maximize the range of values in which the Dazzler pulse shaper can manipulate the spectral phase, the second-order dispersion of the pulse can be already compensated in the grating compressor of the laser system. This allows compensation of dispersion by the Dazzler pulse shaper over the widest possible wavelength range. A constant phase can thus be achieved over almost the entire pulse bandwidth (where the pulse intensity is still larger than 5% of the peak intensity).

As seen in Figure 18 b), the XPW spectrum produced by a fundamental pulse with a constant phase (phase after fine compression by feedback loop) is broader than the XPW spectrum produced by a pulse with non-constant spectral phase, see discussion in subsection 2.3.2.

4.1.2 Improvement by a high-resolution spectrometer

With the Anritsu spectrometer, the evaluation can be performed again, whereby the higher resolution provides a more precise determination of the amplitude and phase. The spectra (XPW spectrum, fundamental spectrum, and interferogram) are recorded as described in subsection 3.4 and are shown in Figure 19 a). The main problem with a spectrometer with too small a resolution is that the interference

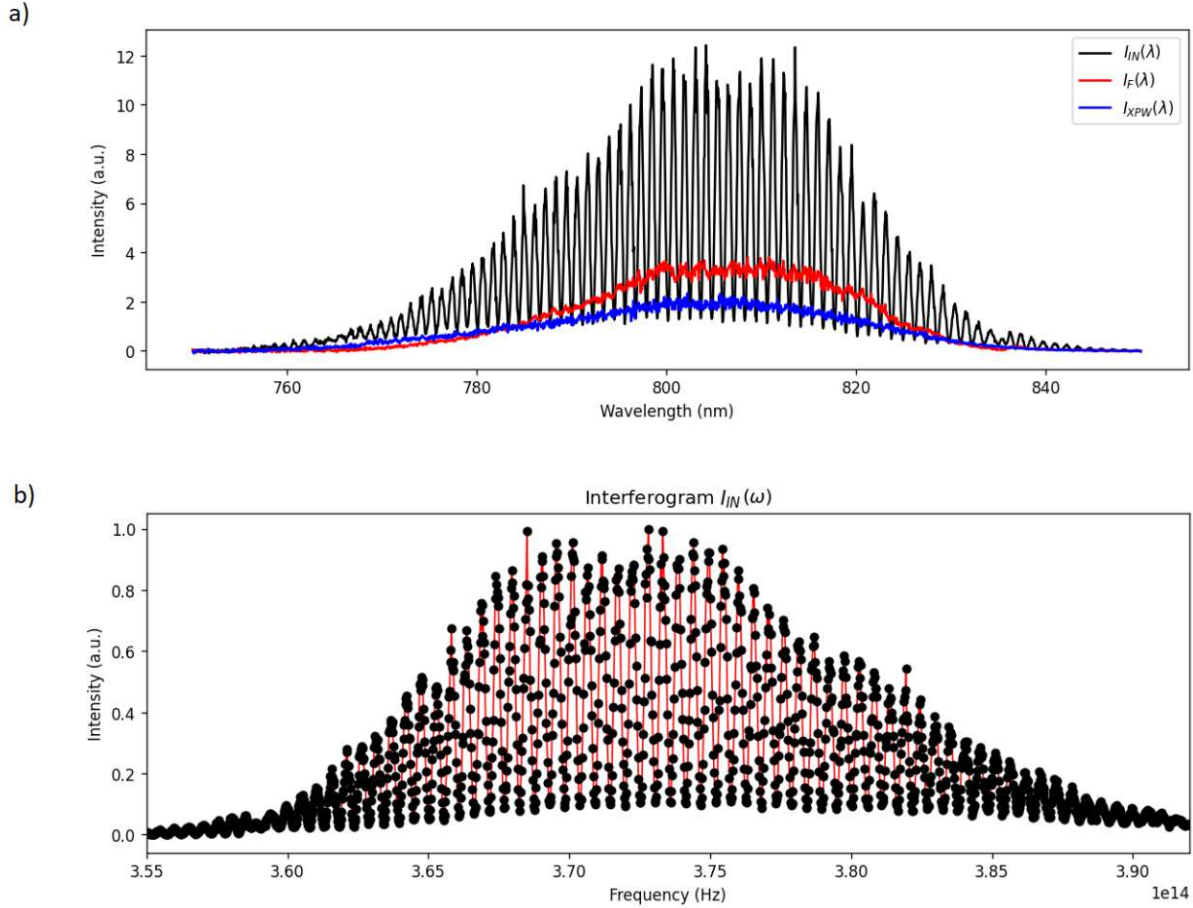


Figure 19: Typical interferogram of an SRSI measurement for a calcite plate with a thickness of 3 mm and a dispersion-compensated femtosecond pulse with a center wavelength of 800 nm, displayed in the wavelength and frequency domain. a) Intensity $I_{IN}(\lambda)$ of the interferogram in the wavelength domain. It serves as input for the evaluation presented in Figure 20 a). Also shown are the intensities of the separately measured XPW spectrum $I_{XPW}(\lambda)$ and fundamental spectrum $I_F(\lambda)$. b) Intensity $I_{IN}(\omega)$ of the interferogram in the frequency domain. Black dots correspond to the measuring points of the spectrometer. The red line corresponds to the linear interpolation. The interferogram was recorded with a high-resolution Anritsu spectrometer (resolution about 0.059 nm).

pattern cannot be resolved well enough and the magnitude of the amplitude of the interference term appears too small. The determined interference term $f(\omega)$ is thus too small and directly affects the analytically calculated spectra for the XPW and the fundamental pulse (see Equation 2.35 and Equation 2.36). This is easily seen by direct comparison by measuring the same signal with spectrometers of different resolutions. Compare the interferogram Figure 12 b) (measured with Ocean Optics HR4000, optical resolution (FWHM) about 0.75 nm) and the interferogram Figure 19 b) (measured with Anritsu spectrometer, resolution about 0.059 nm). Note that both measurements are of the same signal.

As described in the previous paragraphs, the measured interferogram $I_{IN}(\omega)$ can be processed to extract the sum term $S_0(\omega)$ and interference term $f(\omega)$ and consequently calculate the amplitudes and phases of the fundamental and the reference pulse. In Figure 20, a comparison between the XPW and fundamental spectra calculated using the SRSI algorithm (see Equation 2.35 – Equation 2.38) and the separately measured and scaled spectra (see Equation 2.42 – Equation 2.43) is shown.

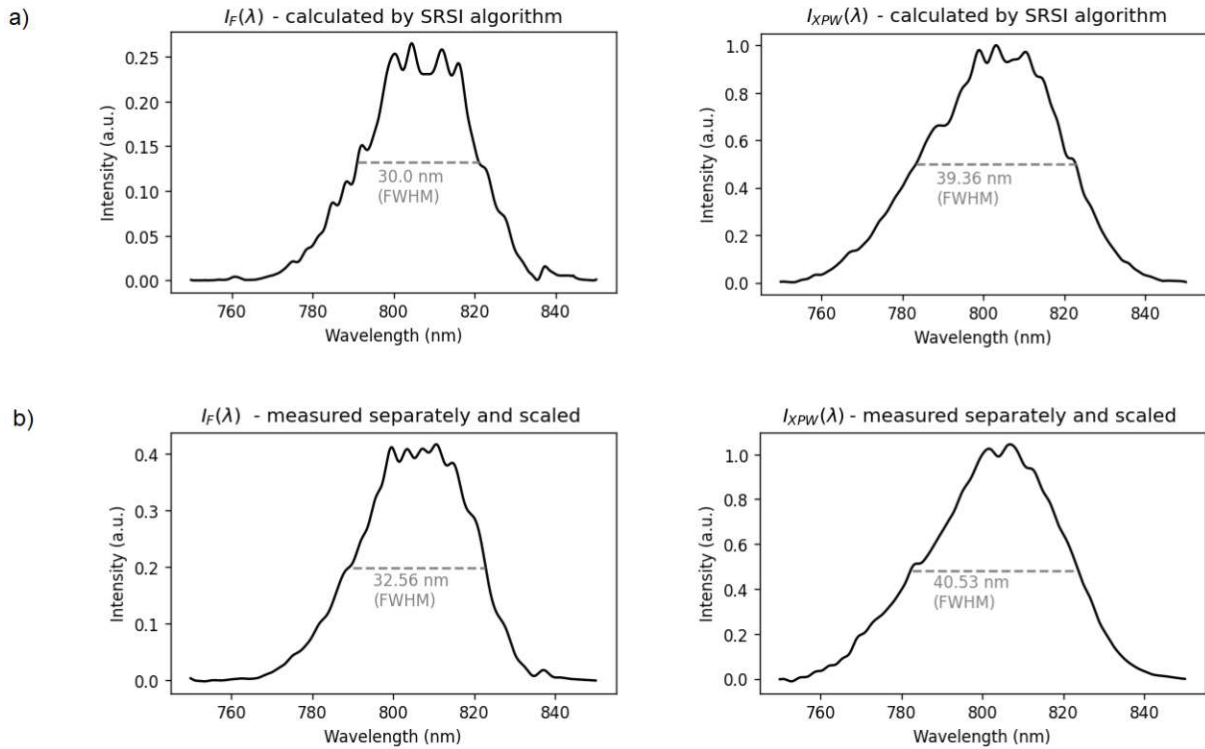


Figure 20: a) The intensities of the XPW and fundamental spectra calculated from the measured interferogram using the SRSI algorithm (see Equation 2.35 – Equation 2.38) are shown. b) The separately measured and scaled spectra (see Equation 2.42 – Equation 2.43) are shown.

In each case, the intensities are scaled with respect to the maximum intensity of the reference signal $I_{XPW}(\lambda)$. The spectra were measured by the high-resolution Anritsu spectrometer. The pulse characterized here is a dispersion-compensated femtosecond pulse with a center wavelength of 800 nm.

It can be seen that the ratio of the maximum intensity of the fundamental spectrum to the maximum intensity of the XPW spectrum still depends on the calculation method, which will be discussed below. The separately measured and scaled XPW and fundamental spectra are smoothed by inverse Fourier transform and multiplication by a Gaussian window function in the time domain. The width of the window is chosen the same as for the interferogram signal to obtain the same filter properties as for the sum and interference term. After multiplication with the window function, the signal is Fourier transformed back to the frequency domain. This method corresponds to a band-pass filter and reduces noise while preserving the underlying structure of the spectrum.

The two differently determined XPW spectra and the fundamental spectra show a similar shape (see Figure 20). In contrast to the determination using the Ocean Optics HR4000 spectrometer (lower resolution) as seen in Figure 16, the ratio of the maximum intensity of the fundamental spectrum to the maximum intensity of the XPW spectrum is similar for both calculation methods. However, there is still a deviation which is due to the amplified spontaneous emission (ASE). The measured fundamental spectrum is not the purely coherent fundamental intensity $I_F(\omega)$, but also includes an incoherent component (ASE). The independently measured spectrum $I_{FA}(\omega)$ is composed of the fundamental intensity $I_F(\omega)$ and the incoherent component $I_{ASE}(\omega)$ and therefore corresponds only approximately to the fundamental spectrum calculated from the measured interferogram using the SRSI algorithm (calculation by Equation 2.36 or Equation 2.38). A detailed treatment of the amplified spontaneous emission is given in subsection 2.5.2.

By further feedback of the determined spectral phase of the fundamental pulse into the pulse shaper using the high-resolution spectrometer, the phase can be flattened even more.

In Figure 21 a) the phase and spectrum of the fundamental pulse and the XPW spectrum determined by SRSI after fine compression of the fundamental pulse (two iterations of the feedback loop) are shown. For

this fine compression, the phase for the feedback into the Dazzler was determined by SRSI, using the Ocean Optics HR4000 spectrometer to measure the interferogram as described in subsection 4.1.1. Note that the fine compression was performed by using the low-resolution Ocean Optics HR4000 spectrometer, but the displayed phase and spectra in Figure 21 were determined by SRSI, using the high-resolution Anritsu spectrometer to measure the interferogram.

By using the high-resolution spectrometer for the fine compression, the dispersion can be compensated even more. The phase and spectrum of the fundamental pulse and the XPW spectrum after an additional iteration of the feedback loop is shown in Figure 21 b), where the phase for the feedback into the Dazzler was now determined by SRSI, using the high-resolution spectrometer.

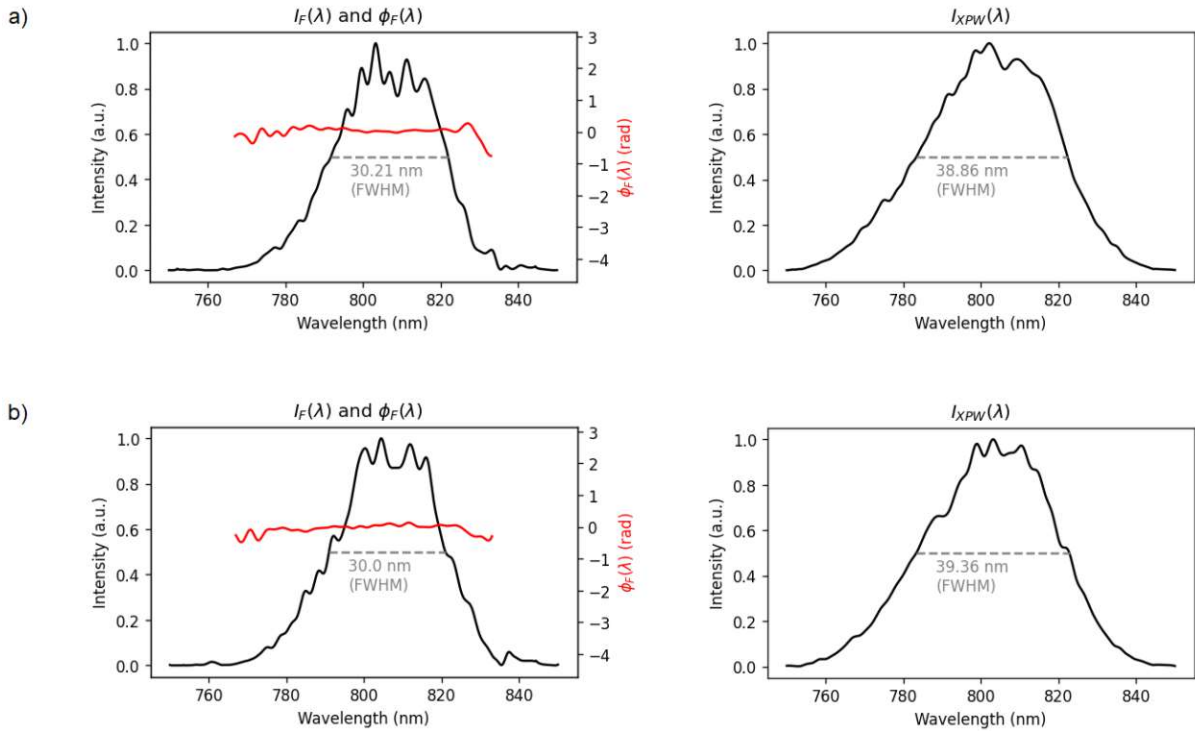


Figure 21: a) Phase and spectrum of fundamental pulse and XPW spectrum determined by SRSI after fine compression by low-resolution Ocean Optics HR4000 spectrometer (two iterations of the feedback loop) b) Phase and spectrum of fundamental pulse and XPW spectrum determined by SRSI after fine compression by high-resolution Anritsu spectrometer (one more iteration of the feedback loop).

Note that in a) the fine compression was performed by using the low-resolution Ocean Optics HR4000 spectrometer, but the displayed phase and spectra were determined by SRSI, using the high-resolution Anritsu spectrometer to measure the interferogram. Also in b), the displayed phase and spectra were obtained by SRSI, utilizing the high-resolution Anritsu spectrometer for interferogram measurement.

The fluctuations of the spectral phase are not necessarily due to higher-order dispersion terms, but can also be caused by the output power fluctuation of the laser.

Also the misalignment of the optical setup could have an impact on the measured interferogram and retrieved phase. For example, a wrong adjustment of the second polarizer results in one of the two perpendicularly polarized fundamental beams not being completely blocked, which leads to interference (detailed discussion in subsection 3.4).

Temporal characterization

By inverse Fourier transform, the electric field of the pulse in the temporal domain can be calculated from the amplitude and phase in the frequency domain to obtain an estimate of the pulse duration (FWHM of the intensity). For a dispersion-compensated pulse (fine compression performed by feedback of the determined spectral phase of the fundamental pulse into the Dazzler pulse shaper using the high-resolution Anritsu spectrometer as described in the upper paragraphs) this results in a pulse duration of about 38 fs. In 22, the temporal intensity of the pulse is illustrated in two scenarios: one determined through SRSI

pulse characterization using the Ocean Optics HR4000 spectrometer for measuring the interferogram (with a resolution of about 0.75 nm), and the other through the utilization of the Anritsu spectrometer (with a resolution of approximately 0.059 nm). No pre-pulses are evident in this plot.

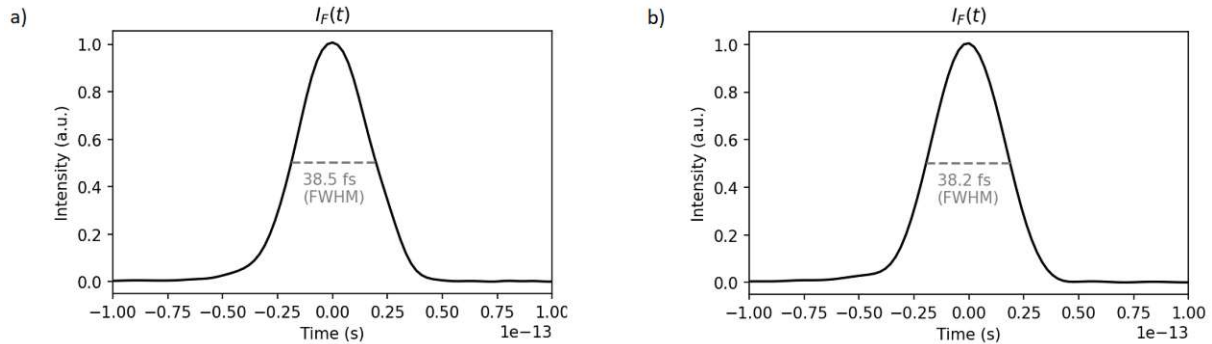


Figure 22: Intensities $I_F(t)$ of a dispersion-compensated pulse in the time domain (fine-compression by feedback of the spectral phase in the Dazzler pulse shaper, see corresponding spectrum and spectral phase in Figure 21 b). In a) the temporal intensity was determined through SRSI pulse characterization using the Ocean Optics HR4000 spectrometer (with a resolution of about 0.75 nm). In b) the temporal intensity was determined through SRSI pulse characterization using the Anritsu spectrometer (with a resolution of approximately 0.059 nm). The pulse duration (FWHM) is about 38 fs.

Also in Figure 23, the temporal intensity of the dispersion-compensated pulse is depicted. In contrast to Figure 22 this is illustrated in a semi-logarithmic plot that spans a time range roughly equivalent to the width of the super-Gaussian window function used in the SRSI evaluation. In this plot, the identification of a potential pre-pulse should be feasible. However, no distinct pre-pulse is detectable. This could also possibly be attributed to the significant noise present, which complicates the analysis.

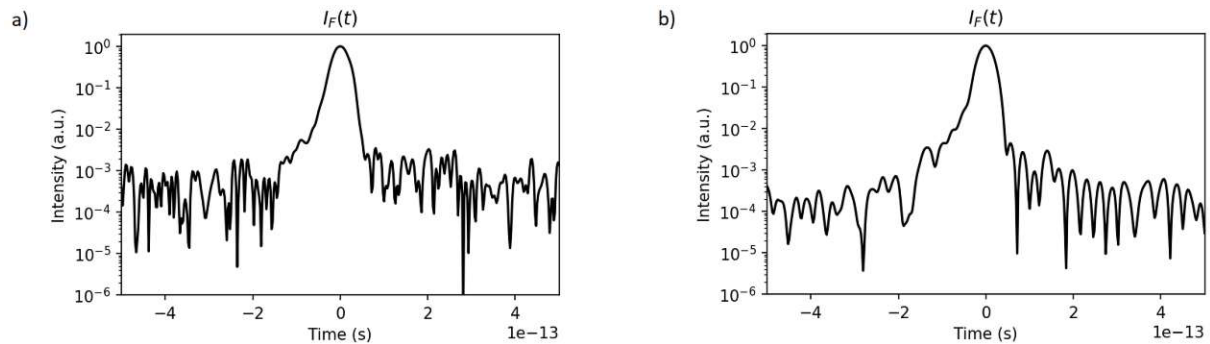


Figure 23: Semi-logarithmic plot of the temporal intensity $I_F(t)$ of a dispersion-compensated pulse in the time domain (fine-compression by feedback of the spectral phase in the Dazzler pulse shaper, see corresponding spectrum and spectral phase in Figure 21 b). In a) the temporal intensity was determined through SRSI pulse characterization using the Ocean Optics HR4000 spectrometer (with a resolution of about 0.75 nm). In b) the temporal intensity was determined through SRSI pulse characterization using the Anritsu spectrometer (with a resolution of approximately 0.059 nm). No distinct pre-pulses are detectable.

4.2 SRSI pulse characterization of a Light Conversion PHAROS laser

For accurate characterization of pulses from the PHAROS laser source, it is crucial to use a suitable thickness of the calcite plate and a high-resolution spectrometer as described in subsection 3.3. Also, it is important to adjust the elements according to the instructions provided in subsection 3.4. This ensures the acquisition of an interferogram with clear fringes, enabling the evaluation and retrieval of pulse characteristics.

The evaluation for the pulse characterization is done as in subsection 2.5.1 where the algorithm to

retrieve pulse characteristics is described. In the following, the individual steps of the evaluation are described on the basis of an example pulse (dispersion-compensated pulse with pulse duration of about 270 fs, center wavelength of 1025 nm and bandwidth of 6.7 nm from a Light Conversion PHAROS PH2-20W laser source).

The most important difference to the measurements and the pulse characterization described for the Thales ALPHA kHz laser source is the now larger pulse duration (and narrower bandwidth). As a consequence a thicker calcite plate is used, otherwise the sum term $S_0(t)$ and the interference term $f(t)$ in the time domain cannot be well separated by the Gaussian window function. The calcite plate used for this experiment has a thickness of 10 mm. A detailed discussion of the estimation of the thickness of the calcite plate can be found in subsection 3.3. Due to the longer delay time τ of the 10 mm calcite plate, the peaks of the interferogram are close to each other. The Anritsu spectrometer with a resolution of 0.059 nm (pixel spacing 0.05 nm), VBW of 200 Hz and point average of 100 is used to record the interferogram. Using the grating compressor of the PHAROS laser system, the spectral phase of the pulses can be flattened and the pulse duration can be shortened.

Regarding the measurement procedure of the interferogram (as described in subsection 3.4), it should be noted that the Ocean Optics HR4000 spectrometer is used for fine adjustment of the optical elements to see the effects of the different settings on the measured spectrum directly (without significant time delay). The Anritsu spectrometer with higher resolution needs up to several minutes for the recording of a single spectrum which is too slow for adjustment and used only for the measurement of the interferogram after the fine adjustments.

Using the Ocean Optics HR4000 spectrometer with lower resolution poses a problem in the adjustment of the second polarizer, which should completely block the fundamental pulse $E_{F,\text{input}}(\omega)$. The interference pattern, which results from the superposition of fundamental pulse $E_{F,\text{input}}(\omega)$ and the generated, time-delayed replica pulse $E_F(\omega)$ if the second polarizer does not block one of the two pulses, cannot be resolved by the Ocean Optics HR4000 spectrometer. The best setting of the second polarizer can still be found by rotating the polarizer until a minimum intensity of the spectrum is measured. At this setting the fundamental pulse $E_{F,\text{input}}(\omega)$ is blocked by the second polarizer. To check the alignment, the Anritsu spectrometer can be used to verify the absence of interference in this spectrum.

4.2.1 Pulse characterization procedure

In the following paragraphs, the experimental procedure of pulse characterization for the PHAROS laser is performed according to the theoretical description in subsection 2.5.1.

Processing of the measured signal

The Anritsu spectrometer records the intensities for the wavelength range 1015–1035 nm with a resolution of 0.059 nm. The interferogram is recorded as described in subsection 3.4 and is shown in Figure 24 for the example of a dispersion-compensated femtosecond pulse with a center wavelength of 1025 nm.

As described in subsection 2.5.1, the spectrum data is mapped to a frequency range $(0-3 \cdot 10^{14} \text{ Hz})$ and linearly interpolated to obtain equidistant data points which are needed for the fast Fourier transform. The pixel spacing of the Anritsu spectrometer corresponds to a frequency interval $|\Delta f| = 1.4 \cdot 10^{10} \text{ Hz}$ (at wavelength 1025 nm and a pixel spacing in the wavelength domain of 0.05 nm, for the calculation see Equation 2.32). Therefore an interpolation step size of 10^{10} Hz is chosen.

The spectrum obtained in the frequency domain $I_N(\omega)$ can be seen in Figure 25. While there is noise present in the interferogram, it's important to note that the smoothing of the interferogram isn't required to achieve smooth spectra through the SRSI algorithm. This is due to the fact that the signal smoothing is already incorporated within the SRSI algorithm. Smoothing occurs during the processing step in which the interferogram is inverse-Fourier-transformed, the sum term and the interference term are extracted by multiplication with a super-Gaussian window function and the extracted signals are Fourier transformed back into the frequency domain. This procedure is elaborated in more detail in the following.

Extracting the sum term and the interference term

The measured signal in the frequency domain $I_N(\omega)$ is composed of a sum term $S_0(\omega)$ and interference term $f(\omega)$. As in the case of the characterization of the pulses of the Thales ALPHA kHz laser, the terms $S_0(\omega)$ and $f(\omega)$ are extracted from the signal $I_N(\omega)$. Therefore in the first step $I_N(\omega)$ is inverse-Fourier-transformed (using fast Fourier transform) to obtain a temporal signal $I_N(t)$, depicted in Figure 26.

The peaks $S_0(t)$ and $f(t - \tau)$ of the signal $I_N(t)$ are separated by the time delay τ , which corresponds to

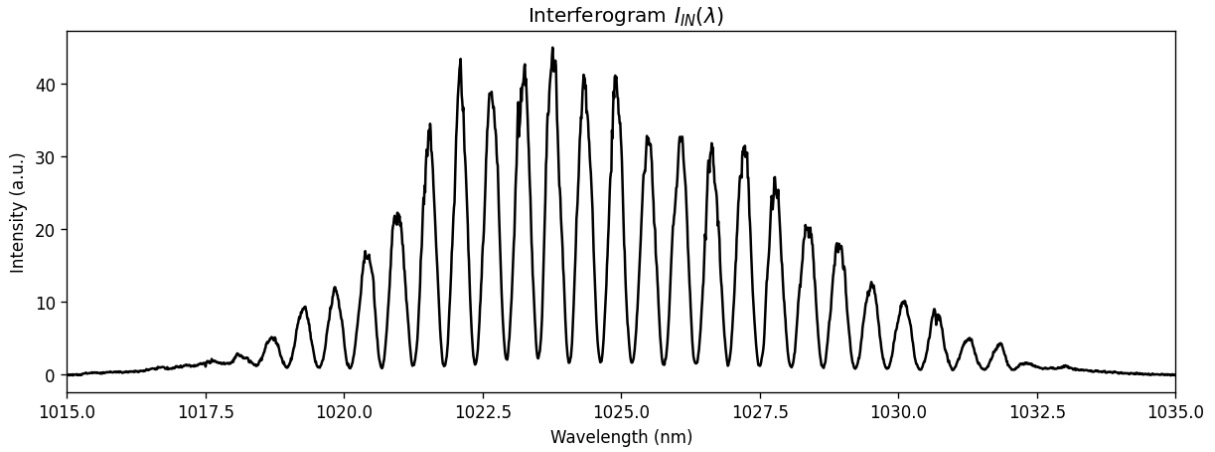


Figure 24: Intensity $I_{IN}(\lambda)$ of a typical interferogram of an SRSI measurement for a calcite plate with a thickness of 10 mm and a dispersion-compensated femtosecond pulse with a center wavelength of 1025 nm. It serves as input for the evaluations presented in Figure 25 – Figure 29. (Spectrometer: Anritsu; resolution 0.059 nm)

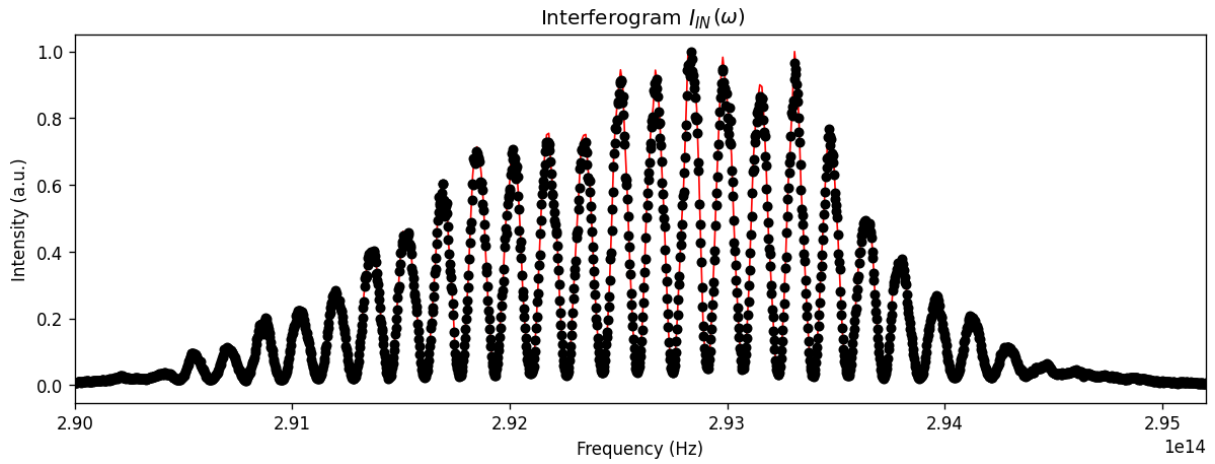


Figure 25: Intensity $I_{IN}(\omega)$ of a typical interferogram of an SRSI measurement for a calcite plate with a thickness of 10 mm and a dispersion-compensated femtosecond pulse with a center wavelength of 1025 nm. Black dots correspond to the measuring points of the spectrometer (Anritsu; resolution about 0.059 nm). The red line corresponds to the linear interpolation.

the delay of the replica pulse caused by the calcite plate. The retardation with a calcite plate of thickness $\Delta s = 10$ mm corresponds approximately to a temporal retardation of $\tau = 5.44$ ps at a mean wavelength of 1025 nm (for the calculation see subsection 3.3).

For a calcite plate with a thickness of 10 mm, the peaks $S_0(t)$ and $f(t - \tau)$ are well separated so that the temporal signals do not overlap. Thus, by multiplying the super-Gaussian window function with the temporal signal $I_{IN}(t)$, the sum term $S_0(t)$ and the interference term $f(t - \tau)$ can be extracted (depicted in Figure 27). After centering the interference term $f(t - \tau)$ around $t = 0$, $S_0(t)$ and $f(t)$ can be Fourier transformed to obtain the now separated components $f(\omega)$ and $S_0(\omega)$ (depicted in Figure 28).

Calculating the amplitudes of the fundamental and the reference pulse

Using the sum term $S_0(\omega)$ and interference term $f(\omega)$ the amplitudes of the reference pulse $|E_{XPW}(\omega)|$ (XPW signal) and the fundamental pulse $|E_F(\omega)|$ can be determined. Assuming that all XPW spectral components are more intense than input pulse ones at each frequency the expressions Equation 2.35 and Equation 2.36 are used. The intensities of the XPW and the fundamental spectrum are shown in Figure 29. As required by the SRSI method, the spectrum of the XPW signal is wider than the spectrum of the fundamental pulse.

Since in the Anritsu spectrometer the intensities of the wavelength intervals are recorded sequentially, a

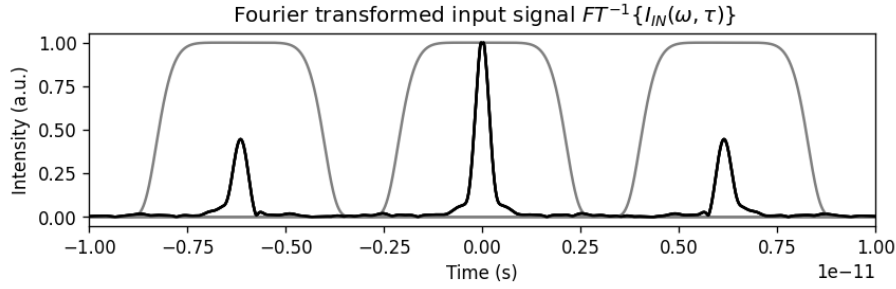


Figure 26: The temporal signal $I_{IN}(t)$ (the real part is shown here in black) is the inverse-Fourier-transformed signal $I_{IN}(\omega)$ measured by the SRSI setup. The signal $I_{IN}(t)$ contains the sum term $S_0(t)$ centered around $t = 0$ and the two interference terms $f(t - \tau)$ and $f^*(t + \tau)$ which are centered around $t = \tau$ and $t = -\tau$. By multiplying a super-Gaussian window function of order four (shown in gray) with the temporal signal $I_{IN}(t)$, the sum term $S_0(t)$ and the interference term $f(t - \tau)$ (respectively $f^*(t + \tau)$) can be separated. The pulse characterized here is a dispersion-compensated femtosecond pulse with a center wavelength of 1025 nm.

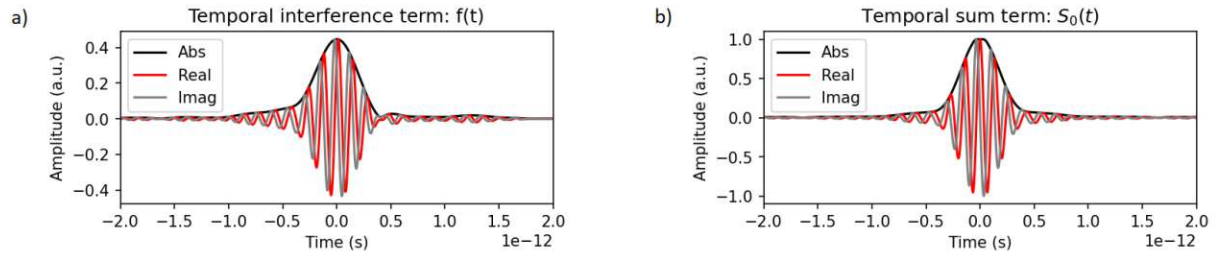


Figure 27: The plots shows the interference term (a) and the sum term (b), which were extracted from the signal $I_{IN}(t)$ by multiplication with a super-Gaussian window. Thereby the sum term corresponds to the sum of the field autocorrelation functions of the fundamental and the reference pulse. The interference term corresponds to the cross-correlation of the two pulses. The signal $I_{IN}(t)$ is the inverse-Fourier-transformed signal $I_{IN}(\omega)$ measured by an SRSI setup. The pulse characterized here is a dispersion-compensated femtosecond pulse with a center wavelength of 1025 nm.

fluctuation of the intensity of the entire input signal means fluctuations in the measured interferogram, since in the implementation it was not averaged over a sufficiently large number of points and sweeps. This results in a fluctuation of the intensity of the determined fundamental and XPW spectrum. This can also be seen in the fundamental intensity spectra $I_F(\lambda)$ for different spectral phases, shown in Figure 30, which theoretically should be the same, since the grating compressor only affects the phase. If more accurately determined spectra are required, the point averaging (per measured wavelength) and sweep averaging can be increased, resulting in a longer measurement time. Alternatively, pulse characterization can be repeated multiple times without making any adjustments or modifications in the experimental procedure. This would provide a more distinct understanding of the noise characteristics.

As an extension of this work, the obtained spectra could be verified by measuring the fundamental and XPW spectra separately, as was done in the characterization of the Thales ALPHA kHz pulses and described theoretically in subsection 3.4.

Phase retrieval and pulse compression

As described in subsection 2.5.1, the spectral phase of the fundamental pulse $\phi_F(\omega)$ is estimated in first approximation (assumption of a constant phase of the reference pulse) by $\arg[f(\omega)]$, see Equation 2.45. To improve the accuracy of the determined spectral phase, the non-constant phase of the reference pulse is taken into account as described in subsection 2.5. Using an iterative algorithm (see Figure 7), a better estimation of the phase of the pulse to be determined can be made. The determined spectral phases of femtosecond pulses with a center wavelength of 1025 nm for different settings of the PHAROS grating compressor are shown in Figure 30.

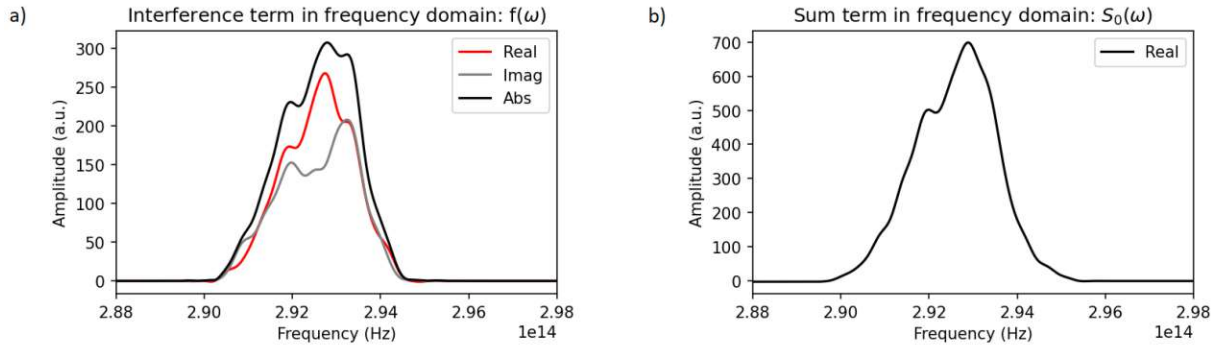


Figure 28: The plots show the interference term (a) and the sum term (b) extracted from the measured SRSI signal $I_{IN}(\omega)$. The pulse characterized here is a dispersion-compensated femtosecond pulse with a center wavelength of 1025 nm.

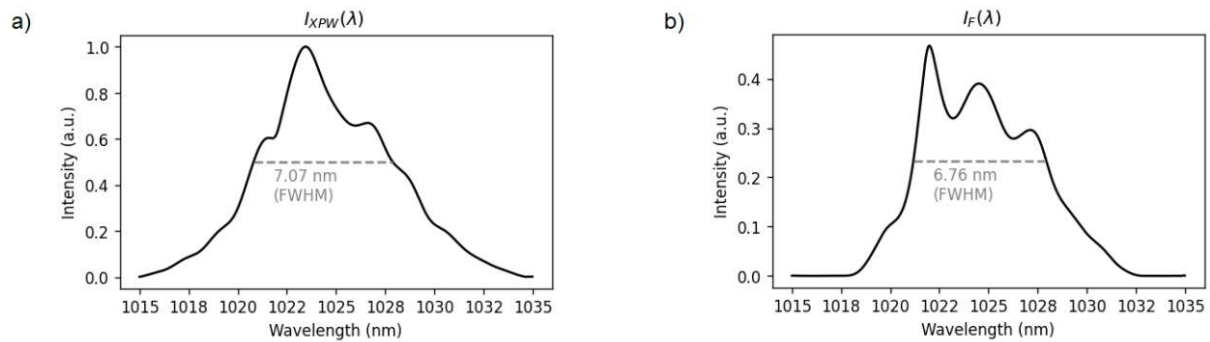


Figure 29: The analytically calculated spectra of the reference pulse $I_{XPW}(\lambda)$ (a) and the fundamental pulse $I_F(\lambda)$ (b) are shown. Intensities are scaled with respect to the maximum intensity of the reference signal $I_{XPW}(\lambda)$. The pulse characterized here is a dispersion-compensated femtosecond pulse with a center wavelength of 1025 nm.

In the case of the PHAROS laser system, the built-in compressor (diffraction grating setup) allows dispersion compensation. By changing the compressor length, a negative or positive chirp can be induced. The best compensation can be determined by gradually changing the compressor length and determining the spectral phase. The best compensation means the flattest possible phase and minimum pulse duration. The determined phases and temporal intensities $I_F(t)$ of pulses for three exemplary settings of the compressor length are displayed in Figure 30. The best compression allowed a pulse with a pulse duration of 271 fs. If the compressor length is changed from this optimum, positive/negative GDD is induced and the pulse duration is increased.

4.3 Determination of dispersion terms and validity ranges using SRSI

In subsection 4.1 the SRSI method to determine the spectral phase and amplitude of a Thales ALPHA kHz pulse (without considering ASE) was presented. The shape of the spectral phase already provides qualitative information about the pulse (flat phase, positive/negative chirp, etc.). For quantification, a polynomial fitting of the spectral phase is performed to determine the chromatic dispersion terms.

As we have seen in Equation 2.9 the spectral phase can be expanded into a Taylor series. Thus it is possible to fit the spectral phase to a p-th degree polynomial to obtain dispersion terms up to p-th order. The fitting polynomial is centered at the peak wavelength of the retrieved spectrum. Note that the calculation and fitting of the spectral phase is performed only for a frequency range where the pulse intensity is larger than 5% of the peak intensity, since the values of the phase are not meaningful at an intensity close to zero. For small intensity values, retrieving the correct phase becomes challenging, which means that if the spectral phase is unwrapped for too large a wavelength range (where the intensity at the edge is very small), the fitted polynomial is not a good approximation of the actual phase. At the same time, however, it is necessary to fit the spectral phase on the largest possible wavelength range where correct retrieval of the phase is still possible in order to obtain the best possible approximation by the polynomial. For the

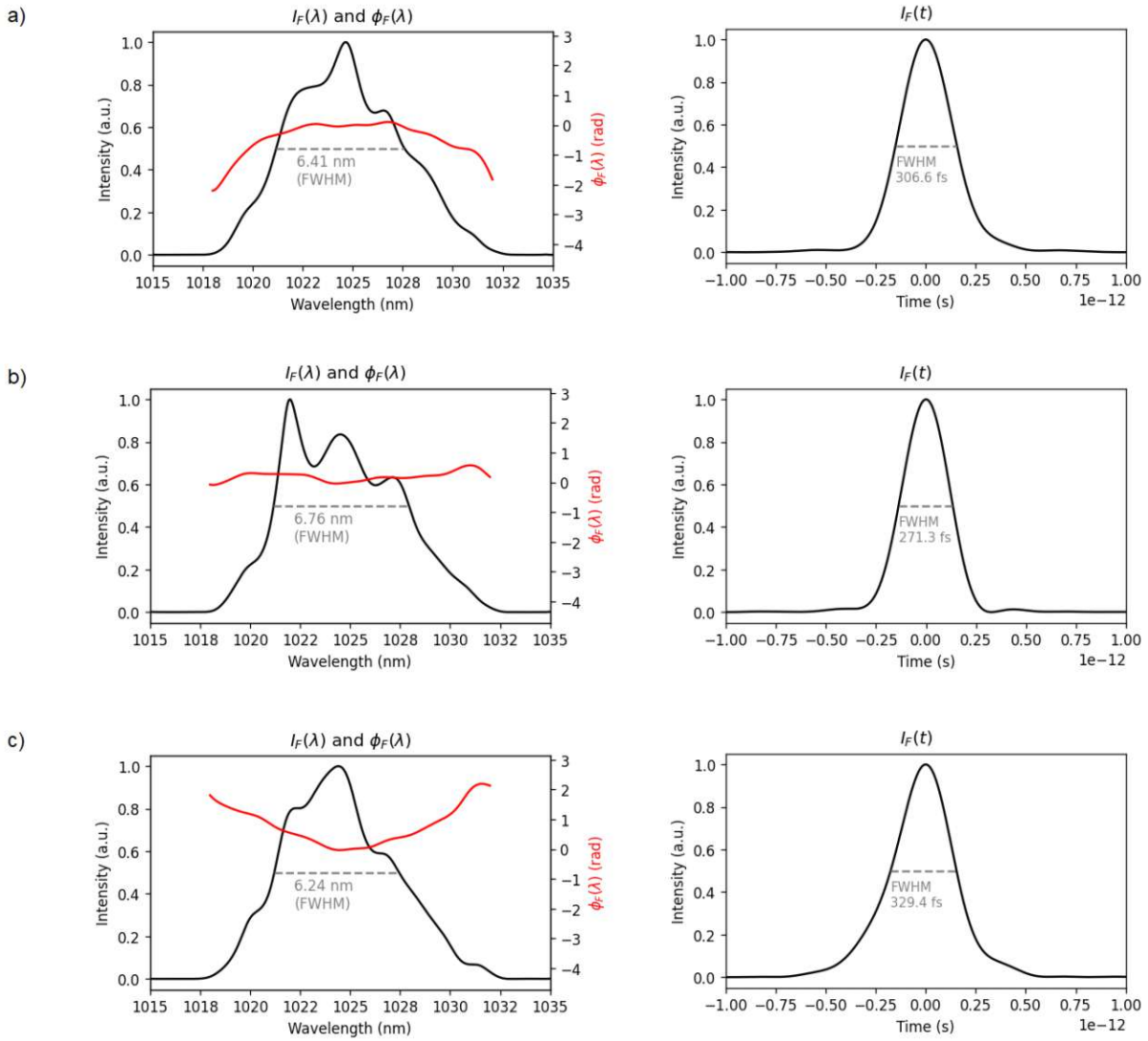


Figure 30: The following plots show the spectral phase and temporal description of different femtosecond pulses with a center wavelength of 1025 nm (PHAROS laser) for different compressor settings. a) Case of negative chirp (compressor length: -10000 steps compared to optimum) b) Case of the best compensation: The phase is approximately constant over the entire bandwidth of the pulse and the pulse duration is shortest possible. c) Case of positive chirp (compressor length: +10000 steps compared to optimum)

polynomial fitting of the spectral phase, no weighting factors were applied. An alternative approach could involve employing an intensity-weighted fit, where the phase is weighted lower at low-intensity frequencies.

For the following experiments the Thales ALPHA kHz laser system, the Fastlite Dazzle pulse shaper and the Ocean Optics HR4000 spectrometer were used.

The experiments in this chapter were performed with a 1 mm thick calcite plate, which yields well-resolved peaks in the interferogram using the Ocean Optics spectrometer. However, it should be noted that the resulting time delay τ between the fundamental and reference pulses is relatively small, as explained in subsection 3.3. This can result in a lack of clear separation between the temporal sum term and the interference term, leading to potential inaccuracies in the pulse characterization. To achieve a more precise determination of the spectral phase and the associated dispersion terms, conducting these experiments with a thicker calcite plate is suggested. However, it is important to consider that for effective resolution of the resulting interferogram, a spectrometer with higher resolution would be required. When using the Anritsu spectrometer, this would significantly increase the time required for the experiments.

Because we characterize pulses with non-negligible dispersion (no flat spectral phase), the dispersion of the reference pulse has to be considered. The estimation of the phase of the fundamental pulse by

$\phi_F(\omega) \approx \arg[f(\omega)]$ is therefore inaccurate and was corrected by taking into account the phase $\phi_{\text{XPW}}(\omega)$ as described in subsection 2.5.1.

A possible incoherent part of the laser output is ignored in the following evaluations.

In the first experiment, the objective is to characterize a sample pulse featuring pure second-order dispersion (GDD of 200 fs²). For this purpose, an initial dispersion-compensated pulse is generated through the fine-compression process involving iterative feedback of the spectral phase into the Dazzler pulse shaper. Subsequently, an additional GDD of 200 fs² is introduced to this dispersion-compensated pulse using the Dazzler pulse shaper. In Figure 31 the spectral phase of this pulse and its fit by a fourth-degree polynomial is shown. The values of the dispersion terms obtained by the polynomial fitting are: GDD = 214.25 fs², TOD = 548.61 fs³, FOD = -96237.98 fs⁴. The magnitude of these values is not as large as it appears. In the case of a pulse with a spectral bandwidth (FWHM) of 30 nm (approximately 14·10¹⁴ Hz), these values result in a change in spectral phase of 0.210, 0.008, and 0.015 rad, respectively, at a distance of half the FWHM from the central wavelength. The calculation of this change in spectral phase, depending on the dispersion terms and the frequency is provided in Equation 2.9.

Since we assumed a dispersion-compensated pulse with additionally introduced GDD, we expect small values for the TOD and FOD terms. Possible reasons for the deviation of the measured GDD value of 214 fs² from the 200 fs² introduced by the Dazzler pulse shaper and the non-zero values of the TOD and FOD are the neglect of higher-order dispersion terms and the inaccurate retrieval of the spectral phase, especially in the edge regions. Moreover, the pulse (without the introduced GDD = 200 fs²) is not exactly dispersion-compensated (see e.g. Figure 21). One way to determine the dispersion terms more accurately is to proceed as discussed in the following paragraph, using a 'reference phase' of a dispersion-compensated pulse.

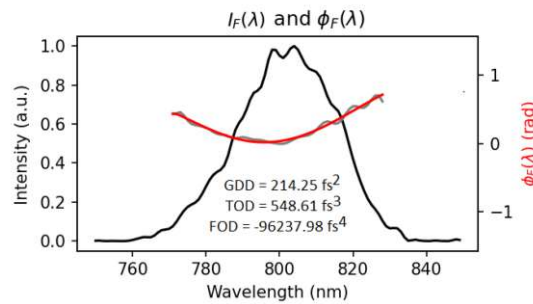


Figure 31: SRSI pulse characterization of a Thales ALPHA kHz laser with center wavelength at 800 nm. The pulse described corresponds to a dispersion compensated pulse (fine compressed by iterative feedback of the spectral phase into the Dazzler pulse shaper), with an additional GDD of 200 fs² subsequently added using the Dazzler pulse shaper. The spectral phase of the pulse with positive GDD is shown in gray. The phase is fitted to a fourth-degree polynomial (red) to obtain the dispersion terms up to order four. (Spectrometer: Ocean Optics HR4000; calcite plate thickness: 1 mm)

4.3.1 Determination of relative GDD and TOD of different pulses

Using a dispersion-compensated pulse as a reference, the method presented here allows the relative GDD and TOD of different pulses to be determined with a higher accuracy than fitting the retrieved spectral phase to a high-order polynomial.

In the Taylor expansion of the spectral phase, in general, higher-order dispersion terms cannot be assumed to be zero, so high-order fitting polynomials would be necessary. However, if only the deviation of the second or third-order dispersion with respect to a certain pulse is of interest, a fitting polynomial of second or third-order is sufficient. In the experiment, this is realized as follows.

An initial pulse is generated through the fine-compression process involving iterative feedback of the spectral phase into the Dazzler pulse shaper. The measured spectral phase of this dispersion compensated pulse can be defined as 'reference phase', see Figure 32 a). If the GDD or TOD is now changed by the Dazzler pulse shaper by a certain value, the spectral phase of the dispersion-compensated pulse can be subtracted from the measured spectral phase of the pulse with nonzero GDD or TOD. The phase thus

obtained should correspond to a polynomial of at most third degree. This means that this difference of spectral phases can be accurately fitted with a third degree polynomial. If the spectral phase (of a pulse with additional GDD or TOD with respect to the compensated pulse) determined in this way deviates from a polynomial of maximum third degree, the deviation is a measure of the error of the determined phase, see Figure 32 b). With the fitting parameters of the fitted polynomial the values for the GDD and TOD can be determined using Equation 2.9.

A dispersion compensated femtosecond pulse with a center wavelength at 800 nm (fine compression process with iterative feedback of the spectral phase into the Dazzler pulse shaper), with an additional GDD of 200 fs² subsequently added using the Dazzler pulse shaper is used as an example, see Figure 32 b). Fitting the retrieved spectral phase corrected by subtracting the spectral phase of the dispersion-compensated pulse to a fourth-degree polynomial yields the following values: GDD = 201.38 fs², TOD = -238.7 fs³ and FOD = 6349.28 fs⁴. Since the pulse shaper only introduces additional GDD with respect to the original dispersion-compensated pulse and the higher-order dispersion is eliminated by subtracting the spectral phase of the dispersion-compensated pulse, the third and fourth-order terms are expected to be zero. The observed deviation of the values from zero is small (smaller than the retrieved dispersion terms by fitting the phase to a fourth-degree polynomial without using a reference phase) and could possibly be explained by the inaccurate retrieval of the spectral phase, especially in the edge regions and the inaccuracy of the phase manipulation by the pulse shaper.

As mentioned before, for better accuracy of the determined phase, an iterative algorithm (see Figure 7) is used to take into account the non-constant phase of the reference pulse, since the spectral phase of the pulse to be characterized is not flat. Note: If the non-constant phase of the reference pulse is neglected and the iterative correction algorithm is not performed (which means that the phase is estimated by $\phi_F(\omega) \approx \arg[f(\omega)]$), the calculated GDD would only be 176.34 fs², resulting in a deviation of more than 10%.

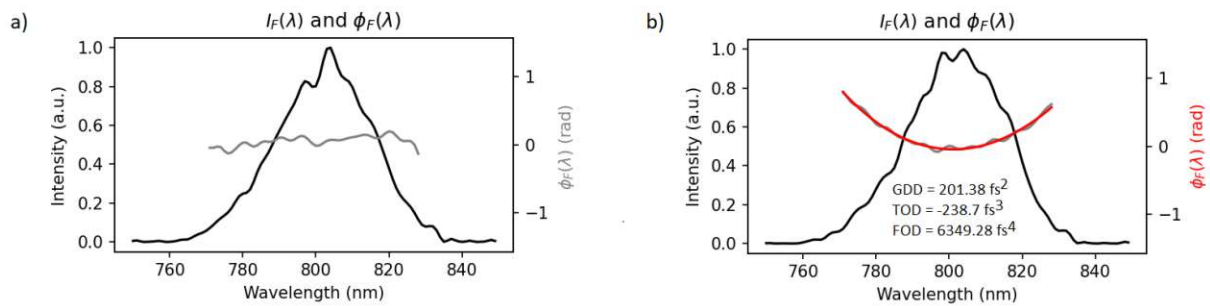


Figure 32: SRSI pulse characterization of Thales ALPHA kHz laser with center wavelength at 800 nm. a) The phase of a dispersion-compensated femtosecond pulse is represented in gray. The compensation is achieved through a fine-compression process that incorporates iterative feedback of the spectral phase into the Dazzler pulse shaper. b) Presented in gray is the spectral phase of the initially dispersion-compensated pulse, with an additional GDD of 200 fs² subsequently added using the Dazzler pulse shaper. It's important to note that the spectral phase of the compensated pulse displayed in a) has been subtracted from this phase to exclude higher-order dispersion. The deviation of the measured phase (gray) from the fitting polynomial (red) is a measure for the error of the determined phase. The dispersion terms up to order four were obtained by fitting the high-order dispersion corrected phase to a fourth-degree polynomial.

(Spectrometer: Ocean Optics HR4000; calcite plate thickness: 1 mm)

4.3.2 Validity range of retrieved GDD and TOD

By changing the second- and third-order dispersion of the pulse to be determined by the Dazzler pulse shaper, it is possible to estimate the range of validity or limitation of the SRSI method for determining the second- and third-order dispersion of the pulse. For this purpose, the GDD and TOD were varied stepwise by the Dazzler pulse shaper and the results of the SRSI analysis plotted against these values. For large GDD and TOD values, a deviation of the GDD and TOD determined by the SRSI method from the GDD and TOD introduced by the pulse shaper is expected. When employing Equation 2.45 to determine the phase, a deviation from the actual values is expected due to the assumption of a constant phase of the XPW pulse. In this experiment, however, the phase is determined using the iterative correc-

tion algorithm described in Figure 7, which takes into account the non-constant phase of the XPW pulse. Nevertheless, even within this approach, accurately extracting the non-constant spectral phase of the fundamental pulse through the SRSI algorithm remains a challenge, as the iterative correction process itself can introduce inaccuracies.

The interferograms for pulse characterization were acquired with the Ocean Optics HR4000 spectrometer.

Procedure:

An initial pulse is generated through the fine-compression process involving iterative feedback of the spectral phase into the Dazzler pulse shaper. The measured spectral phase of this dispersion compensated pulse can be defined as 'reference phase'. Then the GDD and TOD can be changed step by step by the Dazzler pulse shaper, and the spectral phase can be determined respectively. The examined values of TOD are [-6000, -3000, 0, 3000, 6000] fs³ relative to the dispersion-compensated pulse. The examined values of GDD are [-400, -200, 0, 200, 400, 600] fs² relative to the dispersion-compensated pulse. To better understand how these TOD and GDD values affect the spectral phase of the pulse, the following estimation proves to be insightful. For a pulse featuring a spectral bandwidth (FWHM) of 30 nm (approximately 14·10¹⁴ Hz), these values of the dispersion terms lead to a change of the spectral phase of 0.1 rad (for TOD = 6000 fs³) and 0.4 rad (for GDD = 400 fs²) at a distance of half the FWHM from the central wavelength. The calculation of this change in spectral phase, relative to the dispersion terms and frequency, is given in Equation 2.9.

After determining the spectral phases of the pulses with modified GDD or TOD, the 'reference phase' can be subtracted from the retrieved spectral phases. The spectral phases of the pulses with modified GDD should thus correspond to a second-order polynomial and can be fitted with a second-order polynomial. Equivalently, the spectral phases of the pulses with modified TOD can be fitted with a third-order polynomial. The results of the stepwise change of GDD and TOD by the pulse shaper versus the determined GDD and TOD by SRSI can be seen in Figure 33 and Figure 34. It is evident that a deviation from a linear dependence occurs beyond a certain threshold. The findings indicate that when the GDD values exceed ± 400 fs² or TOD values exceed ± 3000 fs³, the experimentally determined dispersion terms by SRSI can deviate by more than 15 % from the actual values.

In addition, the GDD values were determined for the stepwise change of the TOD. Since no GDD was introduced by the pulse shaper, the GDD values obtained from the fit should remain equal to zero (see Figure 34 b)). The results suggest that the pulses manipulated by the pulse shaper with different values of TOD have no relevant influence on the corresponding GDD values determined by SRSI, which is expected.

An improvement of this experiment, the determination of the validity range of the determined GDD and TOD, would be the pulse characterization using a spectrometer with higher resolution. Unfortunately, this is very time-consuming e.g. for the case of the Anritsu spectrometer. Another possibility would be the use of a larger and finer interval of the investigated GDD and TOD values.

A possible future extension for the discussion of the validity range would be the numerical simulation of pulses with different values of the dispersion terms, and their interferogram, and thus the possible validation of the values of these dispersion terms determined by the SRSI algorithm from the simulated interferogram.

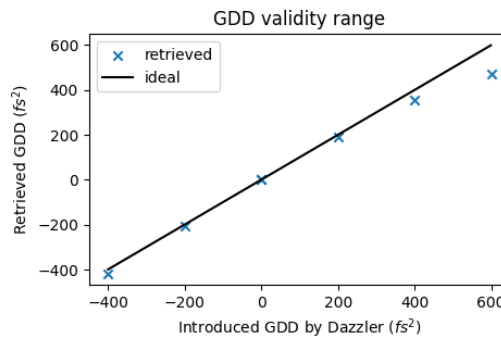


Figure 33: The graph illustrates the GDD terms obtained by fitting the determined spectral phase by SRSI to a second-degree polynomial, versus the GDD values set by the Dazzler pulse shaper. The deviation of the determined values from the ideal allows an estimation for the validity range.

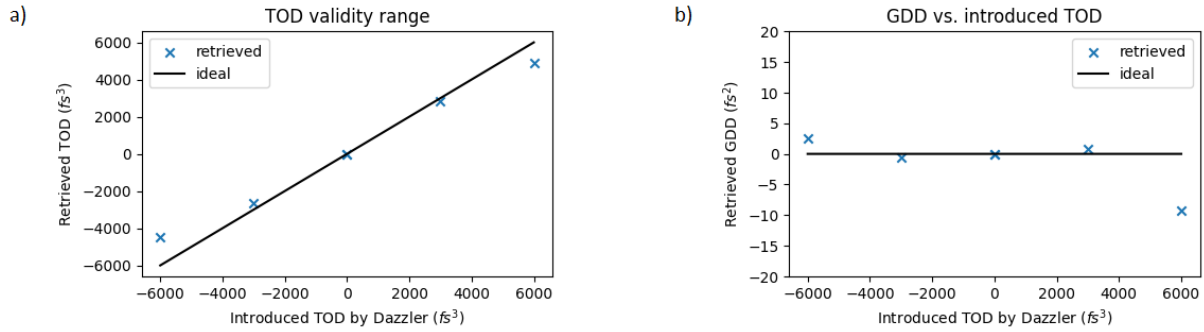


Figure 34: a) The graph illustrates the TOD terms obtained by fitting the determined spectral phase by SRSI to a third-degree polynomial, versus the TOD values set by the Dazzler pulse shaper. The deviation of the determined values from the ideal allows an estimation of the validity range. b) GDD values determined for the stepwise change of the TOD by the pulse shaper. The GDD should remain equal to zero.

4.4 Consideration of ASE in SRSI pulse characterization of a Thales ALPHA kHz laser

To determine the incoherent ASE part of the laser output, the measured interferogram of a conventional SRSI measurement alone is not sufficient. In the chosen approach to determine the ASE, in addition to the interferogram, the spectrum of the XPW signal and the spectrum of the output signal of the laser are recorded separately. It is important to emphasize that the measured XPW spectrum does not contain ASE. This is due to the fact that XPW is a third-order nonlinear phenomenon that occurs only at high intensities, making it insignificant for small amplitudes. Consequently, if the intensity of the ASE signal is low, its contribution is negligible in the XPW signal. The XPW signal can therefore be considered purely coherent. In contrast, the output signal of the laser consists of a coherent part, in the following called fundamental signal with intensity $I_F(\omega)$, and an incoherent part, due to ASE with intensity $I_{ASE}(\omega)$. The three required spectra of the XPW signal $I_{XPW}(\omega)$, output signal $I_{FA}(\omega) = I_F(\omega) + I_{ASE}(\omega)$ and interferogram $I_{IN}(\omega)$ are measured as described in subsection 3.4. In contrast to subsection 3.4, the measured signal of the laser output is now treated as $I_{FA}(\omega)$ instead of $I_F(\omega)$.

The pulse to be characterized is a dispersion-compensated pulse of a Thales Alpha Ti:Sa laser. The dispersion-compensated pulse was obtained as described in subsection 4.1 by the fine-compression process involving iterative feedback of the spectral phase into the Dazzler pulse shaper. The used calcite plate has a thickness of 3 mm and the used Anritsu spectrometer has a resolution of 0.059 nm. The high resolution of the spectrometer is crucial for effectively resolving the interferogram, allowing for a distinct separation between the interference term and the sum term. The following analysis uses the spectra depicted in Figure 19 a) as input data.

To be able to distinguish in the following the intensities of the directly measured spectra ($I_{FA}^M(\omega)$ and $I_{XPW}^M(\omega)$) from the intensities correctly scaled for the evaluations and calculations ($I_{FA}(\omega)$ and $I_{XPW}(\omega)$) the superscript 'M' is used for the measured spectra.

4.4.1 Estimation of the ASE spectrum

In the first step, the measured interferogram is processed and the sum term $S_0(\omega)$ and interference term $f(\omega)$ are determined analogously to subsection 4.1.

The independently measured XPW spectrum $I_{XPW}^M(\omega)$ and fundamental spectrum $I_{FA}^M(\omega)$ can be smoothed by an inverse Fourier transform followed by multiplying a super-Gaussian window function in the time domain. The width of the window is chosen the same as for the interferogram to obtain the same filter properties as for the sum and interference term. After multiplication with the window function, the signal is Fourier transformed again. This method corresponds to a band-pass filter.

After that, the spectra $I_{FA}^M(\omega)$ and $I_{XPW}^M(\omega)$ are scaled as described in Equation 2.49 by fitting them to the sum term $S_0(\omega)$ using scaling factors, see Figure 35. A deviation of the sum of $I_{FA}^M(\omega)$ and $I_{XPW}^M(\omega)$ from the sum term $S_0(\omega)$ is due to the noise of the measurement signal (fluctuation of the laser output power and noise of the detector in the spectrometer) and the used filters in the data processing for sep-

arating the sum and interference term (multiplication of the Fourier transformed signal with a window function in the time domain to extract the sum and interference term). This error also limits the accuracy of the ASE signal determination.

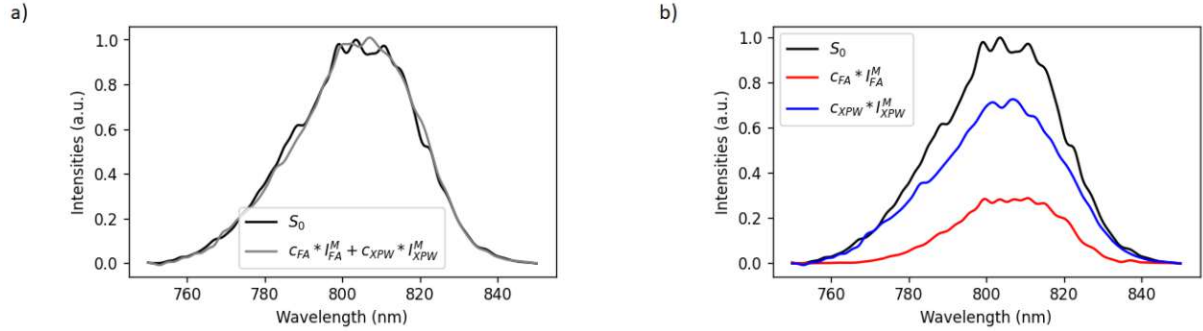


Figure 35: a) The separately measured spectra $I_{FA}^M(\lambda)$ and $I_{XPW}^M(\lambda)$ are scaled by fitting them to the sum term $S_0(\lambda)$ using scaling factors. b) Shown are the scaled spectra $I_{FA}^M(\lambda)$ and $I_{XPW}^M(\lambda)$ with scaling factors c_{FA} and c_{XPW} . It can be seen that the scaled XPW signal is stronger than the fundamental signal.

Intensities are scaled with respect to the maximum intensity of the sum term $S_0(\lambda)$.

Now, using the sum term, interference term, scaled fundamental spectrum and scaled XPW spectrum, the ASE can be calculated in two ways as described in Equation 2.53 and Equation 2.54. The results of these calculations are shown in Figure 36. It should be noted that the first method of calculating the ASE spectrum is more accurate because it uses the directly measured (and scaled) expression $I_{FA}(\omega) = c_{FA} \cdot I_{FA}^M(\omega)$ instead of the composite term $I_{FA}(\omega) = S_0(\omega) - c_{XPW} \cdot I_{XPW}^M(\omega)$. This is also evident from the negative intensities of the ASE signal depicted in Figure 36 b) (clearly an outcome of inaccuracies in the calculation). The ratio of the integrated intensities over the wavelength range (750 nm

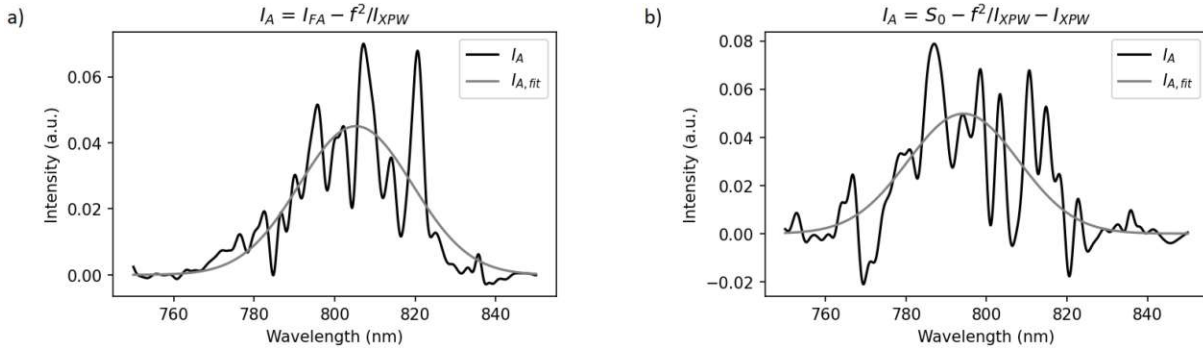


Figure 36: Estimation of the ASE spectrum using the sum term and interference term determined from the interferogram and the two separately measured and scaled XPW and fundamental spectra. A Gaussian fit is shown in gray. a) Calculation of the ASE intensity by $I_{ASE}(\lambda) = I_{FA}(\lambda) - I_F(\lambda)$. b) Calculation of the ASE intensity by $I_{ASE}(\lambda) = S_0(\lambda) - I_F(\lambda) - I_{XPW}(\lambda)$.

Intensities are scaled with respect to the maximum intensity of the sum term $S_0(\lambda)$.

to 850 nm) of the ASE spectrum to the fundamental spectrum ranges from 21.5 % to 23.1 %, depending on the calculation method. The ASE part of the total laser output signal $I_{ASE}(\omega)/(I_{ASE}(\omega) + I_F(\omega))$ thus corresponds to about 17.7 % to 18.8 %.

4.4.2 Influence of ASE on the calculated fundamental and XPW spectrum

By comparing the formulas for the calculation of the amplitude of the XPW spectrum with and without consideration of ASE (Equation 2.35 and Equation 2.55) a statement on the influence of ASE on the amplitude can already be made (the same applies to the fundamental spectrum, see Equation 2.36 and Equation 2.56). The magnitude of the intensity of the actual XPW spectrum (calculation with consideration of ASE) is larger than or equal to the intensity of the calculated XPW spectrum without consideration of ASE. The opposite is true for the magnitude of the intensity of the fundamental

spectrum. It should be noted that the formulas are valid under the assumption that the XPW spectral components are more intense than the fundamental ones at each frequency. (In the case that the fundamental spectral components are more intense than XPW pulse ones at each frequency, the formulas Equation 2.37, Equation 2.38, Equation 2.57 and Equation 2.58 apply.)

The magnitudes of the calculated spectra without consideration of ASE and the actual magnitudes considering ASE can be compared, this is shown in Figure 37 a) and b) and will be discussed in the following.

The magnitude of the fundamental spectrum without consideration of ASE calculated from the measured interferogram using the SRSI algorithm (see Equation 2.36 or Equation 2.38) differs from the actual magnitude (obtained by $I_F(\omega) = |f(\omega)|^2 / (c_{XPW} \cdot I_{XPW}^M(\omega))$, see Equation 2.52). The deviation can be quantified by the ratio of the integral of the spectrum calculated as described in the SRSI algorithm (without consideration of ASE) over the wavelength to the integral of the actual spectrum (obtained by Equation 2.52) over the wavelength. The integration is performed over the wavelength interval 760–840 nm, since the intensities outside this range are close to zero. The ratio determined in this way has a value of 0.940. This means that the magnitude of the analytically calculated fundamental spectrum without consideration of ASE is about 6.0 % smaller than the determined fundamental spectrum with consideration of ASE.

Also the magnitude of the XPW spectrum without considering ASE calculated as described in the SRSI algorithm (using Equation 2.35 or Equation 2.37) differs from the actual magnitude (obtained by direct measurement and scaling $I_{XPW}(\omega) = c_{XPW} \cdot I_{XPW}^M(\omega)$). Again, the deviation can be quantified by the ratio of the integral of the spectrum calculated as described in the SRSI algorithm (without consideration of ASE) over the wavelength to the integral of the directly measured and scaled spectrum over the wavelength, using the same wavelength interval as before. The ratio determined in this way has a value of 1.071. This means that the magnitude of the analytically calculated XPW spectrum without consideration of ASE is about 7.1 % larger than the actual XPW spectrum.

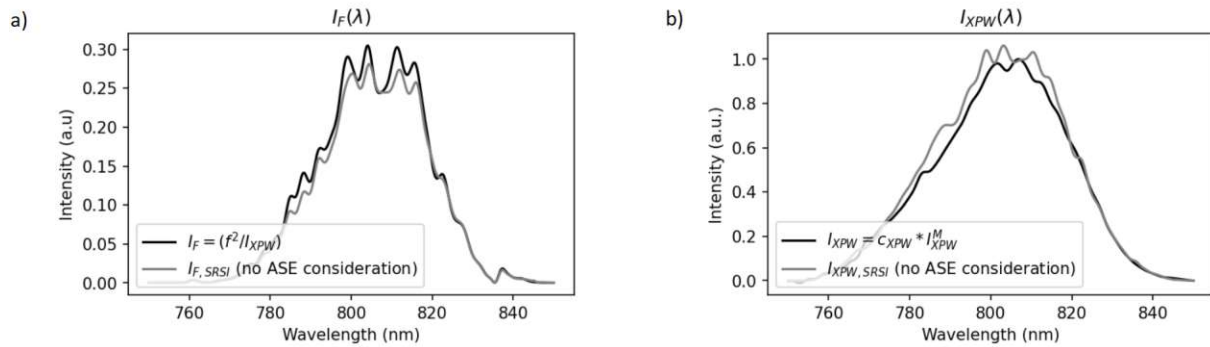


Figure 37: The calculated magnitudes of the fundamental and the XPW spectrum without considering ASE differ from the actual magnitudes considering ASE. Intensities are scaled with respect to the maximum intensity of the measured XPW spectrum $I_{XPW}(\lambda)$. a) The actual XPW spectrum is obtained by direct measurement and scaling $I_{XPW}(\lambda) = c_{XPW} \cdot I_{XPW}^M(\lambda)$, shown in black. The calculation as described in the SRSI algorithm without considering ASE is shown in gray. b) The actual fundamental spectrum is obtained by $I_F(\lambda) = |f(\lambda)|^2 / (c_{XPW} \cdot I_{XPW}^M(\lambda))$, shown in black. The calculation of $I_F(\lambda)$ as described in the SRSI algorithm without considering ASE is shown in gray.

The influence of ASE on the fundamental and XPW spectra calculated as described in the SRSI algorithm without taking ASE into account (using Equation 2.35 – Equation 2.38) can also be calculated in a numerical simulation. For this, first the bandwidths and center wavelengths of the fundamental and the ASE spectrum are determined in order to correctly model the spectra in the numerical simulation. The bandwidth and center wavelength of the ASE spectrum is determined by fitting a Gaussian function to the ASE spectrum (see Figure 36). The ASE spectrum is determined as specified in Equation 2.53, since this calculation method is more accurate than Equation 2.54 (as described in subsection 4.4.1). This results in a bandwidth of 33.1 nm and a center wavelength of 805.2 nm for the ASE spectrum. For the determination of the bandwidth and the center wavelength of the fundamental spectrum (obtained by Equation 2.52) also a Gaussian fit is used. This results in a bandwidth of 31.2 nm and a center wave-

length of 806.0 nm for the fundamental spectrum. Gaussian fits are used for determining the FWHM and central wavelength, as this approach is more precise than directly measuring the spectrum's width at half intensity. When directly measuring the bandwidth at half intensity, the obtained width is influenced by noise or minor local intensity fluctuations.

It is essential to highlight that the central wavelength and bandwidth of the ASE spectrum closely resemble those of the fundamental spectrum. This similarity allows us to assume a proportional relationship between the ASE and fundamental spectrum intensities. Also, the fundamental spectrum, computed using SRSI without accounting for ASE as described in Equation 2.36 or Equation 2.38, has a similar central wavelength (806.3 nm) and bandwidth (30.8 nm), both of which were also determined through Gaussian fitting.

In order to compare the experimentally determined deviation (deviation of the calculated fundamental and XPW spectrum by SRSI without consideration of ASE using Equation 2.35 – Equation 2.38 from the spectra determined by Equation 2.42 – Equation 2.43) with the calculated deviation of the numerical simulation, the following procedure is followed. First, in the numerical simulation in Python, the fundamental and ASE spectra measured and determined in the experiment are reproduced by using their Gaussian fitting functions with the fitting parameters described above. The XPW spectrum is generated using the Fourier transformed fundamental spectrum, the relation Equation 2.24 and Fourier back transformation. The maximum intensity of the fundamental spectrum is scaled to 30.0 % of the maximum intensity of the XPW spectrum (determined by comparing the fitting parameters of the Gaussian fitting functions). The maximum intensity of the ASE spectrum is scaled to 21.5 % of the maximum intensity of the fundamental spectrum.

These three spectra (fundamental, XPW, and ASE) serve as references for subsequent evaluations and comparisons.

The sum term $S_0(\omega)$ and the interference term $f(\omega)$ can be calculated numerically by Equation 2.47 and Equation 2.48. Using these two terms, the fundamental and XPW spectra can now be calculated as described in the SRSI algorithm using Equation 2.35 and Equation 2.36 as suggested in Oksenhendler et al. [10]. This calculation does not consider ASE and the difference between the spectra calculated as described in the SRSI algorithm without considering ASE and the original spectra as defined in the simulation can be analyzed. This is shown in Figure 38 a) and b).

As also seen with the experimentally determined spectra, there is a difference between the magnitudes of the intensities of the spectra calculated as described in the SRSI algorithm without considering ASE and the original spectrum as defined in the simulation. The deviation is quantified by the ratio of the integral of the spectrum calculated as described in the SRSI algorithm over the wavelength to the integral of the actual spectrum over the wavelength. The ratio determined in this way for the fundamental spectrum has a value of 0.939. This means that the magnitude of the fundamental spectrum calculated as described in the SRSI algorithm without consideration of ASE is about 6.1 % smaller than the actual fundamental spectrum.

The deviation of the magnitude of the intensity of the XPW spectrum calculated as described in the SRSI algorithm without considering ASE from the original spectrum as defined in the simulation can be calculated similarly as for the fundamental spectrum. The ratio determined in this way has a value of 1.050. This means that the magnitude of the XPW spectrum calculated as described in the SRSI algorithm without consideration of ASE is about 5.0% larger than the actual XPW spectrum.

The experimentally determined deviations and the deviations determined by the numerical simulation of the magnitudes of the XPW and fundamental spectrum by the calculations without consideration of ASE from the actual magnitudes show good agreement. Discrepancies may be due to the fact that a Gaussian shape is assumed in the modeling (fitting) of the spectra for the numerical simulation, which is only an approximation. In addition, the experimentally determined spectra are subject to errors due to the measurement process of the spectra itself (fluctuations of the intensity of the laser output). Also the procedure described in subsection 2.5 for the determination of the sum and interference terms and the fundamental and XPW spectrum without consideration of ASE can lead to deviations due to the Fourier transforms and filtering.

The evaluation shows that one must be aware that the magnitudes of the determined spectra deviate from the actual magnitudes without taking ASE into account. In the experiment presented here, this discrepancy was of the order of 5 to 7 %. The consideration of ASE also affects the characterization of

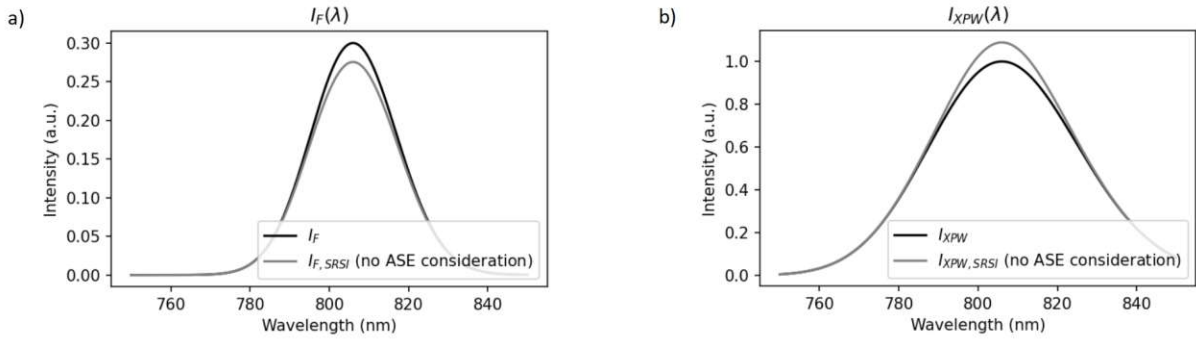


Figure 38: The figure displays the difference between the fundamental and XPW spectra calculated by the SRSI algorithm, where ASE is not taken into account despite its presence, and the original spectra as defined in the simulation. With the help of this numerical simulation, the difference between the spectra calculated as described in the SRSI algorithm without considering ASE and the actual spectra can be shown. Intensities are scaled with respect to the maximum intensity of the actual XPW spectrum. The magnitude of the ASE intensity corresponds in this example to 21.5 % of the magnitude of the fundamental spectrum intensity. The central wavelength of the ASE spectrum (805 nm) corresponds approximately to that of the fundamental spectrum. a) The actual fundamental spectrum $I_F(\lambda)$ is shown in black. The intensity $I_F(\lambda)$ calculated as described in the SRSI algorithm without considering ASE is shown in gray. b) The actual XPW spectrum $I_{XPW}(\lambda)$ is shown in black. The intensity $I_{XPW}(\lambda)$ calculated as described in the SRSI algorithm without considering ASE is shown in gray.

the spectral phase of the fundamental pulse, since the iterative correction (consideration of a non-flat XPW spectral phase) depends on the fundamental spectrum (see Figure 7).

If the ASE spectrum is determined by an alternative method (for example by measuring the optical spectrum before and after the optical amplifier to evaluate the optical gain and the ASE noise spectral density, as described in [45]), the extended formulas (Equation 2.55) and (Equation 2.56) (respectively (Equation 2.57) and (Equation 2.58)) can be employed to calculate the XPW and fundamental spectra based on the interferogram measured during the SRSI evaluation, taking into account the presence of an incoherent laser output component such as ASE. Thus, the fundamental spectrum (as described in Equation 2.52) can be determined without the necessity of a separate measurement of the XPW spectrum.

5 Conclusion

In this thesis, the characterization of pulses from two solid-state femtosecond lasers in the near-infrared region was investigated. The main objective was to determine the characteristics of the pulses using self-referenced spectral interferometry (SRSI). SRSI is a technique that allows to determine both the spectral phase and the spectral amplitude of laser pulses. A thorough analysis was conducted on the experimental setup, emphasizing the critical role of the calcite plate's thickness as a significant parameter. A detailed description of the impact of the calcite plate's thickness on the SRSI evaluation has been provided. It was demonstrated that the resolution of the spectrometer used played a significant role in the accuracy of pulse characterization, whereby the resolution has a greater impact on the accurate determination of the spectra's magnitude rather than on the precise determination of the spectral phase.

In the process of determining the spectral phase, polynomial fitting was utilized to determine the second, third and fourth-order dispersion terms. By employing dispersion compensation devices like a grating compressor or an AOPDF pulse shaper, it was possible to flatten the phase across the entire spectral bandwidth, thereby achieving minimum pulse durations. For the Thales ALPHA kHz laser, a dispersion-compensated pulse yielded a duration of 38 fs. In the case of the Light Conversion PHAROS laser, the best dispersion compensation resulted in pulse durations of 271 fs. Measured pulse durations may vary from the manufacturer's indicated minimum values due to their sensitivity to environmental conditions like temperature and humidity. Furthermore, any deviation of the laser output spectrum from a Gaussian profile could result in an extended minimum pulse duration.

To ensure the validity of the SRSI algorithm, the range of applicability for determining the second- and third-order dispersion terms was estimated based on SRSI measurements of pulses with well-defined dispersion. This estimation was employed in characterizing femtosecond pulses from the Thales ALPHA kHz laser (38 fs) using the Ocean Optics HR4000 spectrometer with a resolution of 0.75 nm. The results indicated that for pulses with GDD (group delay dispersion) values exceeding $\pm 400 \text{ fs}^2$ or TOD (third-order dispersion) values exceeding $\pm 3000 \text{ fs}^3$, a deviation of more than 15 % in the experimentally determined dispersion terms can be expected. Consequently, for pulses with significant dispersion, the spectral phase determined by SRSI may not correspond to the actual phase. The accuracy of the SRSI method is therefore enhanced when the phase is further flattened during the SRSI procedure.

An extended pulse characterization using SRSI was also studied, incorporating an incoherent component in the analytical description. This allowed the determination of the amplified spontaneous emission (ASE) spectrum. This extension shows that for the determination of the incoherent ASE component the measured interferogram of a conventional SRSI measurement alone is not sufficient, but also the XPW spectrum and the spectrum of the output signal of the laser must be recorded separately. The experimentally determined ASE spectrum of the Thales ALPHA kHz was acquired, revealing an ASE spectrum intensity equivalent to 21.5 % of the intensity of the fundamental spectrum. The analysis demonstrates that the central wavelength and bandwidth of the ASE spectrum closely resemble those of the fundamental spectrum. This similarity indicates a proportional relationship between the intensities of the ASE spectrum and the fundamental spectrum. ASE also influenced the fundamental and XPW spectra calculated using the SRSI algorithm. Taking ASE into account, the spectra deviate by about 5 % in magnitude with respect to the calculated spectra without taking ASE into account (at an ASE intensity of about one third of the fundamental spectrum intensity).

One possible extension of this work could involve conducting range of applicability experiments to estimate the range of validity of the SRSI method for determining the second- and third-order dispersion terms using a higher resolution spectrometer, such as the Anritsu spectrometer. This enhancement would lead to increased accuracy in determining the spectral phase, subsequently enhancing the precision of the dispersion terms as well. In addition, studying a broader range and finer interval of GDD and TOD values would allow a more precise determination of the range of applicability.

One approach to reduce the pulse duration of the Thales ALPHA kHz laser involves manipulating the spectral amplitude in addition to the spectral phase in the AOPDF pulse shaper. By shaping the amplitude profile to resemble a Gaussian distribution, for instance, by slightly reducing the intensity around the center wavelength, the bandwidth can be increased, resulting in a shorter pulse duration. This approach helps prevent gain narrowing and yields a smoother spectral shape. Optimizing this amplitude shaping in the pulse shaper could be a potential focus for future investigations.

References

- [1] P. A. Franken et al. “Generation of Optical Harmonics”. In: *Phys. Rev. Lett.* 7 (4 Aug. 1961), pp. 118–119. DOI: 10.1103/PhysRevLett.7.118.
- [2] F. Brunel. “Harmonic generation due to plasma effects in a gas undergoing multiphoton ionization in the high-intensity limit”. In: *J. Opt. Soc. Am. B* 7.4 (Apr. 1990), pp. 521–526. DOI: 10.1364/JOSAB.7.000521.
- [3] A. L’Huillier, X. F. Li, and L. A. Lompré. “Propagation effects in high-order harmonic generation in rare gases”. In: *J. Opt. Soc. Am. B* 7.4 (Apr. 1990), pp. 527–536. DOI: 10.1364/JOSAB.7.000527.
- [4] R.W. Boyd and D. Prato. *Nonlinear Optics*. Elsevier Science, 2008. ISBN: 9780080485966.
- [5] B. Rethfeld et al. “Timescales in the response of materials to femtosecond laser excitation”. In: *Applied Physics A* 79 (Sept. 2004), pp. 767–769. DOI: 10.1007/s00339-004-2805-9.
- [6] X. Liu, D. Du, and Gé. Mourou. “Laser ablation and micromachining with ultrashort laser pulses”. In: *IEEE Journal of Quantum Electronics* 33 (1997), pp. 1706–1716.
- [7] Ahmed H. Zewail. “Laser Femtochemistry”. In: *Science* 242.4886 (1988), pp. 1645–1653. DOI: 10.1126/science.242.4886.1645.
- [8] Rick Trebino. *Frequency-Resolved Optical Gating: The Measurement of Ultrashort Laser Pulses*. Springer Science+Business Media New York, 2000. ISBN: 978-1-4613-5432-1.
- [9] C. Iaconis and I. A. Walmsley. “Self-referencing spectral interferometry for measuring ultrashort optical pulses”. In: *IEEE Journal of Quantum Electronics* 35.4 (1999), pp. 501–509. DOI: 10.1109/3.753654.
- [10] N. Forget et al. T. Oksenhendler S. Coudreau. “Self-referenced spectral interferometry”. In: *Applied Physics B* 99 (Apr. 2010), pp. 7–12. DOI: <https://doi.org/10.1007/s00340-010-3916-y>.
- [11] Dimitar Popmintchev et al. “Theory of the Chromatic Dispersion, Revisited”. In: *arXiv: Optics* (Oct. 2020). DOI: <https://doi.org/10.48550/arXiv.2011.00066>.
- [12] Sebastian Keppler et al. “The generation of amplified spontaneous emission in high-power CPA laser systems”. In: *Laser & Photonics Reviews* 10.2 (2016), pp. 264–277. DOI: <https://doi.org/10.1002/lpor.201500186>.
- [13] N.P. Barnes and B.M. Walsh. “Amplified spontaneous emission-application to Nd:YAG lasers”. In: *IEEE Journal of Quantum Electronics* 35.1 (1999), pp. 101–109. DOI: 10.1109/3.737626.
- [14] J.C. Diels et al. *Ultrashort Laser Pulse Phenomena*. Optics and photonics. Elsevier Science, 2006. ISBN: 9780080466408.
- [15] Yong-Ho Cha et al. “Simple method for the temporal characterization of amplified spontaneous emission in femtosecond terawatt Ti:sapphire lasers”. In: *Appl. Opt.* 46.28 (Oct. 2007), pp. 6854–6858. DOI: 10.1364/AO.46.006854.
- [16] F. Träger. *Springer Handbook of Lasers and Optics*. Springer Handbooks. Springer Berlin Heidelberg, 2012. ISBN: 9783642194092.
- [17] C.B. Hitz, J.J. Ewing, and J. Hecht. *Introduction to Laser Technology*. Wiley, 2012. ISBN: 9780470916209.
- [18] Donna Strickland and Gerard Mourou. “Compression of amplified chirped optical pulses”. In: *Optics Communications* 56.3 (1985), pp. 219–221. ISSN: 0030-4018. DOI: [https://doi.org/10.1016/0030-4018\(85\)90120-8](https://doi.org/10.1016/0030-4018(85)90120-8).
- [19] Tae Moon Jeong and Jongmin Lee. “Femtosecond petawatt laser”. In: *Annalen der Physik* 526.3-4 (2014), pp. 157–172. DOI: <https://doi.org/10.1002/andp.201300192>.
- [20] *Femtopower Compact Pro, Femtosecond Multi-pass Amplifier, User’s Manual, Version 3.3*. FEM-TOLASERS Produktions GmbH.
- [21] Ursula Keller. *Ultrafast lasers : a comprehensive introduction to fundamental principles with practical applications*. Graduate Texts in Physics. Springer, 2021. ISBN: 3030825310.
- [22] Pierre Tournois. “Acousto-optic programmable dispersive filter for adaptive compensation of group delay time dispersion in laser systems”. In: *Optics Communications* 140.4 (1997), pp. 245–249. ISSN: 0030-4018. DOI: [https://doi.org/10.1016/S0030-4018\(97\)00153-3](https://doi.org/10.1016/S0030-4018(97)00153-3).
- [23] N. Menn. *Practical Optics*. Elsevier Science & Technology Books, 2004. ISBN: 9781493301577.

- [24] *DAZZLERTM system manual Part I : installation operation, V3.00*. Fastlite, Apr. 2019.
- [25] Moana Pittman et al. “Design and characterization of a near-diffraction-limited femtosecond 100-TW 10-Hz high-intensity laser system”. In: *Applied Physics B: Lasers and Optics* 74 (Jan. 2002). DOI: 10.1007/s003400200838.
- [26] P.E. Powers. *Fundamentals of Nonlinear Optics*. Taylor & Francis, 2011. ISBN: 9781420093513.
- [27] N. Minkovski et al. “Nonlinear polarization rotation and orthogonal polarization generation experienced in a single-beam configuration”. In: *J. Opt. Soc. Am. B* 21.9 (Sept. 2004), pp. 1659–1664. DOI: 10.1364/JOSAB.21.001659.
- [28] Lorenzo Canova et al. “Efficient generation of cross-polarized femtosecond pulses in cubic crystals with holographic cut orientation”. In: *Applied Physics Letters* 92.23 (June 2008), p. 231102. ISSN: 0003-6951. DOI: 10.1063/1.2939584.
- [29] A. Jullien et al. “Spectral broadening and pulse duration reduction during cross-polarized wave generation: influence of the quadratic spectral phase”. In: *Applied Physics B - Laser and Optics* 87.4 (May 2007), pp. 595–601. DOI: 10.1007/s00340-007-2685-8.
- [30] Patrick O’Shea et al. “Highly simplified device for ultrashort-pulse measurement”. In: *Opt. Lett.* 26.12 (June 2001), pp. 932–934. DOI: 10.1364/OL.26.000932.
- [31] K. W. DeLong et al. “Frequency-resolved optical gating with the use of second-harmonic generation”. In: *J. Opt. Soc. Am. B* 11.11 (Nov. 1994), pp. 2206–2215. DOI: 10.1364/JOSAB.11.002206.
- [32] D.J. Kane and R. Trebino. “Characterization of arbitrary femtosecond pulses using frequency-resolved optical gating”. In: *IEEE Journal of Quantum Electronics* 29.2 (1993), pp. 571–579. DOI: 10.1109/3.199311.
- [33] Byung-Kwan Yang et al. “Design, Construction and Calibration of a GRENOUILLE, Single-Shot, Ultrashort-Pulse Measurement System”. In: *Journal of The Korean Physical Society* 52 (Feb. 2008). DOI: 10.3938/jkps.52.269.
- [34] M. Kimmel et al. R. Trebino P. O’Shea. “Measuring Ultrashort Laser Pulses Just Got a Lot Easier”. In: *Optics Photonics News* 12.6 (2001), pp. 22–25.
- [35] Cl Froehly, A Lacourt, and J Ch Viénot. “Time impulse response and time frequency response of optical pupils.:Experimental confirmations and applications”. In: *Nouvelle Revue d’Optique* 4.4 (July 1973), p. 183. DOI: 10.1088/0335-7368/4/4/301.
- [36] Xiong Shen et al. “Self-Referenced Spectral Interferometry for Femtosecond Pulse Characterization”. In: *Applied Sciences* 7 (Apr. 2017), p. 407. DOI: 10.3390/app7040407.
- [37] Michelle Rhodes, Günter Steinmeyer, and Rick Trebino. “Standards for ultrashort-laser-pulse-measurement techniques and their consideration for self-referenced spectral interferometry”. In: *Appl. Opt.* 53.16 (June 2014), pp. D1–D11. DOI: 10.1364/AO.53.0000D1.
- [38] Marin Iliev et al. “Measurement of energy contrast of amplified ultrashort pulses using cross-polarized wave generation and spectral interferometry”. In: *Opt. Express* 22.15 (July 2014), pp. 17968–17978. DOI: 10.1364/OE.22.017968.
- [39] *ALPHA kHz High Repetition Rate Ti:Sa Laser Series*. Thales Group, 2021.
- [40] *PHAROS LIGHT CONVERSION User’s Manual*. Light Conversion Ltd., 2011.
- [41] *HR4000 and HR4000CG-UV-NIR Series Spectrometers Installation and Operation Manual, Document No: 210-00000-000-02-201604*. Ocean Optics, Inc., 2008.
- [42] *MS9740B Optical Spectrum Analyzer Operation Manual, Fourth Edition, Document No.: M-W3998AE-4.0*. ANRITSU CORPORATION, Sept. 2021.
- [43] Gorachand Ghosh. “Dispersion-equation coefficients for the refractive index and birefringence of calcite and quartz crystals”. In: *Optics Communications* 163.1 (1999), pp. 95–102. ISSN: 0030-4018. DOI: [https://doi.org/10.1016/S0030-4018\(99\)00091-7](https://doi.org/10.1016/S0030-4018(99)00091-7).
- [44] Christophe Dorrer et al. “Spectral resolution and sampling issues in Fourier-transform spectral interferometry”. In: *J. Opt. Soc. Am. B* 17.10 (Oct. 2000), pp. 1795–1802. DOI: 10.1364/JOSAB.17.001795.
- [45] Rongqing Hui and Maurice S. O’Sullivan. *Fiber optic measurement techniques*. eng. Elsevier/Academic Press, 2009. ISBN: 1282286897.

A Source code

In this section, the Python implementation of the SRSI algorithm is described, and demonstrated by the characterization of pulses from a Thales ALPHA kHz laser. The pulse under consideration is a dispersion-compensated pulse with a duration of 38 fs, a center wavelength of 800 nm and a bandwidth spanning approximately 30 nm. The spectral data, which includes the interferogram, fundamental spectrum, and XPW spectrum, was recorded using the Anritsu MS9740B spectrometer with a resolution of 0.059 nm. The pulse characterization process and the ASE spectrum determination were conducted following the procedures outlined in subsection 2.5.1 and subsection 2.5.2. The results presented in this evaluation partially coincide with those described in subsection 4.1.2 and subsection 4.4, due to the use of the same sample pulse and spectrometer for pulse characterization. Below, the source code and its corresponding outputs are displayed.

```
# import libraries
import pandas as pd
import scipy
import scipy.constants as c
import scipy.signal as sig
import scipy.fftpack as fft
import numpy as np
import matplotlib.pyplot as plt
import math

# set resolution of plots
plt.rcParams['figure.dpi'] = 150

# path to spectra
path = 'C:/Users/Public/Documents/'

# -----
# read .txt files (fundamental spectrum, XPW spectrum and interferogram) into pandas DataFrame
# -----

# read the interferogram
df = pd.read_csv(path+'interferogram.txt', sep='\t')
# columns for wavelength (wl) and intensity (int)
df.columns = ['wl', 'int']
# manual 'calibration' of the spectrum's intensity values
# intensities at the edge (at the smallest and largest wavelengths) are set equal to zero
df['int'] -= np.arange(np.mean(df['int'][0:20]), np.mean(df['int'][-20:]),
                      -(np.mean(df['int'][0:20]) - np.mean(df['int'][-20:]))) / len(df['int'])

# insert frequency column and convert wavelength to frequencies
df.insert(2, "frequency", c.c/(df.loc[:, "wl"]*10**(-9)))

# read the XPW spectrum
dfXPW = pd.read_csv(path+'spectrumXPW.txt', sep='\t')
# columns for wavelength (wl) and intensity (int)
dfXPW.columns = ['wl', 'int']
# manual 'calibration' of the spectrum's intensity values
# intensities at the edge (at the smallest and largest wavelengths) are set equal to zero
dfXPW['int'] -= np.arange(np.mean(dfXPW['int'][0:20]), np.mean(dfXPW['int'][-20:]),
                          -(np.mean(dfXPW['int'][0:20]) - np.mean(dfXPW['int'][-20:]))) / len(dfXPW['int'])

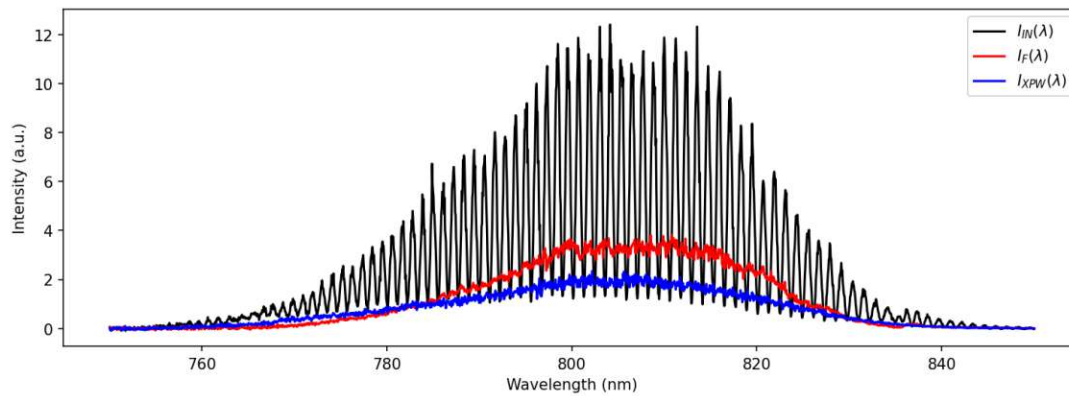
# insert frequency column and convert wavelength to frequencies
dfXPW.insert(2, "frequency", c.c/(dfXPW.loc[:, "wl"]*10**(-9)))

# read the fundamental spectrum
dfF = pd.read_csv(path+'spectrumFA.txt', sep='\t')
# columns for wavelength (wl) and intensity (int)
dfF.columns = ['wl', 'int']
# manual 'calibration' of the spectrum's intensity values
# intensities at the edge (at the smallest and largest wavelengths) are set equal to zero
dfF['int'] -= np.arange(np.mean(dfF['int'][0:20]), np.mean(dfF['int'][-20:]),
                        -(np.mean(dfF['int'][0:20]) - np.mean(dfF['int'][-20:]))) / len(dfF['int'])

# insert frequency column and convert wavelength to frequencies
dfF.insert(2, "frequency", c.c/(dfF.loc[:, "wl"]*10**(-9)))

# set the size of the plot
plt.rcParams['figure.figsize'] = [12, 4]

# plot the spectra
plt.plot(df['wl'][:-1], df['int'][:-1], label='$I_{IN}(\lambda)$', color="black")
plt.plot(df['wl'][:-1], dfF['int'][:-1], label='$I_F(\lambda)$', color="red")
plt.plot(df['wl'][:-1], dfXPW['int'][:-1], label='$I_{XPW}(\lambda)$', color="blue")
plt.xlabel("Wavelength (nm)")
plt.ylabel("Intensity (a.u.)")
plt.legend()
plt.show()
```



```

# -----
# processing of the measured signals
# -----

# set figure size
plt.rcParams['figure.figsize'] = [12, 3]

# set array with frequencies (from top to bottom)
xp = df['frequency'][:, :-1]

# define frequency interval
dfreq = 1*10**10

# create array of frequencies with spacing of the size of the frequency interval
f = np.arange(0*3*10**14, 4.2*(10**14), dfreq)
N = len(f)

# define time interval
dt = 1/(N*dfreq)

# time array t with interval dt
t = np.arange(-(N/2)*dt, (N-(N/2))*dt, dt)

# interpolate the interferogram in frequency domain
signal_inter_spec = np.interp(f, xp, df['int'][:, :-1])

# scale values
signal_inter_spec /= np.max(signal_inter_spec)

# filter high (and low) frequencies so that the temporal signal is not distorted
# find peaks of signal
peaks, _ = sig.find_peaks(abs(signal_inter_spec), height=0.99, distance=3000)
# choose width of Gaussian filter
sigma = math.floor(0.2*10**14/dfreq)
# multiply Gaussian function with the data to cut off very low and high frequencies
signal_inter_spec *= np.exp(-(((np.arange(0, 1, 1/N) - (3.75*10**14/dfreq)/N)**2)/(2*(sigma/N)**2))**8)

# plot measured intensity data points per wavelength and interpolated curve
plt.plot(f, signal_inter_spec, linewidth=1, color='black')
plt.plot(xp, df['int'][:, :-1]/np.max(df['int'][:, :-1]), 'ro', ms=5)
plt.plot(f, np.exp(-(((np.arange(0, 1, 1/N) - (3.75*10**14/dfreq)/N)**2)/(2*(sigma/N)**2))**8), color='black')
plt.xlim([0.34*10**15, 0.41*10**15])
plt.title("Input signal $I_{IN}(\omega, \tau)$")
plt.xlabel("Frequency (Hz)")
plt.ylabel("Intensity")
plt.show()

# create array for the temporal signal, Fourier-transform the interpolated spectrum
signal_temp = fft.ifft(signal_inter_spec)
# shift the temporal signal;
# array has to be shifted because Fourier-transform returns an array sorted from [0, t/2] concatenated with [-t/2, 0]
# an array sorted from [-t, t] is needed
signal_temp = fft.ifftshift(signal_temp)

# create array with frequencies of the signal (from bottom to top)
xp_Unk = df['frequency'][:, :-1]
# interpolate the data for the fundamental (=unknown) spectrum
Fund_inter_spec = np.interp(f, xp_Unk, df['int'][:, :-1])

# filter high frequencies so that the temporal signal is not distorted
# find peaks of signal
peaks, _ = sig.find_peaks(abs(Fund_inter_spec)/np.max(abs(Fund_inter_spec)), height=0.99, distance=3000)
# choose width of Gaussian filter
sigma = math.floor(0.6*10**14/dfreq)
# multiply Gaussian function with the data to cut off very low and high frequencies

```

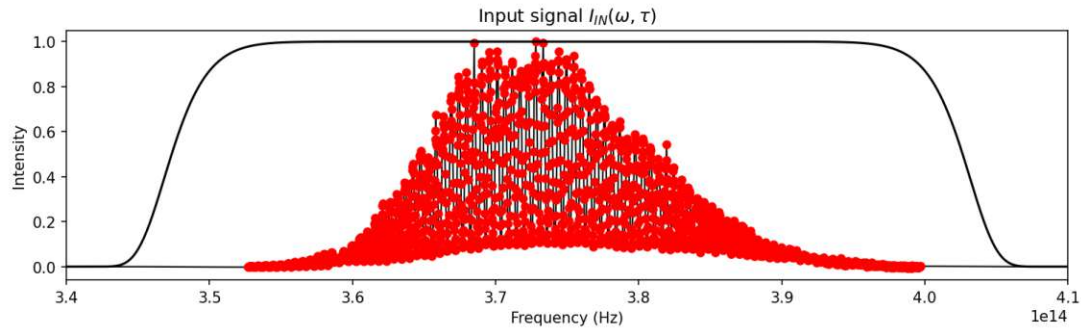
```

Fund_inter_spec *= np.exp(-(((np.arange(0,1,1/N)-(3.75*10**14/dfreq)/N)**2)/(2*(sigma/N)**2))**4)+10**(-10)

# create array with frequencies of the signal (from bottom to top)
xp_XPW = dfXPW['frequency'][:,::-1]
# interpolate the data for the XPW (=reference) spectrum
XPW_inter_spec = np.interp(f, xp_XPW, dfXPW['int'][:,::-1])

# filter high frequencies so that the temporal signal is not distorted
# find peaks of signal
peaks, _ = sig.find_peaks(abs(XPW_inter_spec)/np.max(abs(XPW_inter_spec)), height=0.99, distance=3000)
# choose width of Gaussian filter
sigma = math.floor(0.8*10**14/dfreq)
# multiply Gaussian function with the data to cut off very low and high frequencies
XPW_inter_spec *= np.exp(-(((np.arange(0,1,1/N)-(3.75*10**14/dfreq)/N)**2)/(2*(sigma/N)**2))**4)+10**(-10)

```



```

# -----
# Fourier transform interferogram to extract sum term and interference term in temporal domain
# -----

# set figure size
plt.rcParams['figure.figsize'] = [5, 2]

# scale temporal signal
signal_temp /= np.max(abs(signal_temp))

# find peaks of the Fourier-transformed interferogram signal and plot the temporal signal
peaks, properties = sig.find_peaks(np.abs(signal_temp), height=0.05, distance=500, prominence=(0.05, None))
plt.plot(t, np.abs(signal_temp))
plt.plot(peaks*dt-N/2*dt, np.abs(signal_temp)[peaks], "x")
plt.xlim([-3*10**(-12), 3*10**(-12)])
plt.title("Fourier transformed input signal $FT^{-1}\{I_{IN}(\omega, \tau)\}$")
plt.xlabel("Time (s)")
plt.ylabel("Intensity")
plt.show()

# tau corresponds to the temporal retardation between the fundamental and the reference pulse
tau=abs(peaks[0]-peaks[1])

window = []
# sigma for the super Gaussian function to separate the sum term and interference term from the temporal signal
# sigma defines the width of the window function
sigma = [math.floor((tau)+1)/4, math.floor((tau)+1)/4, math.floor((tau)+1)/4]

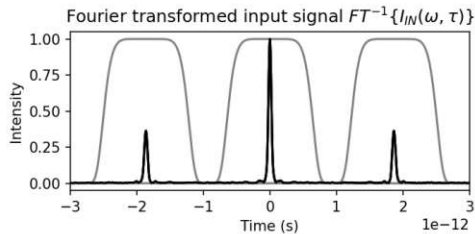
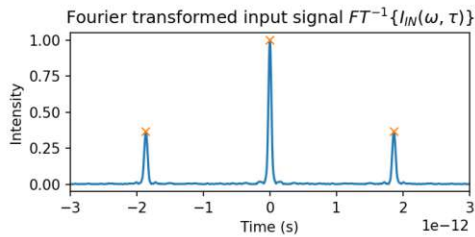
for i in range(0,3):

    # all divided by N - otherwise too large values in exponent
    window.append(np.exp(-(((np.arange(0,1,1/N)-peaks[i]/N)**2)/(2*(sigma[i]/N)**2))**4))

    b=window[i]

    # plot the temporal signal with its corresponding window functions to separate sum term and interference term
    plt.plot(t, b, color="grey")
    plt.plot(t, np.abs(signal_temp), color="black")
    plt.xlim([-3*10**(-12), 3*10**(-12)])
plt.xlabel("Time (s)")
plt.ylabel("Intensity")
plt.title("Fourier transformed input signal $FT^{-1}\{I_{IN}(\omega, \tau)\}$")
plt.show()

```



```

# -----
# extract sum term and interference term from Fourier-transformed interferogram
# inverse Fourier-transform sum term and interference term to obtain it in the frequency domain
# -----

# separate sum term from the temporal signal
sumpeak_temporal = signal_temp*window[1]

# plot the temporal sum term
# attention: sum term is displayed from -t/2 to t/2 but data is ordered in range [0,t/2] to [-t/2:0] (periodicity)
plt.plot(t,np.abs(sumpeak_temporal),label="Abs")
plt.plot(t,(sumpeak_temporal).real,label="Real")
plt.plot(t,(sumpeak_temporal).imag,label="Imag")
plt.title("Temporal sum term:  $S_0(t)$ ")
plt.xlabel("Time (s)")
plt.ylabel(" $S_0(t)$ ")
plt.xlim([-2*10**(-13), 2*10**(-13)])
plt.legend()
plt.show()

# plot the temporal interference term
# separate interference term from the temporal signal
interferencePeak_temporal = signal_temp*window[0]
interferencePeak_temporal=np.roll(interferencePeak_temporal,-(peaks[0]+math.floor(N/2)))
# attention: sum term is displayed from -t/2 to t/2 but data is ordered in range [0:t/2] to [-t/2:0] (periodicity)
plt.plot(t,np.abs((interferencePeak_temporal)),label="Abs")
plt.plot(t,((interferencePeak_temporal).real),label="Real")
plt.plot(t,((interferencePeak_temporal).imag,label="Imag")
plt.title("Temporal interference term:  $f(t)$ ")
plt.xlabel("Time (s)")
plt.ylabel(" $f(t)$ ")
plt.xlim([-2*10**(-13), 2*10**(-13)])
plt.legend()
plt.show()

# auxiliary variables
N=len(sumpeak_temporal)
dfreq = 1/((N)*dt)

# shift array of the sum term in temporal domain
sumpeak_temporal = fft.ifftshift(sumpeak_temporal)
# Fourier-transform to obtain sum term in frequency domain
sumPeak = fft.fft(sumpeak_temporal)

# filter high (and low) frequencies so that the temporal signal is not distorted
# choose width of Gaussian filter
sigma = math.floor(0.15*10**14/dfreq)
# multiply Gaussian function with the data to cut off very low and high frequencies
sumPeak = sumPeak*np.exp(-((np.arange(0,1,1/N)-(3.75*10**14/dfreq)/N)**2)/(2*(sigma/N)**2))**12)

# plot sum term in frequency domain
plt.plot(f,(abs(sumPeak)),label="Abs",color="black")
plt.xlim([0.34*10**15, 0.41*10**15])
plt.title("Sum term in frequency domain:  $S_0(\omega)$ ")
plt.xlabel("Frequency (Hz)")
plt.ylabel(" $S_0(\omega)$ ")
plt.legend()
plt.show()

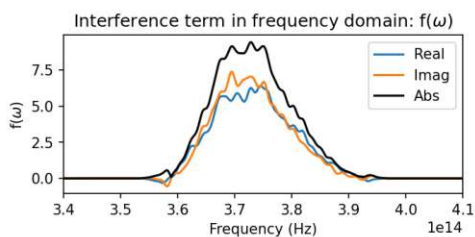
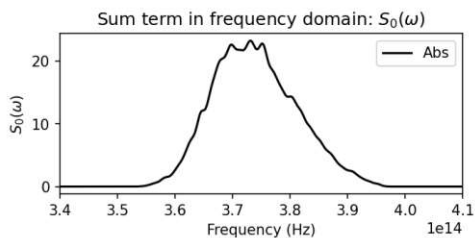
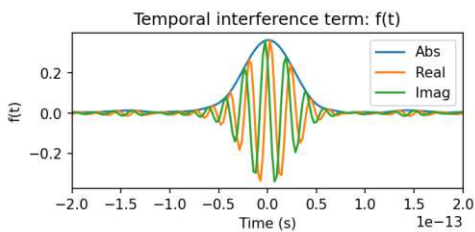
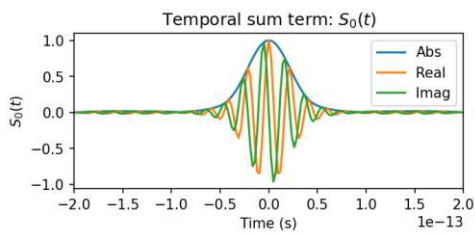
# shift array of the interference term in temporal domain

```

```
interferencePeak_temporal = fft.ifftshift(interferencePeak_temporal)
# Fourier-transform to obtain interference term in frequency domain
interPeak = fft.fft(interferencePeak_temporal)

# filter high (and low) frequencies so that the temporal signal is not distorted
# choose width of Gaussian filter
sigma = math.floor(0.148*10**14/dfreq)
# multiply Gaussian function with the data to cut off very low and high frequencies
interPeak *= np.exp(-((np.arange(0,1,1/N)-(3.75*10**14/dfreq)/N)**2)/(2*(sigma/N)**2))**12

# plot sum term in frequency domain
plt.plot(f,(interPeak.real),label="Real")
plt.plot(f,(interPeak.imag),label="Imag")
plt.plot(f,(abs(interPeak)),label="Abs",color="black")
plt.xlim([0.34*10**15, 0.41*10**15])
plt.title("Interference term in frequency domain: f($\omega$)")
plt.xlabel("Frequency (Hz)")
plt.ylabel("f($\omega$)")
plt.legend()
plt.show()
```



```
# -----
# calculating amplitudes of fundamental and reference pulse
# method by Oksenhendler, original SRSI algorithm, without consideration of incoherent component (ASE)
# -----

# set figure size
plt.rcParams['figure.figsize'] = [5, 3]

# formulas for  $E_{XPW} \gg E_{FA}$ 
# calculation of XPW and fundamental amplitudes
E_ref_abs_spec = (1/2*((abs(sumPeak)+2*abs(interPeak))**(1/2) + abs(abs(sumPeak)-2*abs(interPeak))**(1/2)))
E_F_abs_spec = (1/2*((abs(sumPeak)+2*abs(interPeak))**(1/2)-abs(abs(sumPeak)-2*abs(interPeak))**(1/2)))
```

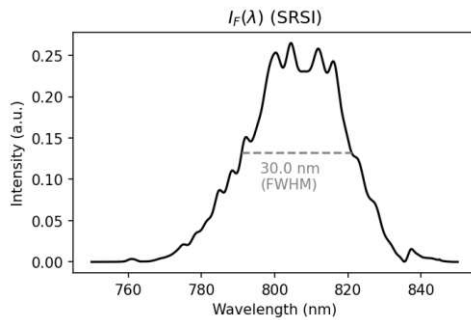
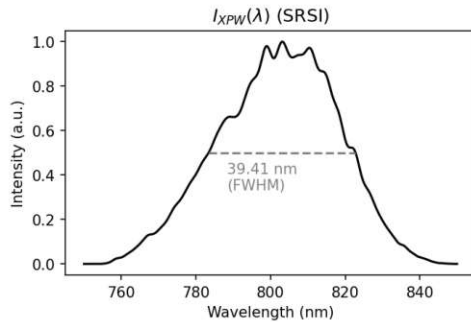
```

# define a scaling factor
norm_factor = np.max(E_ref_abs_spec)

# interpolate data to display spectrum on wavelength scale
x = np.arange(750,850,0.01)
interE_ref_abs_specSq = np.interp(x,(c.c/(f[1:])*10**9)[::-1], ((E_ref_abs_spec[1:])*2)[::-1])
# find peaks of signal to calculate FWHM
peaks, _ = sig.find_peaks(interE_ref_abs_specSq/np.max(interE_ref_abs_specSq), distance=300, prominence=(0.5,None))
fwhm = sig.peak_widths(interE_ref_abs_specSq/np.max(interE_ref_abs_specSq), peaks, rel_height=0.5)
FWHMofIref = 'FWHM of $I_{XPW}(\lambda)$ = ' + str(np.round(fwhm[0][0]/100,4)) + ' nm'
# plot XPW spectrum
plt.plot(x,interE_ref_abs_specSq/np.max(interE_ref_abs_specSq),color="black")
plt.title("$I_{XPW}(\lambda)$ (SRSI)")
plt.xlabel("Wavelength (nm)")
plt.ylabel("Intensity (a.u.)")
# plot line to mark FWHM
plt.hlines(fwhm[1:][0][0],fwhm[1:][1][0]*(x[1]-x[0])+x[0],fwhm[1:][2][0]*(x[1]-x[0])+x[0], color="grey",ls="--")
fwhmText = str(np.round(fwhm[0][0]/100,2)) + ' nm \n(FWHM)'
plt.text(fwhm[1:][1][0]*(x[1]-x[0])+x[0]+5,fwhm[1:][0][0]/1.5, fwhmText, color = 'grey')
plt.show()

# interpolate data to display spectrum on wavelength scale
interpolE_F_abs_specSq = np.interp(x,(c.c/(f[1:])*10**9)[::-1], ((E_F_abs_spec[1:])*2)[::-1])
plt.plot(x,interpolE_F_abs_specSq/np.max(interE_ref_abs_specSq),color="black")
# find peaks of signal to calculate FWHM
peaks, _ = sig.find_peaks(interpolE_F_abs_specSq/np.max(interE_ref_abs_specSq), distance=300, prominence=(0.2,None))
fwhm = sig.peak_widths(interpolE_F_abs_specSq/np.max(interE_ref_abs_specSq), peaks, rel_height=0.5)
FWHMofIunk = 'FWHM of $I_F(\lambda)$ = ' + str(np.round(fwhm[0][0]/100,4)) + ' nm'
# plot fundamental spectrum
plt.title("$I_F(\lambda)$ (SRSI)")
plt.xlabel("Wavelength (nm)")
plt.ylabel("Intensity (a.u.)")
# plot line to mark FWHM
plt.hlines(fwhm[1:][0][0],fwhm[1:][1][0]*(x[1]-x[0])+x[0],fwhm[1:][2][0]*(x[1]-x[0])+x[0], color="grey",ls="--")
fwhmText = str(np.round(fwhm[0][0]/100,2)) + ' nm \n(FWHM)'
plt.text(fwhm[1:][1][0]*(x[1]-x[0])+x[0]+5,fwhm[1:][0][0]/1.5, fwhmText, color = 'grey')
plt.show()

```



```

# -----
# fitting of separately measured XPW spectrum and fundamental spectrum to the sum term S_0
# -----

# set figure size
plt.rcParams['figure.figsize'] = [5, 3]

# scale spectra
Fund_inter_spec /= np.max(Fund_inter_spec)
XPW_inter_spec /= np.max(XPW_inter_spec)

```

```

# define interval in which the minimization is performed; edge-regions are excluded
interval=np.r_[round(3.5*10**14/dfreq):round(4.1*10**14/dfreq)]

# function to minimize; parameters c_FA and c_X can be determined this way
# the parameters are used to scale the XPW and fundamental spectrum
# function is the sum over all entries i: (S_0)_i - c_FA*(I_FA)_i - c_X*(I_XPW)_i
def fittingFunction(params):
    c_FA, c_X = params

    # initialization of variable a
    a = ((np.array(sumPeak[interval])[0] - c_FA*np.array(Fund_inter_spec[interval])[0]
           - c_X*np.array(XPW_inter_spec[interval])[0]).real**2)**(1/2)
    # for every intensity data point
    for i in range(len(sumPeak[interval])):
        if i != 0:
            a+=((np.array(sumPeak[interval])[i] - c_FA*np.array(Fund_inter_spec[interval])[i]
                 - c_X*np.array(XPW_inter_spec[interval])[i]).real**2)**(1/2))

    return a

# optimize the fitting function by least-squares method, giving an initial guess by the factors [26,71]
r = scipy.optimize.least_squares(fittingFunction, [26, 71])
# Alternative, faster method: Powell
#r = scipy.optimize.minimize(fittingFunction, [70, 15],method="Powell")

# scaling factors for the separately measured fundamental and XPW signal
scalingFactorFA = r.x[0]
scalingFactorXPW = r.x[1]

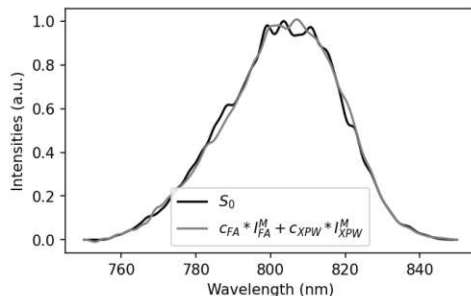
# filtering of XPW and FA signal (smoothing of spectra)
# same temporal filter as for sum term and interference term
Fund_inter_spec=(fft.fft(fft.ifftshift(fft.ifftshift(scipy.fft.ifft(Fund_inter_spec))*window[1])))
XPW_inter_spec=(fft.fft(fft.ifftshift(fft.ifftshift(scipy.fft.ifft(XPW_inter_spec))*window[1])))

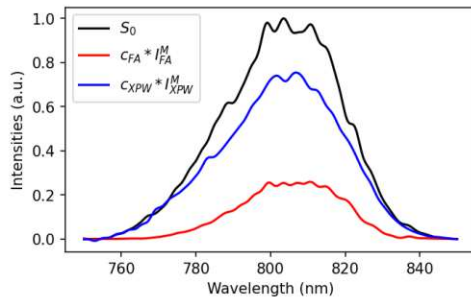
# define wavelength-range for spectrum
x = np.arange(750,850,0.01)

# plot the sum term obtained by the SRSI algorithm and sum of fundamental and XPW spectrum
# interpolate data to display spectrum on wavelength scale
inter_S0 = np.interp(x,(c.c/(f[1:])*10**9)[::-1], ((sumPeak)[1:]))[::-1])
inter_S0_2 = np.interp(x,(c.c/(f[1:])*10**9)[::-1], ((r.x[0]*Fund_inter_spec+r.x[1]*XPW_inter_spec)[1:]))[::-1])
plt.plot(x,(inter_S0/np.max(inter_S0)).real,label="$S_0$",color="black")
plt.plot(x,(inter_S0_2/np.max(inter_S0)).real,label="$c_{FA} * I_{FA}^M + c_{XPW} * I_{XPW}^M$",color="grey")
plt.legend()
plt.xlabel("Wavelength (nm)")
plt.ylabel("Intensities (a.u.)")
plt.show()

# plot the sum term, fundamental and XPW spectrum
# interpolate data to display spectrum on wavelength scale
interpol_F_measured = np.interp(x,(c.c/(f[1:])*10**9)[::-1], ((r.x[0]*Fund_inter_spec)[1:]))[::-1])
interpol_xpw_measured = np.interp(x,(c.c/(f[1:])*10**9)[::-1], ((r.x[1]*XPW_inter_spec)[1:]))[::-1])
plt.plot(x,(inter_S0/np.max(inter_S0)).real,label="$S_0$",color="black")
plt.plot(x,(interpol_F_measured/np.max(inter_S0)).real,label="$c_{FA} * I_{FA}^M$",color="red")
plt.plot(x,(interpol_xpw_measured/np.max(inter_S0)).real,label="$c_{XPW} * I_{XPW}^M$",color="blue")
plt.legend()
plt.xlabel("Wavelength (nm)")
plt.ylabel("Intensities (a.u.)")
plt.show()

```





```

# -----
# calculate ASE spectra
# -----

# set figure size
plt.rcParams['figure.figsize'] = [5, 3]

# calculate ASE spectra using two methods I_ASE = I_FA - f^2/I_XPW and I_ASE = S_0 - f^2/I_XPW - I_XPW
ASEsignal2 = -(abs(interPeak)/np.sqrt(r.x[1]*XPW_inter_spec)**2)+r.x[0]*Fund_inter_spec
ASEsignal = (sumPeak-(abs(interPeak)/np.sqrt(r.x[1]*XPW_inter_spec)**2)-r.x[1]*XPW_inter_spec)

# convert NaN values to zero
ASEsignal2 = np.nan_to_num(ASEsignal2)
ASEsignal = np.nan_to_num(ASEsignal)

# clip negative values of ASE signal since it is only due to noise and has no physical relevance
ASEsignal2 = ASEsignal2.clip(min=-2)
ASEsignal = ASEsignal.clip(min=-2)

# interpolate data to display spectrum on wavelength scale
x = np.arange(750,850,0.01)
interpol_ASEsignal = np.interp(x,(c.c/(f[1:])*10**9)[::-1], ((ASEsignal)[1:]))[::-1])
interpol_ASEsignal2 = np.interp(x,(c.c/(f[1:])*10**9)[::-1], ((ASEsignal2)[1:]))[::-1])

# Gauss fitting of ASE spectrum
# define the Gaussian function
# x_0 is the deviation of the shift of the center of the gaussian function from 790 nm
def Gauss(x, A, sigma, x0):
    y = A*np.exp(-1/2*(x-(x0+790))**2/(sigma**2))
    return y

# fit the ASE data to a Gauss curve; amongst others, the center wavelength (relative to 790 nm) is returned
parameters, covariance = scipy.optimize.curve_fit(Gauss, x, interpol_ASEsignal/np.max(inter_S0))

# fitting parameters of Gaussian function (amplitude, sigma and center of peak)
fit_A = parameters[0]
fit_Sigma = parameters[1]
fit_x0 = parameters[2]

# plot original ASE signal (I_A = S_0 - f^2/I_XPW - I_XPW) and the Gaussian fit
fit_y = Gauss(x, fit_A, fit_Sigma, fit_x0)
plt.plot(x, interpol_ASEsignal/np.max(inter_S0),label="$I_A$",color="black")
plt.plot(x, fit_y, '-', label='$I_{A,fit}$',color="gray")
plt.legend()
plt.xlabel("Wavelength (nm)")
plt.ylabel("Intensity (a.u.)")
plt.title("$I_A$ = $S_0 - f^2/I_{XPW} - I_{XPW}$")
plt.show()

# fit the ASE data to a Gauss curve; amongst others, the center wavelength (relative to 790 nm) is returned
parameters2, covariance2 = scipy.optimize.curve_fit(Gauss, x, interpol_ASEsignal2/np.max(inter_S0))

# fitting parameters of Gaussian function (amplitude, sigma and center of peak)
fit_A_2 = parameters2[0]
fit_Sigma_2 = parameters2[1]
fit_x0_2 = parameters2[2]

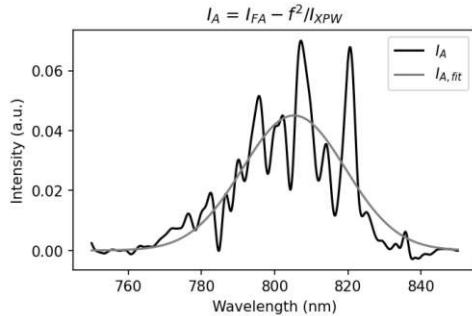
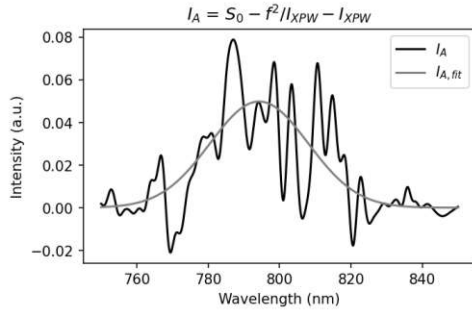
# plot original ASE signal (I_A = I_FA - f^2/I_XPW) and the Gaussian fit
fit_y_2_ASE = Gauss(x, fit_A_2, fit_Sigma_2, fit_x0_2)
plt.plot(x, interpol_ASEsignal2/np.max(inter_S0),label="$I_A$",color="black")
plt.plot(x, fit_y_2_ASE, '-', label='$I_{A,fit}$',color="gray")
plt.legend()
plt.xlabel("Wavelength (nm)")
plt.ylabel("Intensity (a.u.)")
plt.title("$I_A$ = $I_{FA} - f^2/I_{XPW}$")
plt.show()

# print center wavelength and FWHM of XPW signal (I_A = S_0 - f^2/I_XPW - I_XPW)
print("\n\nI_A = S_0 - f^2/I_XPW - I_XPW")
# [OUT]: I_A = S_0 - f^2/I_XPW - I_XPW

```

```
print("center wavelength of ASE spectrum (Gauss fit) = " + str(round(fit_x0+790,2)) + " nm")
# [OUT]: center wavelength of ASE spectrum (Gauss fit) = 794.27 nm
print("FWHM of ASE spectrum (Gauss fit) = " + str(round(2*np.sqrt(2*np.log(2))*fit_Sigma,2)) + " nm")
# [OUT]: FWHM of ASE spectrum (Gauss fit) = 32.37 nm

# print center wavelength and FWHM of XPW signal (I_A = I_FA - f^2/I_XPW)
print("\n\nI_A = I_FA - f^2/I_XPW")
# [OUT]: I_A = I_FA - f^2/I_XPW
print("center wavelength of ASE spectrum (Gauss fit) = " + str(round(fit_x0_2+790,2)) + " nm")
# [OUT]: center wavelength of ASE spectrum (Gauss fit) = 805.25 nm
print("FWHM of ASE spectrum (Gauss fit) = " + str(round(2*np.sqrt(2*np.log(2))*fit_Sigma_2,2)) + " nm")
# [OUT]: FWHM of ASE spectrum (Gauss fit) = 33.11 nm
```



```
# -----
# comparison of fundamental and XPW spectrum for calculation with and without consideration of ASE
# -----

# define wavelength-range for spectrum
x = np.arange(750,850,0.01)

# interpolate the measured and scaled XPW spectrum and plot
interE_ref_abs_specSq_fit = np.interp(x,(c.c/(f[1:::])*10**9)[::-1], ((r.x[1]*XPW_inter_spec)[1:::])[::-1])
scalingFactor = 1*np.max(interE_ref_abs_specSq_fit)
plt.plot(x,interE_ref_abs_specSq_fit/scalingFactor,label="$I_{XPW} = c_{XPW} * I_{XPW}^{-M}$",color="black")

# interpolate the calculated XPW spectrum (without ASE consideration) and plot
interE_E_ref_abs_spec_ana = np.interp(x,(c.c/(f[1:::])*10**9)[::-1], ((E_ref_abs_spec**2)[1:::])[::-1])
plt.plot(x,interE_E_ref_abs_spec_ana/scalingFactor,label="$I_{XPW, SRSI}$ (no ASE consideration)",color="grey")
plt.title("$I_{XPW}(\lambda)$")
plt.xlabel("Wavelength (nm)")
plt.ylabel("Intensity (a.u.)")
plt.legend(loc="lower left")
plt.show()

# interpolate the measured and scaled fundamental spectrum and plot
interE_F_abs_specSq_fit = np.interp(x,(c.c/(f[1:::])*10**9)[::-1], ((abs(interPeak)/np.sqrt(r.x[1]*XPW_inter_spec))**2)[1:::])[::-1])
interE_F_abs_specSq_fit = np.nan_to_num(interE_F_abs_specSq_fit)

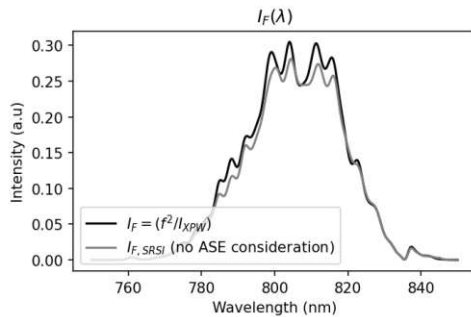
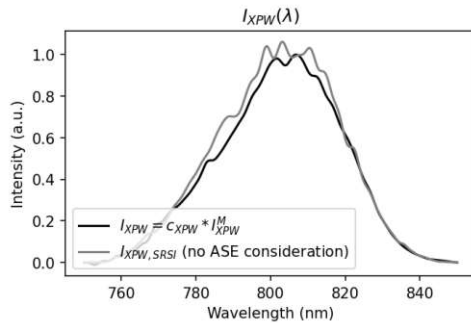
# plot the interpolated, measured and scaled fundamental spectrum
plt.plot(x,interE_F_abs_specSq_fit/scalingFactor,label="$I_F = (f^2/I_{XPW})$",color="black")

# interpolate the calculated fundamental spectrum (without ASE consideration) and plot
interpolE_E_F_abs_spec_ana = np.interp(x,(c.c/(f[1:::])*10**9)[::-1], ((E_F_abs_spec**2)[1:::])[::-1])
plt.plot(x,interpolE_E_F_abs_spec_ana/scalingFactor,label="$I_F, SRSI$ (no ASE consideration)",color="grey")
plt.title("$I_F(\lambda)$")
plt.xlabel("Wavelength (nm)")
plt.ylabel("Intensity (a.u)")
plt.legend(loc="lower left")
plt.show()
```

```
# calculate ratio of calculated XPW spectrum without consideration of ASE to directly measured and scaled XPW spectrum
print('ratio of XPW spectrum without consideration of ASE to directly measured and scaled XPW spectrum = ' +
      str(round(np.mean((interE_E_ref_abs_spec_ana[round(15/0.01):-round(10/0.01)] /
                      interE_ref_abs_specSq_fit[round(15/0.01):-round(10/0.01)]).real),3)))
# [OUT]: ratio of XPW spectrum without consideration of ASE to directly measured and scaled XPW spectrum = 1.071

# print ratio of fundamental spectrum without consideration of ASE to directly measured and scaled fundamental spectrum
print('ratio of fundamental spectrum without consideration of ASE to directly measured and scaled fundamental spectrum = '
      + str(round(np.mean((interpolE_E_F_abs_spec_ana[round(15/0.01):-round(10/0.01)] /
                      interE_F_abs_specSq_fit[round(15/0.01):-round(10/0.01)]).real),3)))
# [OUT]: ratio of fundamental spectrum without consideration of ASE to directly measured and scaled fund. spectrum = 0.94

# calculate the ratio of ASE to I_FA and I_F
# this is done by an integral (sum) over the whole spectrum divided by the integral over the other spectrum
# alternative: ratio of the fitting functions' maxima of the two spectra
print('\nratio of ASE to I_FA (1) = ' + str(round((1/(np.sum(interpol_F_measured)/np.sum(interpol_ASEsignal2))).real),3)))
# [OUT]: ratio of ASE to I_FA (1) = 0.177
print('ratio of ASE to I_FA (2) = ' + str(round((1/(np.sum(interpol_F_measured)/np.sum(interpol_ASEsignal))).real),3)))
# [OUT]: ratio of ASE to I_FA (2) = 0.190
print('\nratio of ASE to I_F (1) = ' + str(round((1/(np.sum(interE_F_abs_specSq_fit)/np.sum(interpol_ASEsignal2))).real),3)))
# [OUT]: ratio of ASE to I_F (1) = 0.215
print('ratio of ASE to I_F (2) = ' + str(round((1/(np.sum(interE_F_abs_specSq_fit)/np.sum(interpol_ASEsignal))).real),3)))
# [OUT]: ratio of ASE to I_F (2) = 0.231
```



```
# -----
# Gaussian fit of fundamental and XPW spectrum
# -----

# define the Gaussian function
# x_0 is the deviation of the shift of the center of the gaussian function from 790 nm
def Gauss(x, A, sigma, x0):
    y = A*np.exp(-1/2*(x-(x0+790))**2/(sigma**2))
    return y

# fit the ASE data to a Gauss curve; amongst others, the center wavelength (relative to 790 nm) is returned
parameters, covariance = scipy.optimize.curve_fit(Gauss, x, interE_ref_abs_specSq_fit/np.max(interE_ref_abs_specSq_fit))

# fitting parameters of Gaussian function (amplitude, sigma and center of peak)
fit_A = parameters[0]
fit_Sigma = parameters[1]
fit_x0 = parameters[2]

# fit the ASE data to a Gauss curve; amongst others, the center wavelength (relative to 790 nm) is returned
parameters2, covariance2 = scipy.optimize.curve_fit(Gauss, x, interE_F_abs_specSq_fit/np.max(interE_ref_abs_specSq_fit))

# fitting parameters of Gaussian function (amplitude, sigma and center of peak)
fit_A_2 = parameters2[0]
fit_Sigma_2 = parameters2[1]
fit_x0_2 = parameters2[2]
```

```

# plot separately measured and scaled XPW and fundamental spectrum (with consideration of ASE) and the ASE spectrum
fit_y = Gauss(x, fit_A, fit_Sigma, fit_x0)
plt.plot(x, interE_ref_abs_specSq_fit/np.max(interE_ref_abs_specSq_fit),label="$I_{XPW}$",color="black")
plt.plot(x, fit_y, '-', label='$I_{XPW,fit}$')
fit_y_2 = Gauss(x, fit_A_2, fit_Sigma_2, fit_x0_2)
plt.plot(x, interE_F_abs_specSq_fit/np.max(interE_ref_abs_specSq_fit),label="$I_F$",color="black")
plt.plot(x, fit_y_2, '-', label='$I_{F,fit}$')
plt.plot(x, interpol_ASEsignal2/np.max(interE_ref_abs_specSq_fit),label="$I_A$",color="black")
plt.plot(x, fit_y_2_ASE, '-', label='$I_{A,fit}$')
plt.legend()
plt.xlabel("Wavelength (nm)")
plt.ylabel("Intensity (a.u.)")
plt.title("$I_{XPW,fit}$, $I_{F,fit}$ and $I_{ASE,fit}$")
plt.show()

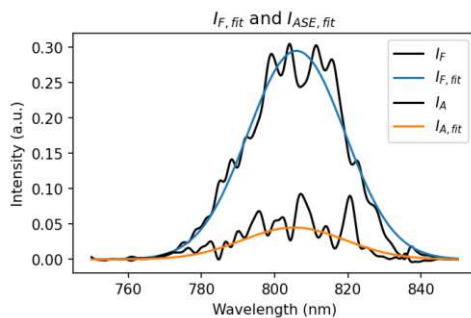
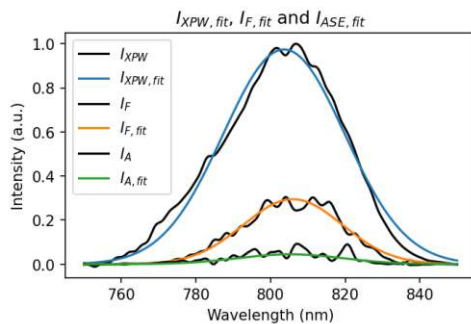
# plot separately measured and fundamental spectrum (with consideration of ASE) and the ASE spectrum
# also Gaussian fits are plotted
fit_y = Gauss(x, fit_A, fit_Sigma, fit_x0)
fit_y_2 = Gauss(x, fit_A_2, fit_Sigma_2, fit_x0_2)
plt.plot(x, interE_F_abs_specSq_fit/np.max(interE_ref_abs_specSq_fit),label="$I_F$",color="black")
plt.plot(x, fit_y_2, '-', label='$I_{F,fit}$')
plt.plot(x, interpol_ASEsignal2/np.max(interE_ref_abs_specSq_fit),label="$I_A$",color="black")
plt.plot(x, fit_y_2_ASE, '-', label='$I_{A,fit}$')
plt.legend()
plt.xlabel("Wavelength (nm)")
plt.ylabel("Intensity (a.u.)")
plt.title("$I_{F,fit}$ and $I_{ASE,fit}$")
plt.show()

# print center wavelength and FWHM of Gaussian fitted fundamental spectrum
print("\n\ncenter wavelength of fundamental spectrum (Gauss fit) = " + str(round(fit_x0_2+790,2)) + " nm")
# [OUT]: center wavelength of fundamental spectrum (Gauss fit) = 805.97 nm
print("FWHM of fundamental spectrum (Gauss fit) = " + str(round(2*np.sqrt(2*np.log(2))*fit_Sigma_2,2)) + " nm")
# [OUT]: FWHM of fundamental spectrum (Gauss fit) = 31.2 nm

# print center wavelength and FWHM of Gaussian fitted XPW spectrum
print("\n\ncenter wavelength of XPW spectrum (Gauss fit) = " + str(round(fit_x0+790,2)) + " nm")
# [OUT]: center wavelength of XPW spectrum (Gauss fit) = 803.61 nm
print("FWHM of XPW spectrum (Gauss fit) = " + str(round(2*np.sqrt(2*np.log(2))*fit_Sigma,2)) + " nm")
# [OUT]: FWHM of XPW spectrum (Gauss fit) = 38.32 nm

# ratio of max intensity of Gaussian-fitted fundamental spectrum to max intensity of Gaussian-fitted XPW spectrum
print("\n\ratio of max. intensity of fundamental spectrum to max. intensity of XPW spectrum = " +
      str(round(fit_A_2/fit_A,3)))
# [OUT]: ratio of max. intensity of fundamental spectrum to max. intensity of XPW spectrum = 0.303

```



```

# -----
# plot spectrum with phase and temporal intensity without ASE consideration of fundamental signal
# (original proposal by Oksenhendler et al.)
# -----

# define electric field of fundamental signal (spectrum and phase)
E_F_spectral_withoutASEconsideration = abs(E_F_abs_spec)*(np.exp(np.unwrap(np.angle(interPeak))*1j))

# unwrap phase of fundamental spectrum
phase = np.unwrap(np.angle(E_F_spectral_withoutASEconsideration))
# rescale phase; phase is zero at centerwavelength 800nm (=3.75*1014 Hz)
phase = phase - phase[round(3.75*10**14/dfreq)]

# plot fundamental spectrum and phase (without ASE consideration)
fig, ax1 = plt.subplots()
ax1.plot(f,phase, color="red")
ax1.set_xlabel("Frequency  $\omega$  (Hz)")
ax1.set_ylim([-math.pi,math.pi])
ax1.set_ylabel("Spectral phase:  $\phi(\omega)$  (rad)",color="red")
ax2 = ax1.twinx()
ax2.plot(f,abs(E_F_spectral_withoutASEconsideration)**2, color="black")
ax2.set_ylabel("Intensity of fundamental signal:  $I_F(\omega)$ ",color="black")
plt.xlim([0.34*10**15, 0.41*10**15])
plt.title(" $I_F(\omega)$  and  $\phi(\omega)$  without ASE consideration")
plt.show()

# calculate temporal intensity of fundamental signal
E_F_temp = fft.ifft(E_F_spectral_withoutASEconsideration)
E_F_temp /= np.max(E_F_temp)
E_F_temp = fft.ifftshift(E_F_temp)

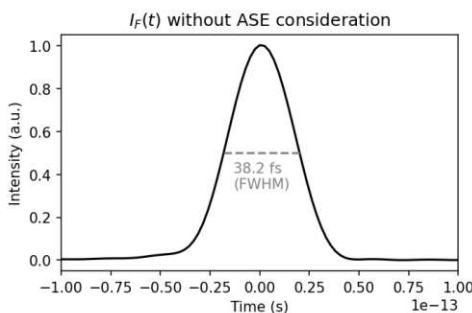
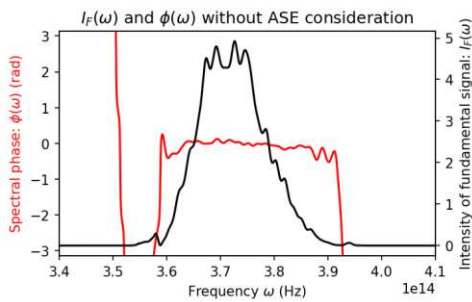
# find temporal peak; necessary for FWHM calculation
peaks, _ = sig.find_peaks(abs(E_F_temp)**2, height=0.5, distance=300, prominence=(0.5,None))
fwhm = sig.peak_widths(abs(E_F_temp)**2, peaks, rel_height=0.5)

# center temporal signal around t = 0 and calculate and print FWHM
E_F_temp = np.roll(E_F_temp,-peaks[0]-N//2)
E_F_temp_without_improved_phase_without_ASE = E_F_temp

# calculate temporal phase; (large linear component)
phi_F_temporal = np.unwrap(np.angle(E_F_temp))
phi_F_temporal = phi_F_temporal - phi_F_temporal[len(t)//2]

# plot temporal intensity of fundamental signal with FWHM
fig, ax1 = plt.subplots()
ax1.plot(t,abs(E_F_temp)**2,color="black")
ax1.set_xlabel("Time (s)")
ax1.set_ylabel("Intensity (a.u.)",color="black")
plt.hlines(fwhm[1:][0][0],fwhm[1:][1][0]*(t[1]-t[0])+t[0],fwhm[1:][2][0]*(t[1]-t[0])+t[0], color="grey",ls="--")
fwhmText = str(np.round(fwhm[0][0]*dt*10**15,1)) + " fs\n(FWHM)"
plt.text(fwhm[1:][1][0]*(t[1]-t[0])+t[0]+5*10**(-15),fwhm[1:][2][0][0]/1.5, fwhmText, color = 'grey')
plt.xlim([-100*10**(-15),100*10**(-15)])
plt.title(" $I_F(t)$  without ASE consideration")
plt.show()

```



```

# -----
# plot spectrum with phase and temporal intensity with ASE consideration
# -----

# define electric field of fundamental signal (spectrum and phase)
E_F_spectral = abs(abs(interPeak)/np.sqrt(r.x[1]*XPW_inter_spec))*(np.exp(np.unwrap(np.angle(interPeak))*1j))

# unwrap phase of fundamental pulse
phase = np.unwrap(np.angle(E_F_spectral))
# rescale phase; phase is set to zero at center wavelength 800nm (=3.75*10^14 Hz)
phase = phase - phase[round(3.75*10**14/dfreq)]

# plot fundamental spectrum and phase
fig, ax1 = plt.subplots()
ax1.plot(f,phase, color="red")
ax1.set_xlabel("Frequency  $\omega$  (Hz)")
ax1.set_ylim([-math.pi,math.pi])
ax1.set_ylabel("Spectral phase:  $\phi(\omega)$  (rad)",color="red")
ax2 = ax1.twinx()
ax2.plot(f,abs(E_F_spectral)**2, color="black")
ax2.set_ylabel("Intensity of fundamental signal:  $I_F(\omega)$ ",color="black")
plt.xlim([0.34*10**15, 0.41*10**15])
plt.title(" $I_F(\omega)$  and  $\phi(\omega)$  with ASE consideration")
plt.show()

# calculate temporal intensity of fundamental signal
E_F_temp = fft.ifft(E_F_spectral)
E_F_temp /= np.max(E_F_temp)
E_F_temp = fft.ifftshift(E_F_temp)

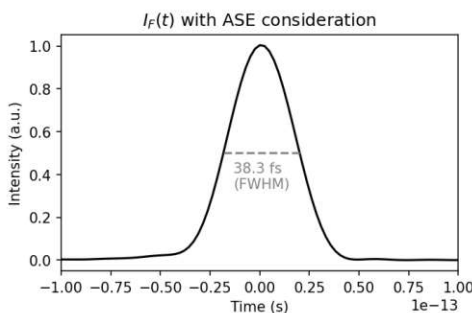
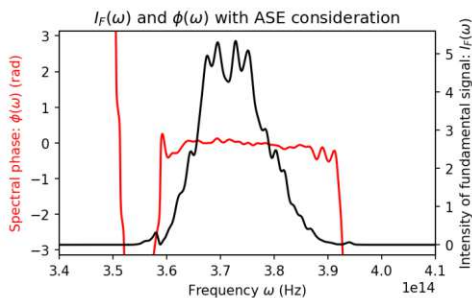
# find temporal peak; necessary for FWHM calculation
peaks, _ = sig.find_peaks(abs(E_F_temp)**2, height=0.5, distance=300, prominence=(0.5,None))
fwhm = sig.peak_widths(abs(E_F_temp)**2, peaks, rel_height=0.5)

# center temporal signal around t = 0 and calculate and print FWHM
E_F_temp = np.roll(E_F_temp,-peaks[0]-N//2)
E_F_temp_without_corr_phase = E_F_temp

# calculate temporal phase; (large linear component)
phi_F_temporal = np.unwrap(np.angle(E_F_temp))
phi_F_temporal = phi_F_temporal - phi_F_temporal[len(t)//2]

# plot temporal intensity of fundamental signal with FWHM
fig, ax1 = plt.subplots()
ax1.plot(t,abs(E_F_temp)**2,color="black")
ax1.set_xlabel("Time (s)")
ax1.set_ylabel("Intensity (a.u.)",color="black")
plt.hlines(fwhm[1:][0][0],fwhm[1:][1][0]*(t[1]-t[0])+t[0],fwhm[1:][2][0]*(t[1]-t[0])+t[0], color="grey",ls="--")
plt.text(fwhm[1:][1][0]*(t[1]-t[0])+t[0]+5*10**(-15),fwhm[1:][2][0]/1.5,
         str(np.round(fwhm[0][0]*dt*10**15,1)) + " fs\n(FWHM)", color = 'grey')
plt.xlim([-100*10**(-15),100*10**(-15)])
plt.title(" $I_F(t)$  with ASE consideration")
plt.show()

```



```

# -----
# calculate iterative phase improvement considering the non-constant phase of the XPW pulse with ASE consideration
# -----

# print pulse duration of the fundamental pulse before the iterative correction algorithm for phase improvement
FWHMofIunk = 'FWHM of I_F(t) without phase correction = ' + str(np.round(fwhm[0][0]*dt*10**15,2)) + "fs"
print(FWHMofIunk)
# [OUT]: FWHM of I_F(t) without phase correction = 38.35fs

# define number of iterations
iterationsNumber = 100
for i in range(1, iterationsNumber+1):

    # approximation of the temporal reference electric field
    E_ref_temporal = abs(E_F_temp)**2*E_F_temp
    E_ref_temporal = E_ref_temporal/np.max(E_ref_temporal)

    # find peak of temporal intensity of reference pulse
    peaks, _ = sig.find_peaks(abs(E_ref_temporal)**2, height=0.5, distance=300, prominence=(0.5,None))
    # center temporal reference signal around t = 0
    E_ref_temporal = np.roll(E_ref_temporal,-peaks[0]-N//2)

    # for Fourier transform the temporal signal has to be shifted
    E_ref_temporal = fft.ifftshift(E_ref_temporal)
    # calculate reference pulse phase by Fourier-transform of temporal reference signal (phase=arg[E_ref(omega)])
    phi_ref_spec = np.unwrap(np.angle(fft.fft(E_ref_temporal)))
    # rescale phase; phase is set to zero at center wavelength 800nm (=3.75*10^14 Hz)
    phi_ref_spec = phi_ref_spec - phi_ref_spec[round(c.c/(800*10**(-9))/dfreq)]

    # new phase of fundamental pulse = existing approximation of fundamental pulse phase + phase of reference pulse
    phi_F_spectral = np.unwrap(np.angle(interPeak)+ phi_ref_spec)
    # rescale phase; phase is set to zero at center wavelength 800nm (=3.75*10^14 Hz)
    phi_F_spectral = phi_F_spectral - phi_F_spectral[round(c.c/(800*10**(-9))/dfreq)]

    # update electric field of fundamental pulse with the new phase
    E_F_spectral = abs(E_F_spectral)*np.exp(phi_F_spectral*1j)

    # calculate temporal amplitude of fundamental pulse with corrected phase
    E_F_temp = fft.ifft(E_F_spectral)
    E_F_temp = fft.ifftshift(E_F_temp)

    # calculate temporal FWHM of corrected fundamental pulse
    peaks, _ = sig.find_peaks(abs(E_F_temp)**2/np.max(abs(E_F_temp)**2), height=0.5, distance=300, prominence=(0.5,None))
    fwhm = sig.peak_widths(abs(E_F_temp)**2/np.max(abs(E_F_temp)**2), peaks, rel_height=0.5)
    E_F_temp = np.roll(E_F_temp,-peaks[0]-N//2)

    # print FWHM of temporal intensity (pulse duration) after phase correction
    FWHMofIunk = 'FWHM of I_F(t) with phase correction = ' + str(np.round(fwhm[0][0]*dt*10**15,2)) + "fs"
    print(FWHMofIunk)
    # [OUT]: FWHM of I_F(t) with phase correction = 38.32fs

# -----
# plot spectrum and phase as well as temporal intensity for the case with and without iterative phase correction
# phase correction corresponds to the consideration of non-constant XPW phase
# ASE is taken into account in this evaluation
# -----

# unwrap phase of fundamental pulse without phase correction
unwrappedPhaseWithoutImprovement = np.unwrap(np.angle(interPeak))
# rescale phase; phase is set to zero at center wavelength 800nm (=3.75*10^14 Hz)
unwrappedPhaseWithoutImprovement -=unwrappedPhaseWithoutImprovement[round(3.75*10**14/dfreq)]

# unwrap phase of fundamental pulse
unwrappedPhase = phi_F_spectral - phi_F_spectral[round(3.75*10**14/dfreq)]

# plot fundamental spectrum and phase with and without consideration of non-constant XPW phase
fig, ax1 = plt.subplots()
ax1.plot(f,abs(fft.fft(fft.ifftshift(E_F_temp)**2)), color="black")
ax1.set_xlabel("Frequency $\omega$ (Hz)")
ax1.set_ylabel("$|I_F(\omega)|$, color="black")
ax2 = ax1.twinx()
ax2.plot(f,unwrappedPhaseWithoutImprovement,color="blue",label="phase without improvement")
ax2.plot(f,unwrappedPhase,color="red",label="phase with improvement")
ax2.set_ylabel("Spectral phase: $\phi_F(\omega)$ (rad)",color="red")
ax2.set_ylim([-math.pi,math.pi])
plt.xlim([0.34*10**15, 0.41*10**15])
plt.title("$|I_F(\omega)$ and $\phi_F(\omega)$")
plt.legend()
plt.show()

# calculate temporal phase; (large linear component)
phi_F_temporal = np.unwrap(np.angle(E_F_temp))
phi_F_temporal = phi_F_temporal - phi_F_temporal[len(t)//2]

```

```

# scale temporal intensities of fundamental pulse for the cases with and without phase correction
E_F_temp /= np.max(E_F_temp)
E_F_temp_without_corr_phase /= np.max(E_F_temp_without_corr_phase)

# plot temporal intensity of fundamental pulse with and without phase correction
fig, ax1 = plt.subplots()
ax1.plot(t,abs(E_F_temp_without_corr_phase)**2/np.max(abs(E_F_temp_without_corr_phase)**2),
         color="blue", label="amplitude without corrected phase")
ax1.plot(t,abs(E_F_temp)**2/np.max(abs(E_F_temp)**2),color="black", label="amplitude with corrected phase")
ax1.set_xlabel("Time (s)")
ax1.set_ylabel("$I_F(t)$",color="black")
ax1.legend(loc='upper right')
ax2 = ax1.twinx()
ax2.plot(t,phi_F_temporal,label="corrected phase",color="red")
ax2.set_ylabel("Temporal phase",color="red")
ax2.set_ylim([-100*math.pi,100*math.pi])
plt.xlim([-100*10**(-15),100*10**(-15)])
plt.title("$I_F(t)$ and $\phi_F(t)$")
plt.show()

# plot spectrum (with FWHM) and phase of fundamental pulse in wavelength-domain
# define wavelength-range for spectrum
x = np.arange(750,850,0.01)
# interpolate data to display spectral phase on wavelength scale
interpPhase = np.interp(x,(c.c/f[1:]*10**9)[::-1], unwrappedPhase[1:][::-1])
# rescale phase; phase is set to zero at center wavelength 800nm (=3.75*10^14 Hz)
yAlignedInterpPhase = interpPhase - interpPhase[math.floor(len(interpPhase)/2)]
# plot the scaled fundamental spectrum
# interpolate data to display spectrum on wavelength scale
interEfund = np.interp(x,(c.c/f[1:]*10**9)[::-1], abs(fft.fftshift(E_F_temp[1:]))**2)[::-1])
peaks, _ = sig.find_peaks(interEfund/np.max(interEfund), height=0.5, distance=300, prominence=(0.5,None))
fwhm = sig.peak_widths(interEfund/np.max(interEfund), peaks, rel_height=0.5)
FWHMofFunk = 'FWHM of $I_{FA}(\lambda)^2$ = ' + str(np.round(fwhm[0][0]/100,4)) + ' nm'
fig, ax1 = plt.subplots()
ax1.plot(x,interEfund/np.max(interEfund), color="black")
ax1.set_xlabel("Wavelength (nm)")
ax1.set_ylabel("Intensity (a.u.)",color="black")
ax2 = ax1.twinx()
ax2.plot(x[17*100:-17*100],yAlignedInterpPhase[17*100:-17*100],color="red")
ax2.set_ylabel("$\phi_F(\lambda)$ (rad)",color="red")
ax2.set_ylim([-math.pi*1.5,math.pi])
plt.title("$I_F(\lambda)$ and $\phi_F(\lambda)$")
# plot FWHM of fundamental spectrum
ax1.hlines(fwhm[1:][0][0],fwhm[1:][1][0]*(x[1]-x[0])+x[0],fwhm[1:][2][0]*(x[1]-x[0])+x[0], color="grey",ls="--")
fwhmText = str(np.round(fwhm[0][0]/100,2)) + ' nm \n(FWHM)'
ax1.text(fwhm[1:][1][0]*(x[1]-x[0])+x[0]+5,fwhm[1:][0][0]/1.5, fwhmText, color = 'grey')
plt.show()

# find temporal peak; necessary for FWHM calculation
peaks, _ = sig.find_peaks(abs(E_F_temp)**2, height=0.5, distance=300, prominence=(0.5,None))
fwhm = sig.peak_widths(abs(E_F_temp)**2, peaks, rel_height=0.5)

# plot temporal intensity of fundamental signal with FWHM
fig, ax1 = plt.subplots()
ax1.plot(t,abs(E_F_temp)**2/np.max(abs(E_F_temp)**2),color="black")
ax1.set_xlabel("Time (s)")
ax1.set_ylabel("Intensity (a.u.)",color="black")
plt.hlines(fwhm[1:][0][0],fwhm[1:][1][0]*(t[1]-t[0])+t[0],fwhm[1:][2][0]*(t[1]-t[0])+t[0], color="grey",ls="--")
fwhmText = str(np.round(fwhm[0][0]*dt*10**15,1)) + " fs\n(FWHM)"
plt.text(fwhm[1:][1][0]*(t[1]-t[0])+t[0]+5*10**(-15),fwhm[1:][0][0]/1.5, fwhmText, color = 'grey')
plt.xlim([-100*10**(-15),100*10**(-15)])
plt.title("$I_F(t)$ with ASE consideration")
plt.show()

# plot temporal intensity of fundamental signal with FWHM in semi-log plot
fig, ax1 = plt.subplots()
ax1.semilogy(t,abs(E_F_temp)**2/np.max(abs(E_F_temp)**2),color="black")
ax1.set_xlabel("Time (s)")
ax1.set_ylabel("Intensity (a.u.)",color="black")
x = t
plt.xlim([-500*10**(-15),500*10**(-15)])
plt.ylim([0.000001,2])
plt.title("$I_F(t)$ with ASE consideration")
plt.show()

```

